

國立臺灣大學電機資訊學院電信工程學研究所

碩士論文

Graduate Institute of Communication Engineering
College of Electrical Engineering and Computer Science
National Taiwan University

Master Thesis

用於高頻譜效益正交分頻多工系統中系統參
數識別之正交恆定振幅序列集

Orthogonal Constant-Amplitude Sequence Families for
System Parameter Identification in Spectrally Compact
OFDM

呂世豪

Shih-Hao Lu

指導教授：鐘嘉德 博士

Advisor: Dr. Char-Dir Chung

共同指導教授：陳維昌 博士

Co-advisor: Dr. Wei-Chang Chen

中華民國 112 年 7 月

July 2023





誌謝

個人參與鐘嘉德教授主持之科技部計畫：高頻寬緊密 OFDM 與 OFDMA 系統的低複雜度頻預編解碼、訓練序列、旁頻波消除符元之設計(3/3)(計畫編號：MOST 109-2221-E-002-156-MY3)的前期研究工作，因此衍生本論文之成果及後續相關研究。此研究期間，在鐘嘉德教授和陳維昌教授的專業指導以及在寫作方面的悉心協助方得以順利完成本論文，在此特別感謝。

當我即將完成在台大電信所碩士班的學業時，想在此向大家表達我的感激之情。在這兩年的學習生活中，有許多人和事對我的成長和進步有著重要的幫助。

首先，我要感謝我的指導教授——鐘嘉德教授。在我的研究過程中，老師提供了許多有價值的建議和指導，讓我更深入地理解了研究領域的重要意義。老師的專業知識和豐富經驗，對我的研究成果和論文寫作起到了極為重要的推動作用。接著要感謝陳維昌教授，在我的研究過程中，老師始終給予我積極的反饋和建議，讓我能夠不斷地改進自己的研究方法和技巧。


當然，我還要感謝我的家人，他們是我生命中最重要支持者和鼓勵者。在我學習的道路上，他們始終支持我、鼓勵我，並為我提供了無私的關愛和照顧。

除此之外，我也要感謝我的朋友們，是你們一直以來的互相激勵和支持，讓我在這兩年的學習生活中能夠進步得更快，學得更深刻。在大家共同努力下，我們一起學習、交流、成長，相信這段經歷會是我人生中難以忘懷的回憶。在未來的道路上，我們仍將是彼此最好的後盾，共同面對未來的挑戰。

在這段時間裡，我學到了許多知識和技能，更學會了如何與人相處、如何面對困難和挑戰。這些經驗和收穫將是我未來的寶貴財富，也將在我的人生道路上為我引路。無論是在學術還是在生活中，我都將繼續努力，不斷挑戰自己，學習成長。

再次感謝每一位給予我支持和幫助的人，你們的貢獻和付出讓我能夠順利完成碩士學業，也讓我更加自信和堅定地迎接未來的挑戰。我希望在未來的人生道路上，我也能像你們一樣成為他人的支持和幫助，讓我們共同成長，共創美好的未來。

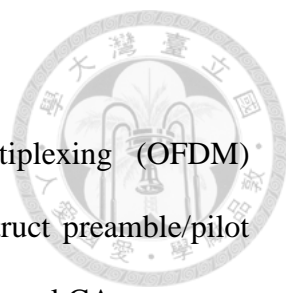
摘要



在矩形脈衝正交分頻多工系統中，恆定振幅序列對於構建前導/領航波形以促進系統參數識別非常有用。在各種系統參數識別應用中，如隨機接入通道識別和多輸入多輸出系統中的上行通道探測，通常優先採用正交恆定振幅序列。然而，在現行的無線通訊標準中採用的傳統正交恆定振幅序列（例如 Zadoff-Chu 序列）數量不足。這種不足會導致需要大量識別序列的系統參數識別性能嚴重降低。此外，攜帶傳統恆定振幅序列的矩形脈衝正交分頻多工前導/領航波形會受到大的旁帶頻譜功率影響，因此具有較低的頻譜緊密度。因此，本文旨在開發幾個 I 階恆定振幅序列集，其中包含更多正交恆定振幅序列，同時賦予相應的正交分頻多工前導/領航波形高頻譜緊密度。由於提供了更多正交序列，所開發的 I 階恆定振幅序列集可以增強在呈現短延遲的多路徑通道上之系統參數識別性能特性，同時構成頻譜緊密的正交分頻多工前導/領航波形。

關鍵字：正交分頻多工、正交恆定振幅序列、領航、前導、系統參數識別、頻譜緊密度。

Abstract



In rectangularly-pulsed orthogonal frequency division multiplexing (OFDM) systems, constant-amplitude (CA) sequences are desirable to construct preamble/pilot waveforms to facilitate system parameter identification (SPI). Orthogonal CA sequences are generally preferred in various SPI applications like random-access channel identification and uplink channel sounding in multiple-input multiple-output systems. However, the number of conventional orthogonal CA sequences (e.g., Zadoff-Chu sequences) that can be adopted in popular wireless communication standards is insufficient. Such insufficiency causes heavy performance degradation for SPI requiring a large number of identification sequences. Moreover, rectangularly-pulsed OFDM preamble/pilot waveforms carrying conventional CA sequences suffer from large power spectral sidelobes and thus exhibit low spectral compactness. This paper is thus motivated to develop several order- I CA sequence families which contain more orthogonal CA sequences while endowing the corresponding OFDM preamble/pilot waveforms with fast-decaying spectral sidelobes. Since more orthogonal sequences are provided, the developed order- I CA sequence families can enhance the performance characteristics in SPI over multipath channels exhibiting short-delay channel profiles, while composing spectrally compact OFDM preamble/pilot waveforms.

Index Terms: Orthogonal frequency division multiplexing, orthogonal constant-amplitude sequences, pilot, preamble, system parameter identification, spectral compactness.

Contents



致謝	i
摘要	ii
Abstract	iii
Contents	iv
List of Figures	vii
List of Tables	viii
1 Introduction	1
1.1 Conventional CA Sequences	3
1.2 Order- I CA Sequences	5
1.3 Contribution	7
1.4 Organization	9
1.5 Notations	9
2 Review of Order-I Constant-Amplitude Sequences	11
2.1 Signal Model	11
2.2 Sequence \mathcal{G}_I	13
2.3 Sequence \mathcal{J}_I	15
2.4 Sequence $\hat{\mathcal{G}}_I$ and $\hat{\mathcal{J}}_I$	16
3 Families $\mathcal{G}_{\max, \bar{I}}^{(\text{dpma}, \kappa)}$ and $\tilde{\mathcal{G}}_{\max, \bar{I}}^{(\text{dpma}, \kappa)}$	26
3.1 Review of Proper Level- $(\Omega(N) - 1)$ Factorization for $\Omega(N) > 2$	28
3.2 Review of Proper Level- $(\Omega(N) - 2)$ Factorization		



for $\Omega(N) > 3$	29
3.3 Exclusively Search a Proper Level- $(\Omega(N) - \kappa)$ Factorization.	31
3.4 Near-Proper Level- $(\Omega(N) - \kappa)$ Factorization for $\Omega(N) > 4$ and $\kappa \in \{3, 4, \dots, \Omega(N) - 2\}$	32
3.5 Some Examples of Families $\mathcal{G}_{\max, \bar{I}}^{(\text{dpma}, \kappa)}$ and $\tilde{\mathcal{G}}_{\max, \bar{I}}^{(\text{dpma}, \kappa)}$	33
4 Families $\hat{\mathcal{G}}_I^{(\text{pma})}$, $\hat{\mathcal{G}}_{\max, \bar{I}}^{(\text{dpma}, \kappa)}$, and $\hat{\mathcal{G}}_{\max, \bar{I}}^{(\text{adpma}, \kappa)}$	39
4.1 Degenerate PMA Sequence Family $\hat{\mathcal{G}}_{\max, \bar{I}}^{(\text{dpma}, \kappa)}$ for $\kappa \in \mathcal{Z}_{\Omega(N)-1}^+$	39
4.2 Augmented PMA Sequence Families $\hat{\mathcal{G}}_I^{(\text{apma})}$ and $\hat{\mathcal{G}}_{\max, \bar{I}}^{(\text{adpma}, \kappa)}$ for $\kappa \in \mathcal{Z}_{\Omega(N)-1}^+$	40
4.2.1 Review of Procedure to Finding a Proper θ	41
4.3 Examples of Families $\hat{\mathcal{G}}_I^{(\text{apma})}$, $\hat{\mathcal{G}}_{\max, \bar{I}}^{(\text{dpma}, \kappa)}$, and $\hat{\mathcal{G}}_{\max, \bar{I}}^{(\text{adpma}, \kappa)}$	43
5 Random Access Channel Identification	45
5.1 Scenario for RA Channel Identification	45
5.2 Performance Analysis	46
5.3 Performance Results	49
6 Simultaneous Channel Estimation	57
6.1 Scenario for Simultaneous Channel Estimation	57
6.1.1 SCE System	58
6.2 Performance Analysis	61
6.3 Performance Results	64
7 Conclusion	70

Appendix

.....

72

Reference

.....

75



List of Figures



Fig. 1.	Performance characteristics for random access channel identification under Rayleigh channel profiles	52
Fig. 2.	Performance characteristics for random access channel identification under Rician channel profiles	54
Fig. 3.	Average out-of-band power fraction characteristics for OFDM random access preamble waveforms.	56
Fig. 4.	Simultaneous channel estimation system.	58
Fig. 5.	Performance characteristics for simultaneous channel estimation under Rayleigh channel.	66
Fig. 6.	Performance characteristics for simultaneous channel estimation under Rician channel.	67
Fig. 7.	Average out-of-band power fraction characteristics for OFDM channel estimation pilot waveforms.	69
Fig. 8.	Gosper's Hack algorithm.	74
Fig. 9.	Codeword conversion algorithm.	74

List of Tables



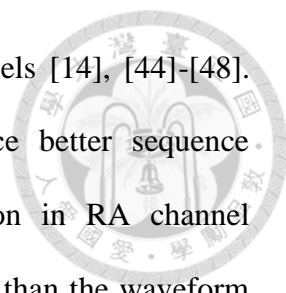
Table I	Some examples of \mathcal{G}_I and \mathcal{J}_I sequences.	16
Table II	Some examples of $\hat{\mathcal{G}}_I$ and $\hat{\mathcal{J}}_I$ sequences.	20
Table III	The construction of families $\mathcal{G}_{\max, \bar{I}}^{(\text{dpma}, \kappa)}$, $\tilde{\mathcal{G}}_{\max, \bar{I}}^{(\text{dpma}, \kappa)}$, $\mathcal{J}_{\max, \bar{I}}^{(\text{dpma}, \kappa)}$, and $\tilde{\mathcal{J}}_{\max, \bar{I}}^{(\text{dpma}, \kappa)}$	21
Table IV	The construction of families $\hat{\mathcal{G}}_{\max, \bar{I}}^{(\text{dpma}, \kappa)}$, $\hat{\mathcal{G}}_{\max, \bar{I}}^{(\text{adpma}, \kappa)}$, $\hat{\mathcal{J}}_{\max, \bar{I}}^{(\text{dpma}, \kappa)}$, and $\hat{\mathcal{J}}_{\max, \bar{I}}^{(\text{adpma}, \kappa)}$	23
Table V	The closed-form expression for proper and near-proper factorizations.	25
Table VI	The numbers of available sounding sequences provided by families $\mathcal{G}_{\max, \bar{I}}^{(\text{dpma}, \kappa)}$ and $\tilde{\mathcal{G}}_{\max, \bar{I}}^{(\text{dpma}, \kappa)}$ for sequence lengths (a) $N = 48$, (b) $N =$ 144 , and (c) $N = 288$ adopted for channel sounding application in 5G NR standard.	36
Table VII	The numbers of available preamble sequences provided by families $\hat{\mathcal{G}}_{\max, \bar{I}}^{(\text{dpma}, \kappa)}$ and $\hat{\mathcal{G}}_{\max, \bar{I}}^{(\text{adpma}, \kappa)}$ for sequence lengths (a) $N = 139$, (b) $N =$ 571 , (c) $N = 839$, and (d) $N = 1151$ adopted for random access application in 5G NR standard.	37
Table VIII	RA system parameters	49
Table IX	Average PAPR of OFDM preamble waveforms	56
Table X	SCE system and channel parameters	66
Table XI	Average PAPR of OFDM pilot waveforms	69

Chapter 1

Introduction



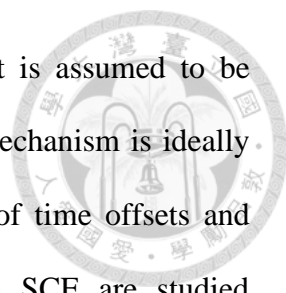
Rectangularly-pulsed orthogonal frequency division multiplexing (OFDM) waveforms are commonly adopted in modern wireless communication systems [1]-[3] due to their feasibility of efficient implementation by fast Fourier transform, easy incorporation of cyclic prefix (CP) to facilitate initial synchronization and channel estimation, and robustness against frequency-selective channel dispersion. In rectangularly-pulsed OFDM systems, constant amplitude (CA) sequences are often used as the training sequence in frequency domain to modulate uniformly spaced subcarriers and thereby enable robust fine initial time/frequency synchronization [4]-[9] and accurate channel estimation [9]-[14] at the receiver combating frequency-selective channel dispersion. When exact or near orthogonality is sustained among sequences, multiple CA training sequences are also adopted to facilitate the identification of different system parameters for establishing initial connection, including the identification of cell/sector/antenna, random access (RA) channel, duplex mode, guard ratio, etc. [1]-[3], [15]-[17]. Two typical applications based on system parameter identification (SPI) are RA channel identification [17]-[21] and multiple-input multiple-output (MIMO) simultaneous channel estimation (SCE) [14], [44]-[48]. Specifically, the received OFDM waveforms carrying different CA sequences in frequency domain are identified by cross-correlating the received frequency-domain samples with all possible identification/sounding sequences, thereby enabling RA channel identification [17]-[21]. Several sounding waveforms carrying different CA sequences in frequency domain are concurrently transmitted by different transmit antennas and separated at different receive antennas by dispreading the received frequency-domain samples with all sounding



sequences, thereby enabling SCE for several uplink MIMO channels [14], [44]-[48]. Multiple orthogonal CA sequences are generally preferred since better sequence identification can be achieved to ensure less false identification in RA channel identification when the channel coherence bandwidth [25] is larger than the waveform bandwidth. Meanwhile, it is analytically shown that the large-size SCE can be achieved with less disturbance from ISI when the adopted CA sequence family is composed of orthogonal sequence subfamilies, each containing as many as permissible cyclically-shiftable CA sequences as possible.

In [17]-[21], they focus on RA applications in various communication systems. They aim to improve the detection performance and efficiency of RA preambles while mitigating interference [17]-[20] or collision issues [21]. For RA application, Zadoff-Chu (ZC) sequences are commonly employed as part of their preamble designs. However, insufficient number of adopted orthogonal ZC sequences may reduce the performance of RA applications. Overall, these papers collectively contribute to advancing RA procedures, enhancing detection performance, reducing collision issues, and improving resource utilization by the proposed techniques in various communication systems.

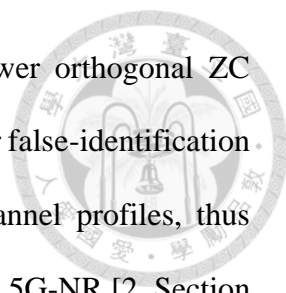
Using cyclically-shiftable ZC sequences as sounding sequences, various SCE approaches have been developed to estimate channel frequency responses (CFRs) on all pilot subcarriers in the least-square (LS) manner directly [48] or estimate channel impulse responses (CIRs) in the LS manner first and then transformed into CFR estimates through discrete Fourier transform (DFT) on all subcarriers indirectly [24], [44]-[47], after separating multiple received sounding signals with the aid of cyclically-shiftable sounding sequences. Within the assumption of perfect time and frequency alignment among all received sounding signals, the SCE performance has been analytically studied for independent Rayleigh multipath channels in [44], [46], [48] and for correlated



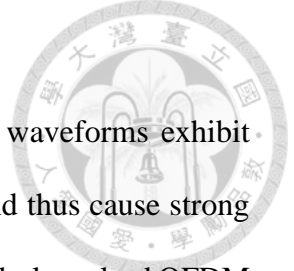
Rayleigh multipath channels in [45], [47]. Perfect time alignment is assumed to be achieved under the cellular system setup that the timing advance mechanism is ideally conducted by all uplink transmitters [46]. The detrimental effect of time offsets and frequency offsets among multiple received sounding signals on SCE are studied analytically in [24] for independent Rayleigh multipath channels.

1.1 Conventional CA Sequences

In practice, ZC sequences [26]-[27] are commonly used as such training/identification/sounding sequences due to their features of CA and zero periodic autocorrelation (ZAC) in both time and frequency domains [8], [28]. Particularly, ZC sequences are popular in SPI applications due to the ZAC-enabled feasibility by generating all orthogonal ZC sequences through cyclically shifting a root ZC sequence in time domain. However, adjacent cyclically-shifted ZC sequences cannot be identified by the receiver in the presence of timing uncertainty under which the start time of the useful signaling subinterval is practically synchronized only within the CP subinterval [18], [29]. Due to such sequence ambiguity [29], not every cyclically shifted ZC sequence can be adopted for SPI in the uplink cellular environment since a minimum cyclic shifting distance (CSD) is required to differentiate distinct received sequences sent from uplink transmitters in different locations [1]-[3], [17]-[21], [29]. As the cell radius is increased, a larger minimum CSD is required to avoid such sequence ambiguity [29]. The latter issue results in the shortage of adoptable orthogonal ZC sequences in many standard preamble/pilot signaling formats for SPI [1]-[3]. For example, a total of 64 ZC sequences are required for RA channel identification in uplink 5G-NR [2, Section 6.3.3.1], [17]-[21]. Among the various adopted pairs of sequence length and minimum CSD, the numbers of adoptable orthogonal ZC sequences are upper bounded by the ratio of sequence length to

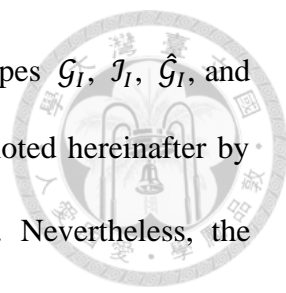


minimum CSD and turn out to be much smaller than 64. Since fewer orthogonal ZC sequences are available, RA channel identification suffers from larger false-identification error (FIE) in multipath environments exhibiting longer-delay channel profiles, thus entailing worse false identification [17]- [18]. As another example in 5G-NR [2, Section 6.4.1.4.1], a MIMO base station in SCE system can receive uplink pilot waveforms from at most 12 transmit antennas concurrently, and thus requires up to 12 cyclically-shiftable orthogonal ZC sequences to identify and separate different uplink channels in order to achieve high estimation accuracy for static multipath channels [14], [22], [24]. Under this setup, the minimum CSD required to avoid sequence ambiguity is specified by $N/12$ for the adopted ZC sequences of different sequence lengths N [2, Section 6.4.1.4.3]. Since at most 12 cyclically-shiftable orthogonal ZC sequences are available for all adopted pairs of sequence length and minimum CSD [2, Section 6.4.1.4], nonorthogonal ZC sequences generated from different root indices would be adopted if more than 12 uplink channels were required to be estimated simultaneously. When a base station receives multiple pilot waveforms carrying nonorthogonal ZC sequences simultaneously, the SCE performance is heavily degraded due to inter-pilot-interference and this causes the pilot contamination problem [14], [22]-[24]. To alleviate the effect of pilot contamination, orthogonal Yu-Lee (YL) sequences are constructed in [14] from phase-rotating ZC sequences generated from a single root index appropriately, and shown to outperform nonorthogonal ZC sequences in uplink SCE under perfectly time-synchronized reception of multiple sounding signals. However, the SCE performance is yet to be enhanced under asynchronous signal reception since the maximum number of adoptable orthogonal YL sequences is still limited by the ratio of sequence length to minimum CSD.



1.2 Order- I CA Sequences

Although efficient to implement, rectangularly-pulsed OFDM waveforms exhibit large power spectral sidelobes due to discontinuity at pulse edges and thus cause strong interference to adjacent channels [9], [30]-[32]. Specifically, rectangularly-pulsed OFDM waveforms carrying ZC sequences have been shown to render widely spread waveform spectrum with baseband spectral sidelobes decaying asymptotically as f^{-2} [8]-[11]. Although highly compact training waveform spectrum can be composed by suppressing spectral sidelobes through delicate signal processing techniques [30]- [35], the feature of frequency-domain CA is altered in the transmitted waveform after sidelobe suppression, thus compromising the performance characteristics of initial synchronization, channel estimation, and SPI at the receiver. To resolve the problem, several order- I CA sequences have been recently developed in [8]-[11] to render extremely small baseband power spectral sidelobes decaying asymptotically as f^{-2I-2} with sidelobe-decaying order $I \geq 1$, and thus compose spectrally compact training waveforms for robust fine initial synchronization [8]-[9] and accurate channel estimation [9]- [11]. The larger the sidelobe-decaying order I is, the higher spectral compactness the corresponding training waveform can achieve. Since frequency-domain CA is sustained, order- I CA sequences enable the same performance characteristics as ZC sequences in initial synchronization and channel estimation, while yielding much higher spectral compactness [8]-[11]. In [10]-[11], order- I CA sequences \mathcal{G}_I and \mathcal{J}_I were first developed for a large number of sequence lengths. For all composite and prime sequence lengths larger than 11, order- I CA sequences $\hat{\mathcal{G}}_I$ and $\hat{\mathcal{J}}_I$ were further developed in [9] and shown to provide the sidelobe-decaying order not smaller than order- \tilde{I} CA sequences $\mathcal{G}_{\tilde{I}}$ and $\mathcal{J}_{\tilde{I}}$. To meet the needs of various SPI applications, four families containing mutually orthogonal order- I



CA sequences were also developed in [9] for respective sequence types \mathcal{G}_I , \mathcal{J}_I , $\hat{\mathcal{G}}_I$, and $\hat{\mathcal{J}}_I$, based on the method of phase model assigning (PMA), and denoted hereinafter by families $\mathcal{G}_I^{(\text{pma})}$, $\mathcal{J}_I^{(\text{pma})}$, $\hat{\mathcal{G}}_I^{(\text{pma})}$, and $\hat{\mathcal{J}}_I^{(\text{pma})}$ for convenience. Nevertheless, the numbers of permissible orthogonal sequences provided by these families are still insufficient for some SPI applications requiring a large number of orthogonal CA sequences (like RA channel identification and MIMO channel sounding) [1]-[2]. This paper is thus motivated to develop new families with an attempt to providing more orthogonal order- I CA sequences. Based on the methods of degenerate PMA and augmented PMA, several modified PMA sequence families are constructed herein to provide more orthogonal order- \tilde{I} CA sequences ($\mathcal{G}_{\tilde{I}}$, $\mathcal{J}_{\tilde{I}}$, $\hat{\mathcal{G}}_{\tilde{I}}$, and $\hat{\mathcal{J}}_{\tilde{I}}$) than families $\mathcal{G}_I^{(\text{pma})}$, $\mathcal{J}_I^{(\text{pma})}$, $\hat{\mathcal{G}}_I^{(\text{pma})}$, and $\hat{\mathcal{J}}_I^{(\text{pma})}$ by possibly trading off the sidelobe-decaying order $\tilde{I} \leq I$.

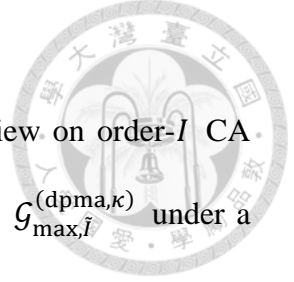
Some modified PMA sequence families were proposed by [43] to obtain more orthogonal sequences, denoted by families $\mathcal{G}_{\max, \tilde{I}}^{(\text{dpma}, \kappa)}$ for $\kappa \in \mathcal{Z}_2^+$ and family $\hat{\mathcal{G}}_I^{(\text{apma})}$. Families $\mathcal{G}_{\max, \tilde{I}}^{(\text{dpma}, \kappa)}$ for $\kappa \in \mathcal{Z}_2^+$ provide larger family sizes than $\mathcal{G}_I^{(\text{pma})}$ and offer the larger family sizes as κ increases, but they may entail reduced sidelobe-decaying order. Family $\hat{\mathcal{G}}_I^{(\text{apma})}$ maintains the same sidelobe-decaying order as family $\hat{\mathcal{G}}_I^{(\text{pma})}$ but increases the number of orthogonal sequences. [43] provides a detailed explanation of the construction and properties of these sequence families. However, the numbers of permissible orthogonal sequences provided by these families are still insufficient for some SPI applications. Therefore, we aim to develop the search method to construct new sequence families $\mathcal{G}_{\max, \tilde{I}}^{(\text{dpma}, \kappa)}$ for $\kappa \in \mathcal{Z}_{\Omega(N)-1}^+ - \mathcal{Z}_2^+$, families $\tilde{\mathcal{G}}_{\max, \tilde{I}}^{(\text{dpma}, \kappa)}$ $\kappa \in \mathcal{Z}_{\Omega(N)-1}^+$, families $\hat{\mathcal{G}}_{\max, \tilde{I}}^{(\text{dpma}, \kappa)}$, and $\mathcal{G}_{\max, \tilde{I}}^{(\text{adpma}, \kappa)}$ for $\kappa \in \mathcal{Z}_{\Omega(N)-1}^+$.

All developed order- \tilde{I} sequences can still provide much higher spectral compactness than ZC, YL, and pseudorandom-noise (PN) sequences for the composed OFDM preamble/pilot waveforms. Since sequences $J_{\tilde{I}}$ and $\hat{J}_{\tilde{I}}$ can be similarly constructed like sequences $G_{\tilde{I}}$ and $\hat{G}_{\tilde{I}}$, only the new families composed of order- \tilde{I} CA sequences $G_{\tilde{I}}$ and $\hat{G}_{\tilde{I}}$ are elaborated in the following. The contribution of the paper is addressed as follows. ^{1.5.1}

1.3 Contribution

- Degenerate PMA sequence families $G_{\max, \tilde{I}}^{(\text{dpma}, \kappa)}$ and $\tilde{G}_{\max, \tilde{I}}^{(\text{dpma}, \kappa)}$ with sequence length N are constructed respectively under a proper level- $(\Omega(N) - \kappa)$ factorization of N for $\kappa \in \mathcal{Z}_{\Omega(N)-1}^+$ and under a near-proper level- $(\Omega(N) - \kappa)$ factorization of N for $\kappa \in \mathcal{Z}_{\Omega(N)-1}^+$, where $\Omega(N)$ is the prime omega value of N and denotes the multiplicity in the prime factorization of N . Families $G_{\max, \tilde{I}}^{(\text{dpma}, \kappa)}$ and $\tilde{G}_{\max, \tilde{I}}^{(\text{dpma}, \kappa)}$ can provide more orthogonal order- \tilde{I} CA sequences than the PMA sequence family $G_{\tilde{I}}^{(\text{pma})}$, with or without trading off sidelobe-decaying order $\tilde{I} \leq I$. When $\tilde{\Omega}(N) > \Omega(N)$, degenerate PMA sequence families $\hat{G}_{\max, \tilde{I}}^{(\text{dpma}, \kappa)}$ are accordingly constructed under a combined proper level- $(\tilde{\Omega}(N) - \kappa)$ factorization of N for $\kappa \in \mathcal{Z}_{\tilde{\Omega}(N)-1}^+$, where $\tilde{\Omega}(N)$ is the modified prime omega (MPO) value defined in [9, eqs. (14)-(15)] and denotes the increased multiplicity provided by all prime factorizations of the properly decomposed values from N . Families $\hat{G}_{\max, \tilde{I}}^{(\text{dpma}, \kappa)}$ can provide more orthogonal order- \tilde{I} CA sequences than the PMA sequence family $\hat{G}_{\tilde{I}}^{(\text{pma})}$, with or without trading off sidelobe-decaying order $\tilde{I} \leq I$.

- When N meets $\tilde{\Omega}(N) > \Omega(N)$, the augmented PMA sequence family $\hat{\mathcal{G}}_I^{(\text{apma})}$ provided in [43] is constructed by virtue of phase-rotating every existing sequence in family $\hat{\mathcal{G}}_I^{(\text{pma})}$ to generate more mutually orthogonal sequence members, and thus provides double the number of orthogonal order- I CA sequences in family $\hat{\mathcal{G}}_I^{(\text{pma})}$ while maintaining the same sidelobe-decaying order. Based on the same phase-rotating method, augmented degenerate PMA sequence family $\hat{\mathcal{G}}_{\max, \tilde{I}}^{(\text{adpma}, \kappa)}$ is constructed from family $\hat{\mathcal{G}}_{\max, \tilde{I}}^{(\text{dpma}, \kappa)}$ for a given $\kappa \in \mathcal{Z}_{\tilde{\Omega}(N)-1}^+$ and provides double the family size of $\hat{\mathcal{G}}_{\max, \tilde{I}}^{(\text{dpma}, \kappa)}$ without trading off the sidelobe-decaying order.
- In comparison with ZC, YL, and PN sequence families, modified PMA sequence families $\hat{\mathcal{G}}_{\max, \tilde{I}}^{(\text{dpma}, \kappa)}$, and $\hat{\mathcal{G}}_{\max, \tilde{I}}^{(\text{adpma}, \kappa)}$ are demonstrated to enhance the performance characteristics in uplink RA channel identification over indoor and urban Rayleigh multipath environments exhibiting short-delay channel profiles. The performance characteristics of SCE over independent Rician multipath channels using the degenerate PMA sequence family $\hat{\mathcal{G}}_{\max, \tilde{I}}^{(\text{dpma}, \kappa)}$ exhibit improvement if a large number of uplink channels were required to be estimated simultaneously under asynchronous signal reception. Such enhancements and improvements are thanks to the provision of more orthogonal CA sequences and thus the mitigation of false identification and inter-sequence-interference. Meanwhile, the preamble/pilot waveforms carrying order- \tilde{I} CA sequences from modified PMA sequence families are attributed with much higher spectral compactness than those carrying ZC, YL, and PN sequences.



1.4 Organization

The paper is organized as follows. **Chapter 2** provides a review on order- I CA sequences \mathcal{G}_I , $\hat{\mathcal{G}}_I$, \mathcal{J}_I , and $\hat{\mathcal{J}}_I$ [9]-[11]. **Chapter 3** develops family $\mathcal{G}_{\max, \tilde{I}}^{(\text{dpma}, \kappa)}$ under a proper level- $(\Omega(N) - \kappa)$ factorization and family $\tilde{\mathcal{G}}_{\max, \tilde{I}}^{(\text{dpma}, \kappa)}$ under a near-proper level- $(\Omega(N) - \kappa)$ factorization, both for $\kappa \in \mathcal{Z}_{\Omega(N)-1}^+$. When $\tilde{\Omega}(N) > \Omega(N)$, family $\hat{\mathcal{G}}_I^{(\text{apma})}$ is constructed in **Chapter 4** by the phase-rotating method. Families $\hat{\mathcal{G}}_{\max, \tilde{I}}^{(\text{dpma}, \kappa)}$ and $\hat{\mathcal{G}}_{\max, \tilde{I}}^{(\text{adpma}, \kappa)}$ are also constructed under a combined proper level- $(\tilde{\Omega}(N) - \kappa)$ factorization for $\kappa \in \mathcal{Z}_{\tilde{\Omega}(N)-1}^+$. In **Chapter 5**, the OFDM systems employing various CA sequence families are compared for RA channel identification and spectral compactness. The performance characteristics of OFDM SCE systems using various CA sequences families are analyzed and demonstrated in **Chapter 6**. **Chapter 7** concludes the paper.

1.5 Notations

1.5.1 Boldface lower-case and upper-case letters denote column vectors and matrices, respectively. Superscripts t , $*$, and h denote transpose, complex conjugate, and conjugate transpose, respectively. \mathcal{Z}^* , \mathcal{Z}_K and \mathcal{Z}_K^+ are the set of nonnegative integers, $\{0, 1, \dots, K-1\}$ and $\{1, 2, \dots, K\}$, respectively. By default, \mathcal{Z}_0^+ is an empty set. We also use $[x_k; k \in \mathcal{Z}_K]$ to represent a $K \times 1$ vector with x_k being the k -th entry, $\min\{x, y\}$ the smaller between x and y , $((n))_N$ the modulo- N value of n , $\|\mathbf{x}\|$ the Frobenius norm of vector \mathbf{x} , $\lceil x \rceil$ the smallest integer that is not smaller than x , and $\lfloor x \rfloor$ the largest integer that is not larger than x . We let $\omega_K \triangleq \exp\left\{-j \frac{2\pi}{K}\right\}$ and denote $\mathbf{W}_K \triangleq [K^{-1/2} \omega_K^{mk}; m \in \mathcal{Z}_K, k \in \mathcal{Z}_K]$ as a $K \times K$ unitary discrete-

Fourier-transform (DFT) matrix with normalized columns and rows. $\mathcal{E}\{\cdot\}$ denotes the expectation operator. $j \triangleq \sqrt{-1}$ is the imaginary unit.

1.5.2 A polygon is said to be cyclic if all vertices of this polygon can circumscribe a circle.

1.5.3 Due to the time-offset uncertainty, only the cyclically-shifted sequences generated from a given time-domain ZAC sequence with the CSD of at least ω_{\min} can be adopted as the sounding sequences in $\{\tilde{\mathbf{q}}_k; k \in \mathcal{Z}_K\}$ in order to avoid sequence identification ambiguity in the SCE process. As such, there are at most $\lfloor N/\omega_{\min} \rfloor$ permissible cyclically-shiftable CA sequences in $\{\mathbf{q}_k; k \in \mathcal{Z}_K\}$ in the case with $K > \lfloor N/\omega_{\min} \rfloor$.

1.5.4 Notably, $\tilde{w}_0 = \Omega(N)$ and all Hamming weights w_m sum to $\Omega(N)$.

Chapter 2

Review of Order- I Constant-Amplitude Sequences



2.1 Signal Model

Consider the rectangularly-pulsed OFDM waveform carrying a sequence of N complex symbols. In the nominal time interval of length T , these symbols are modulated into N uniformly-spaced subcarriers interleaved among γN subcarriers with a positive-integer-valued interleaving factor γ . The time interval is partitioned into a guard CP subinterval of length T_g followed by a useful signaling subinterval of length $T_d = T - T_g$, where $T_g = \alpha T_d$ and α is the guard ratio with $0 < \alpha < 1$. Denote $\mathbf{q} \triangleq [q[n]; n \in \mathcal{Z}_N]$ as the sequence in frequency domain and $\tilde{\mathbf{q}} \triangleq [\tilde{q}[m]; m \in \mathcal{Z}_N] = \mathbf{W}_N^H \mathbf{q}$ as its inverse DFT with $\|\mathbf{q}\|^2 = \|\tilde{\mathbf{q}}\|^2 = 1$. Throughout, \mathbf{q} is restricted to have CA symbols with $|q[n]|^2 = 1/N$, and thus its inverse DFT $\tilde{\mathbf{q}}$ possesses the ZAC property, i.e., $\sum_{m \in \mathcal{Z}_N} \tilde{q} \left[\binom{m-n}{N} \right] (\tilde{q}[m])^* = 0$ for all integers $\binom{(n)}{N} \neq 0$ [8], [28].

Rectangularly-pulsed OFDM preamble/pilot waveforms are discontinuous if identification symbols are not properly restricted and thus render large baseband power spectral sidelobes decaying asymptotically as f^{-2} . In practical OFDM systems, rectangularly pulsed preamble/pilot waveforms carrying PN and ZC sequences render widely spread waveform spectrum with baseband spectral sidelobes decaying asymptotically as f^{-2} [8]-[11]. By properly restricting identification symbols, various order- I CA sequences have been recently developed in [8]-[11] to render extremely small baseband power spectral sidelobes decaying asymptotically as f^{-2I-2} and thus the corresponding baseband power spectrum exhibits I -decaying sidelobes. Due to fast sidelobe decaying, these order- I CA sequences enhance the spectral compactness of the

corresponding OFDM preamble/pilot waveforms, while achieving accurate channel estimation and robust fine initial time and frequency synchronization owing to dual-sequence properties of frequency-domain CA and time-domain ZAC [8]- [9]. Particularly in [9], four types of order- I CA sequences \mathcal{G}_I , $\hat{\mathcal{G}}_I$, \mathcal{J}_I , and $\hat{\mathcal{J}}_I$ with sequence length N have been developed in explicit expressions for all composite sequence lengths and all prime sequence lengths larger than 11 under all parametric conditions on $\alpha\gamma$. In what follows, sequences \mathcal{G}_I , $\hat{\mathcal{G}}_I$, \mathcal{J}_I , and $\hat{\mathcal{J}}_I$ are briefly reviewed.

For convenience, an order- I CA sequence $\mathbf{q} = [N^{-1/2}(-1)^{n\gamma}\chi[n]; n \in \mathcal{Z}_N]$ is described by a CA sequence $\chi = [\chi[n]; n \in \mathcal{Z}_N]$ with $|\chi[n]| = 1$ for all $n \in \mathcal{Z}_N$, and presented in two separate conditions, namely *Condition A* that $\alpha\gamma$ is an integer and *Condition B* that $\alpha\gamma$ is not an integer [9]. Under *Condition A*, if \mathbf{q} satisfies

Constraint A: $\boldsymbol{\mu}_\beta^t \chi = 0$ for all $\beta \in \mathcal{Z}_I$ but $\boldsymbol{\mu}_I^t \chi \neq 0$

for a positive integer $I \in \mathcal{Z}_{N-1}^+$ where $\boldsymbol{\mu}_\beta \triangleq [n^\beta; n \in \mathcal{Z}_N]$, the corresponding baseband power spectrum exhibits I -decaying sidelobes. Under *Condition B*, if \mathbf{q} satisfies

Constraint B: $\boldsymbol{\mu}_\beta^t \chi = 0$ and $\tilde{\boldsymbol{\mu}}_\beta^t \chi = 0$ for all $\beta \in \mathcal{Z}_I$ but $\boldsymbol{\mu}_I^t \chi \neq 0$ or $\tilde{\boldsymbol{\mu}}_I^t \chi \neq 0$

for a positive integer $I \in \mathcal{Z}_{\lfloor (N-1)/2 \rfloor}^+$ where $\tilde{\boldsymbol{\mu}}_\beta \triangleq [e^{-j2\pi n\alpha\gamma} n^\beta; n \in \mathcal{Z}_N]$, the

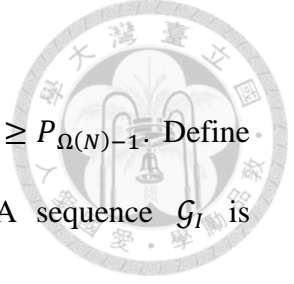
corresponding baseband power spectrum exhibits I -decaying sidelobes. Throughout, we

consider the prime factorization $N = \prod_{m=0}^{\Omega(N)-1} P_m$ where prime integers P_m may not be

all distinct. Due to the constraints, the largest possible family size $\Psi_{\max}(N)$ is limited

by $\Psi_{\max}(N) = N - I$ under *Condition A* and $\Psi_{\max}(N) = N - 2I$ under *Condition B*,

for any sequence family containing mutually orthogonal sequences of length N .



2.2 Sequence \mathcal{G}_I

Arrange prime factors P_m in descending order $P_0 \geq P_1 \geq \dots \geq P_{\Omega(N)-1}$. Define $\phi_m \triangleq \prod_{k=0}^{m-1} P_k$ for $m \in \mathcal{Z}_{\Omega(N)-1}^+$ and $\phi_0 = 1$. An order- I CA sequence \mathcal{G}_I is described as

$$\chi \left[\sum_{m \in \mathcal{Z}_{\Omega(N)}} l_m \phi_m \right] = \exp \left\{ j \sum_{m \in \mathcal{Z}_{\Omega(N)}} \theta_m[l_m] \right\} \quad (1)$$

for all $l_0 \in \mathcal{Z}_{P_0}$, $l_1 \in \mathcal{Z}_{P_1}$, \dots , $l_{\Omega(N)-1} \in \mathcal{Z}_{P_{\Omega(N)-1}}$ under *Condition A*, and

$$\chi \left[\sum_{m \in \mathcal{Z}_{\Omega(N)}} l_m \phi_m \right] = \exp \left\{ j \sum_{m \in \mathcal{Z}_{\Omega(N)}} \theta_m[l_m] + j2\pi\alpha\gamma \sum_{n \in \mathcal{Z}_{\lfloor \frac{\Omega(N)}{2} \rfloor}} l_{2n+1} \phi_{2n+1} \right\} \quad (2)$$

for all $l_0 \in \mathcal{Z}_{P_0}$, $l_1 \in \mathcal{Z}_{P_1}$, \dots , $l_{\Omega(N)-1} \in \mathcal{Z}_{P_{\Omega(N)-1}}$ under *Condition B*. Here, the phases $\theta_m[l_m]$ are restricted by

$$\sum_{l_m \in \mathcal{Z}_{P_m}} \exp\{j\theta_m[l_m]\} = 0 \text{ for all } m \in \mathcal{Z}_{\Omega(N)}. \quad (3)$$

For a given N , sequence \mathcal{G}_I yields the sidelobe-decaying order $I \geq \Omega(N)$ under *Condition A* and $I \geq \lfloor \Omega(N)/2 \rfloor$ under *Condition B*.

Orthogonal sequence family $\mathcal{G}_I^{(\text{pma})}$ have been obtained from the PMA method in [9, Subsection III.B]. For a given index vector $\mathbf{v} = [v_m; m \in \mathcal{Z}_{\Omega(N)}]$ with $v_m \in \mathcal{Z}_{P_m}^+$ for all $m \in \mathcal{Z}_{\Omega(N)}$, a sequence in family $\mathcal{G}_I^{(\text{pma})}$ can be uniquely specified by \mathbf{v} and formed by assigning

$$\theta_m[l_m] = \frac{2\pi v_m l_m}{P_m} \text{ for all } l_m \in \mathcal{Z}_{P_m} \text{ and } m \in \mathcal{Z}_{\Omega(N)} \quad (4)$$

under either *Condition A* or *Condition B*. By varying \mathbf{v} exclusively, family $\mathcal{G}_I^{(\text{pma})}$ can be constructed accordingly and it contains $\Psi(N) \triangleq \prod_{m=0}^{\Omega(N)-1} (P_m - 1)$ orthogonal order-

I CA sequences. Apparently, all order- I sequences in $\mathcal{G}_I^{(\text{pma})}$ are mutually orthogonal, i.e., $\mathbf{q}_l^h \mathbf{q}_k = \tilde{\mathbf{q}}_l^h \tilde{\mathbf{q}}_k = 0$ for any two different sequences \mathbf{q}_l and \mathbf{q}_k in family $\mathcal{G}_I^{(\text{pma})}$.

Consider a leader sequence \mathbf{q}_{lead} in $\mathcal{G}_I^{(\text{pma})}$, specified by $\mathbf{v} = [v_0, v_1, \dots, v_{\Omega(N)-1}]^t$. Denote $\tilde{\mathbf{q}}_{\text{lead}}^{(k)} = [\tilde{q}_{\text{lead}}[(i+k)_N]; i \in \mathcal{Z}_N]$ as the k -cyclically-shifted version of $\tilde{\mathbf{q}}_{\text{lead}}$ (i.e., the inverse DFT of \mathbf{q}_{lead}) and $\mathbf{q}_{\text{lead}}^{(k)} = [q_{\text{lead}}[n] \exp\{j2\pi nk/N\}; n \in \mathcal{Z}_N]$ as its DFT. According to [9], the set of admissible cyclic shifts for which $\mathbf{q}_{\text{lead}}^{(k)}$ is still an order- I CA sequence in $\mathcal{G}_I^{(\text{pma})}$ is specified by $\mathcal{U}(v_0) \triangleq \{lN/P_{\text{max}} | l \in \mathcal{Z}_{P_{\text{max}}} \text{ but } l \neq P_{\text{max}} - v_0\}$ where $P_{\text{max}} \triangleq \max_{m \in \mathcal{Z}_{\Omega(N)}} P_m$ is the largest prime factor and v_0 is the leading entry in \mathbf{v} . From \mathbf{q}_{lead} , we can thus specify the cyclically-shiftable (CS) sequence subfamily $\mathcal{G}_I^{(\text{cs})}(\mathbf{q}_{\text{lead}})$ which contains all mutually orthogonal order- I CA sequences obtained by cyclically shifting $\tilde{\mathbf{q}}_{\text{lead}}$ with shifts in $\mathcal{U}(v_0)$, as

$$\mathcal{G}_I^{(\text{cs})}(\mathbf{q}_{\text{lead}}) \triangleq \{\mathbf{q}_{\text{lead}}^{(k)} | k \in \mathcal{U}(v_0)\} \text{ if } \mathbf{q}_{\text{lead}} \in \mathcal{G}_I^{(\text{pma})} \quad (5)$$

under either *Condition A* or *Condition B*. The factor N/P_{max} defining $\mathcal{U}(v_0)$ is the family CSD for generating $\mathcal{G}_I^{(\text{cs})}(\mathbf{q}_{\text{lead}})$. Notably, $\mathcal{G}_I^{(\text{cs})}(\mathbf{q}_{\text{lead}})$ contains $P_{\text{max}} - 1$ different sequences in $\mathcal{G}_I^{(\text{pma})}$, which are specified by identical indices $v_1, v_2, \dots, v_{\Omega(N)-1}$. Therefore, by varying $v_1, v_2, \dots, v_{\Omega(N)-1}$, we can obtain $\Psi(N)/(P_{\text{max}} - 1)$ mutually exclusive subfamilies $\mathcal{G}_I^{(\text{cs})}(\mathbf{q}_{\text{lead}})$ constructed from all permissible subfamily leaders \mathbf{q}_{lead} specified by different index subvectors $[v_1, v_2, \dots, v_{\Omega(N)-1}]^t$. In $\mathcal{G}_I^{(\text{cs})}(\mathbf{q}_{\text{lead}})$, all orthogonal order- I CA sequences can be easily obtained by cyclically shifting the inverse DFT of a subfamily leader \mathbf{q}_{lead} .

2.3 Sequence \mathcal{J}_I

Arrange prime factors P_m in ascending order $P_0 \leq P_1 \leq \dots \leq P_{\Omega(N)-1}$. Define $\psi_m = N/\phi_{m+1}$ for $m \in \mathcal{Z}_{\Omega(N)-1}$ and $\psi_{\Omega(N)-1} = 1$. An order- I CA sequence \mathcal{J}_I is defined similarly to sequence \mathcal{G}_I as in (1)-(4) with $\phi_m \rightarrow \psi_m$ for $m \in \mathcal{Z}_{\Omega(N)}$. Table I gives some example sequences of length $N = 15$ under *Condition A* and *Condition B*, respectively. With sequence length N , sequence \mathcal{J}_I yields the sidelobe-decaying order $I \geq \Omega(N)$ under *Condition A* and $I \geq \lfloor \Omega(N)/2 \rfloor$ under *Condition B*. By varying the index vector \mathbf{v} exclusively, the orthogonal sequence family $\mathcal{J}_I^{(\text{pma})}$ can be likewise constructed and it contains $\Psi(N)$ mutually orthogonal order- I CA sequences. For a given \mathbf{q}_{lead} in $\mathcal{J}_I^{(\text{pma})}$ specified by $\mathbf{v} = [v_0, v_1, \dots, v_{\Omega(N)-1}]^t$, the cyclically-shiftable sequence subfamily $\mathcal{J}_I^{(\text{cs})}(\mathbf{q}_{\text{lead}})$ can be obtained as

$$\mathcal{J}_I^{(\text{cs})}(\mathbf{q}_{\text{lead}}) \triangleq \left\{ \mathbf{q}_{\text{lead}}^{(k)} \mid k \in \mathcal{U}(v_{\Omega(N)-1}) \right\} \text{ if } \mathbf{q}_{\text{lead}} \in \mathcal{J}_I^{(\text{pma})} \quad (6)$$

under *Condition A* or *Condition B*. Thus, $\mathcal{J}_I^{(\text{cs})}(\mathbf{q}_{\text{lead}})$ contains $P_{\max} - 1$ different sequences in $\mathcal{J}_I^{(\text{pma})}$, which are specified by identical indices $v_0, v_1, \dots, v_{\Omega(N)-2}$. We can obtain $\Psi(N)/(P_{\max} - 1)$ mutually exclusive subfamilies $\mathcal{J}_I^{(\text{cs})}(\mathbf{q}_{\text{lead}})$ constructed from all permissible subfamily leaders \mathbf{q}_{lead} specified by different index subvectors $[v_0, v_1, \dots, v_{\Omega(N)-2}]^t$.

Due to the similarity between $\mathcal{G}_I^{(\text{pma})}$ and $\mathcal{J}_I^{(\text{pma})}$, only modified PMA families from $\mathcal{G}_I^{(\text{pma})}$ are elaborated below.

Table I

Some example sequences of length $N = 14$ under (a) *Condition A* and (b) *Condition B* with $\alpha\gamma = 1/2$. In the tables, ζ is defined by $\zeta \triangleq \exp\{j\pi/7\}$.

(a) Sequences under <i>Condition A</i>	
Sequence	Sequence Expression
\mathcal{G}_I	$\sqrt{\frac{1}{14}} [1, \zeta^2, \zeta^4, \zeta^6, \zeta^8, \zeta^{10}, \zeta^{12}, -1, \zeta^9, \zeta^{11}, \zeta^{13}, \zeta, \zeta^3, \zeta^5]$
\mathcal{J}_I	$\sqrt{\frac{1}{14}} [1, -1, \zeta^2, \zeta^9, \zeta^4, \zeta^{11}, \zeta^6, \zeta^{13}, \zeta^8, \zeta, \zeta^{10}, \zeta^3, \zeta^{12}, \zeta^5]$
(b) Sequences under <i>Condition B</i>	
Sequence	Sequence Expression
\mathcal{G}_I	$\sqrt{\frac{1}{14}} [1, \zeta^2, \zeta^4, \zeta^6, \zeta^8, \zeta^{10}, \zeta^{12}, 1, \zeta^2, \zeta^4, \zeta^6, \zeta^8, \zeta^{10}, \zeta^{12}]$
\mathcal{J}_I	$\sqrt{\frac{1}{14}} [1, 1, \zeta^2, \zeta^2, \zeta^4, \zeta^4, \zeta^6, \zeta^6, \zeta^8, \zeta^8, \zeta^{10}, \zeta^{10}, \zeta^{12}, \zeta^{12}]$

2.4 Sequence $\hat{\mathcal{G}}_I$ and $\hat{\mathcal{J}}_I$

For a given sequence length N , order- I CA sequences $\hat{\mathcal{G}}_I$ and $\hat{\mathcal{J}}_I$ are constructed from concatenating component CA subsequences with shorter lengths as follows. First, N is properly decomposed into $N = \sum_{\rho \in \mathcal{Z}_L} \tilde{N}^{(\rho)}$ where $\tilde{N}^{(\rho)} = \prod_{m=0}^{\Omega(\tilde{N}^{(\rho)})-1} P_m^{(\rho)}$ with prime factors $P_0^{(\rho)} \geq P_1^{(\rho)} \geq \dots \geq P_{\Omega(\tilde{N}^{(\rho)})-1}^{(\rho)}$ arranged for all $\rho \in \mathcal{Z}_L$, and \mathcal{X} is accordingly partitioned into L subsequences $\mathcal{X}_0, \mathcal{X}_1, \dots, \mathcal{X}_{L-1}$ of lengths $\tilde{N}^{(0)}, \tilde{N}^{(1)}, \dots, \tilde{N}^{(L-1)}$, respectively, i.e., $\mathcal{X} = [\mathcal{X}_0^t, \mathcal{X}_1^t, \dots, \mathcal{X}_{L-1}^t]^t$. Second, subsequences $\mathcal{X}_0, \mathcal{X}_1, \dots, \mathcal{X}_{L-1}$ are constructed in forms (1)-(4) with $\phi_m \rightarrow \phi_m^{(\rho)}$ for $m \in \mathcal{Z}_{\Omega(\tilde{N}^{(\rho)})}$ and $\rho \in \mathcal{Z}_L$, and then concatenated to form sequence $\hat{\mathcal{G}}_I$. Sequence $\hat{\mathcal{J}}_I$ is formed similarly with subsequences constructed in the forms (1)-(4) for all $\rho \in \mathcal{Z}_L$ with $\phi_m \rightarrow \psi_m^{(\rho)}$ for $m \in \mathcal{Z}_{\Omega(\tilde{N}^{(\rho)})}$ and $P_0^{(\rho)} \leq P_1^{(\rho)} \leq \dots \leq P_{\Omega(\tilde{N}^{(\rho)})-1}^{(\rho)}$ rearranged. Table II gives some example sequences of length $N = 23$ under *Condition A* and *Condition B*, respectively.

With a proper decomposition $N = \sum_{\rho \in \mathcal{Z}_L} \tilde{N}^{(\rho)}$, order- I CA sequences $\hat{\mathcal{G}}_I$ and $\hat{\mathcal{J}}_I$ yield the sidelobe-decaying order $I \geq \tilde{\Omega}(N)$ under *Condition A* and $I \geq \lfloor \tilde{\Omega}(N)/2 \rfloor$ under *Condition B*, where the *proper* decomposition $\{\tilde{N}^{(\rho)}; \rho \in \mathcal{Z}_L\}$ can achieve the MPO value $\tilde{\Omega}(N)$, defined in [9, eqs. 14-15] as

$$\tilde{\Omega}(N) = \max_{\substack{L \in \mathcal{Z}_2^+ \\ \lfloor \frac{N}{2} \rfloor}} \max_{\substack{\tilde{N}^{(0)} \geq \tilde{N}^{(1)} \geq \dots \geq \tilde{N}^{(L-1)} \geq 2 \\ \tilde{N}^{(0)} + \tilde{N}^{(1)} + \dots + \tilde{N}^{(L-1)} = N}} \min_{\rho \in \mathcal{Z}_L} \Omega(\tilde{N}^{(\rho)}). \quad (7)$$

Notably, the proper decomposition is not necessarily unique for arbitrary lengths N and can assure $\tilde{\Omega}(N) \geq \Omega(N)$ is guaranteed if and only if (iff) N is not any one of the following forms

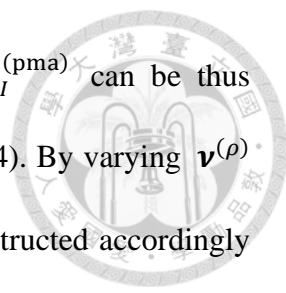
$$N = 2^a \times 3^b \times 5^c \quad (8)$$

$$N = 2^a \times 3^b \times 7^d \quad (9)$$

$$N = 2^a \times 3^b \times 11^e \quad (10)$$

where the nature numbers a, b, c, d , and e are restricted to $a, b \in \mathcal{Z}^*$, $c \in \mathcal{Z}_4$, $d \in \mathcal{Z}_3$, and $e \in \mathcal{Z}_2$ [9, *Property 5*]. In the case, order- I CA sequences $\hat{\mathcal{G}}_I$ and $\hat{\mathcal{J}}_I$ can yield higher sidelobe-decaying order than order- \tilde{I} CA sequences $\mathcal{G}_{\tilde{I}}$ and $\mathcal{J}_{\tilde{I}}$. Conversely, when N is one of the above three forms, sequences $\mathcal{G}_{\tilde{I}}$ and $\mathcal{J}_{\tilde{I}}$ can provide comparable sidelobe-decaying order to sequences $\hat{\mathcal{G}}_I$ and $\hat{\mathcal{J}}_I$ due to $\tilde{\Omega}(N) = \Omega(N)$. For a given N , a proper decomposition and the associated $\tilde{\Omega}(N)$ can be efficiently sought from *Procedure 1* and *Property 4* in [9], where some examples for medium and large N values are also listed in [9, Tables I and II].

Orthogonal sequence family $\hat{\mathcal{G}}_I^{(\text{pma})}$ has also been obtained from the PMA method [9]. Consider the prime factorizations $\tilde{N}^{(\rho)} = \prod_{m=0}^{\Omega(\tilde{N}^{(\rho)})-1} P_m^{(\rho)}$ for all $\rho \in \mathcal{Z}_L$. For the given index vectors $\mathbf{v}^{(\rho)} = \left[v_m^{(\rho)}; m \in \mathcal{Z}_{\Omega(\tilde{N}^{(\rho)})} \right]$ with $v_m^{(\rho)} \in \mathcal{Z}_{P_m^{(\rho)}-1}^+$ for all $\rho \in \mathcal{Z}_L$,

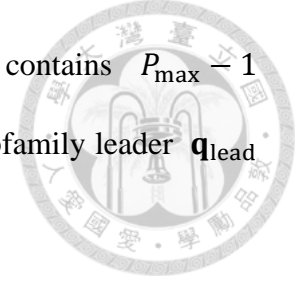


all subsequences of the corresponding sequence \hat{G}_I in family $\hat{G}_I^{(\text{pma})}$ can be thus specified by these $\mathbf{v}^{(\rho)}$ and formed from the phase assignment in (4). By varying $\mathbf{v}^{(\rho)}$ exclusively and concurrently for all $\rho \in \mathcal{Z}_L$, family $\hat{G}_I^{(\text{pma})}$ is constructed accordingly and it contains $\hat{\Psi}(N) \triangleq \min_{\rho \in \mathcal{Z}_L} \Psi(\tilde{N}^{(\rho)})$ orthogonal order- I CA sequences, where $\Psi(\tilde{N}^{(\rho)}) = \prod_{m=0}^{\Omega(\tilde{N}^{(\rho)})-1} (P_m^{(\rho)} - 1)$ for all $\rho \in \mathcal{Z}_L$. Notably, the orthogonal sequence family $\hat{G}_I^{(\text{pma})}$ is not necessarily unique for a given length N since the proper decomposition for N is not necessarily unique. When N is not any one of the forms in (8)-(10), any orthogonal sequence in family $\hat{G}_I^{(\text{pma})}$ can not be obtained from cyclically shifting another sequence (in time domain) in the family, due to the proper decomposition of N [9]. Without limitation by minimum CSD, the latter feature permits the use of all orthogonal sequences in such family $\hat{G}_I^{(\text{pma})}$ and its modified families for SPI applications in the uplink cellular environment.

The orthogonal sequence family $\hat{J}_I^{(\text{pma})}$ is likewise constructed. Due to the similarity between $\hat{G}_I^{(\text{pma})}$ and $\hat{J}_I^{(\text{pma})}$, only modified PMA families from $\hat{G}_I^{(\text{pma})}$ are elaborated herein.

When the sequence length N is not any one of the forms in (8)-(10) and has $\tilde{\Omega}(N) > \Omega(N)$, we can construct family $\hat{G}_I^{(\text{pma})}$ with larger sidelobe-decaying order than family $\mathcal{G}_I^{(\text{pma})}$. Different from family $\mathcal{G}_I^{(\text{pma})}$, all sequences in family $\hat{G}_I^{(\text{pma})}$ can not be obtained through mutual cyclic shifting. Conversely, when N follows any one of the forms in (8)-(10) and exhibits $\tilde{\Omega}(N) = \Omega(N)$, family $\mathcal{G}_I^{(\text{pma})}$ can yield comparable sidelobe-decaying order to family $\hat{G}_I^{(\text{pma})}$ and is composed of $\Psi(N)/(P_{\max} - 1)$ mutually exclusive subfamilies $\mathcal{G}_I^{(\text{cs})}(\mathbf{q}_{\text{lead}})$ for all permissible subfamily leaders \mathbf{q}_{lead} ,

as shown in Subsection II.A. Each subfamily $\mathcal{G}_I^{(\text{cs})}(\mathbf{q}_{\text{lead}})$ contains $P_{\text{max}} - 1$ sequences generated by cyclically shifting the inverse DFT of a subfamily leader \mathbf{q}_{lead} in family $\mathcal{G}_I^{(\text{pma})}$ with family CSD N/P_{max} .



The following sections are devoted to the development of two types of new orthogonal sequence families, namely degenerate PMA sequence families $\mathcal{G}_I^{(\text{dpma}, \kappa)}$, $\hat{\mathcal{G}}_I^{(\text{dpma}, \kappa)}$ and augmented PMA sequence families $\hat{\mathcal{G}}_I^{(\text{apma})}$, $\hat{\mathcal{G}}_I^{(\text{adpma}, \kappa)}$. For a composite length N , family $\mathcal{G}_I^{(\text{dpma}, \kappa)}$ contains orthogonal order- \tilde{I} CA sequences \mathcal{G}_I with the larger family size than family $\mathcal{G}_I^{(\text{pma})}$ by sacrificing the sidelobe-decaying order in some cases. When N meets $\tilde{\Omega}(N) > \Omega(N)$, family $\hat{\mathcal{G}}_I^{(\text{apma})}$ exhibits double the family size as family $\hat{\mathcal{G}}_I^{(\text{pma})}$ while maintaining the same sidelobe-decaying order. Moreover, degenerate PMA sequence family $\hat{\mathcal{G}}_I^{(\text{dpma}, \kappa)}$ and augmented degenerate PMA sequence family $\hat{\mathcal{G}}_I^{(\text{adpma}, \kappa)}$ are also developed from degenerating families $\hat{\mathcal{G}}_I^{(\text{pma})}$ and $\hat{\mathcal{G}}_I^{(\text{apma})}$, respectively, by trading off the sidelobe-decaying order. Table III and IV summarize the proposed modified PMA sequence families.

Table II

Some example sequences of length $N = 23$ with proper decomposition $N = 14 + 9$

under (a) *Condition A* and (b) *Condition B* with $\alpha\gamma = 1/2$. In the tables, ζ_l 's are

defined by $\zeta_l \triangleq \exp\{j\pi/l\}$.

(a) Sequences under *Condition A*

Sequence	Sequence Expression
\hat{g}_l	$\sqrt{\frac{1}{23}} [1, \zeta_7^2, \zeta_7^4, \zeta_7^6, \zeta_7^8, \zeta_7^{10}, \zeta_7^{12}, -1, \zeta_7^9, \zeta_7^{11}, \zeta_7^{13}, \zeta_7^3, \zeta_7^5, 1, \zeta_3^2, \zeta_3^4, \zeta_3^2, \zeta_3^4, 1, \zeta_3^4, 1, \zeta_3^2]$
\hat{j}_l	$\sqrt{\frac{1}{23}} [1, -1, \zeta_7^2, \zeta_7^9, \zeta_7^4, \zeta_7^{11}, \zeta_7^6, \zeta_7^{13}, \zeta_7^8, \zeta_7^3, \zeta_7^{10}, \zeta_7^5, \zeta_7^{12}, \zeta_7^5, 1, \zeta_3^2, \zeta_3^4, \zeta_3^2, \zeta_3^4, 1, \zeta_3^4, 1, \zeta_3^2]$

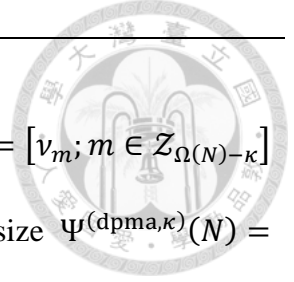
(b) Sequences under *Condition B*

Sequence	Sequence Expression
\hat{g}_l	$\sqrt{\frac{1}{23}} [1, \zeta_7^2, \zeta_7^4, \zeta_7^6, \zeta_7^8, \zeta_7^{10}, \zeta_7^{12}, 1, \zeta_7^2, \zeta_7^4, \zeta_7^6, \zeta_7^8, \zeta_7^{10}, \zeta_7^{12}, 1, \zeta_3^2, \zeta_3^4, \zeta_3^5, \zeta_3, -1, \zeta_3^4, 1, \zeta_3^2]$
\hat{j}_l	$\sqrt{\frac{1}{23}} [1, 1, \zeta_7^2, \zeta_7^2, \zeta_7^4, \zeta_7^4, \zeta_7^6, \zeta_7^6, \zeta_7^8, \zeta_7^8, \zeta_7^{10}, \zeta_7^{10}, \zeta_7^{12}, \zeta_7^{12}, 1, \zeta_3^5, \zeta_3^4, \zeta_3^2, \zeta_3, 1, \zeta_3^4, -1, \zeta_3^2]$

Table III

Families $\mathcal{G}_{\max, \tilde{I}}^{(\text{dpma}, \kappa)}$ and $\mathcal{J}_{\max, \tilde{I}}^{(\text{dpma}, \kappa)}$ under a proper level- $(\Omega(N) - \kappa)$ factorization $N = \prod_{m \in \mathcal{Z}_{\Omega(N) - \kappa}} A_m^{(\kappa)}$ for $\kappa \in \mathcal{Z}_{\Omega(N) - 1}^+$, and families $\tilde{\mathcal{G}}_{\max, \tilde{I}}^{(\text{dpma}, \kappa)}$ and $\tilde{\mathcal{J}}_{\max, \tilde{I}}^{(\text{dpma}, \kappa)}$ under a near-proper level- $(\Omega(N) - \kappa)$ factorization $N = \prod_{m \in \mathcal{Z}_{\Omega(N) - \kappa}} \tilde{A}_m^{(\kappa)}$ for $\kappa \in \mathcal{Z}_{\Omega(N) - 1}^+$ with $\Omega(N) > 2$.

Family	Description
$\mathcal{G}_{\max, \tilde{I}}^{(\text{dpma}, \kappa)}$	<ol style="list-style-type: none"> 1. Arrange factors in descending order $A_0^{(\kappa)} \geq A_1^{(\kappa)} \geq \dots \geq A_{\Omega(N) - \kappa - 1}^{(\kappa)}$. 2. An order-$\tilde{I}$ CA sequence $\mathcal{G}_{\tilde{I}}$ is defined as in (1)-(4) with $P_m \rightarrow A_m^{(\kappa)}$ for $m \in \mathcal{Z}_{\Omega(N) - \kappa}$, $\phi_m = \prod_{i \in \mathcal{Z}_m} A_i^{(\kappa)}$ for $m \in \mathcal{Z}_{\Omega(N) - \kappa - 1}^+$, and $\phi_0 = 1$. 3. Family $\mathcal{G}_{\max, \tilde{I}}^{(\text{dpma}, \kappa)}$ is constructed by varying $\mathbf{v} = [v_m; m \in \mathcal{Z}_{\Omega(N) - \kappa}]$ with $v_m \in \mathcal{Z}_{A_m^{(\kappa)} - 1}^+$ exclusively and has the family size $\Psi^{(\text{dpma}, \kappa)}(N) = \prod_{m \in \mathcal{Z}_{\Omega(N) - \kappa}} (A_m^{(\kappa)} - 1)$.
$\tilde{\mathcal{G}}_{\max, \tilde{I}}^{(\text{dpma}, \kappa)}$	<ol style="list-style-type: none"> 1. Arrange factors in descending order $\tilde{A}_0^{(\kappa)} \geq \tilde{A}_1^{(\kappa)} \geq \dots \geq \tilde{A}_{\Omega(N) - \kappa - 1}^{(\kappa)}$. 2. An order-$\tilde{I}$ CA sequence $\tilde{\mathcal{G}}_{\tilde{I}}$ is defined as in (1)-(4) with $P_m \rightarrow \tilde{A}_m^{(\kappa)}$ for $m \in \mathcal{Z}_{\Omega(N) - \kappa}$, $\phi_m = \prod_{i \in \mathcal{Z}_m} \tilde{A}_i^{(\kappa)}$ for $m \in \mathcal{Z}_{\Omega(N) - \kappa - 1}^+$, and $\phi_0 = 1$. 3. Family $\tilde{\mathcal{G}}_{\max, \tilde{I}}^{(\text{dpma}, \kappa)}$ is constructed by varying $\mathbf{v} = [v_m; m \in \mathcal{Z}_{\Omega(N) - \kappa}]$ with $v_m \in \mathcal{Z}_{\tilde{A}_m^{(\kappa)} - 1}^+$ exclusively and has the family size $\tilde{\Psi}^{(\text{dpma}, \kappa)}(N) = \prod_{m \in \mathcal{Z}_{\Omega(N) - \kappa}} (\tilde{A}_m^{(\kappa)} - 1)$.
$\mathcal{J}_{\max, \tilde{I}}^{(\text{dpma}, \kappa)}$	<ol style="list-style-type: none"> 1. Arrange factors in descending order $A_0^{(\kappa)} \leq A_1^{(\kappa)} \leq \dots \leq A_{\Omega(N) - \kappa - 1}^{(\kappa)}$. 2. An order-$\tilde{I}$ CA sequence $\mathcal{J}_{\tilde{I}}$ is defined as in (1)-(4) with $\phi_m \rightarrow \psi_m$ and $P_m \rightarrow A_m^{(\kappa)}$ for $m \in \mathcal{Z}_{\Omega(N) - \kappa}$, where $\psi_m = N / \phi_{m+1}$ for $m \in$



	<p>$\mathcal{Z}_{\Omega(N)-\kappa-1}$ and $\psi_{\Omega(N)-\kappa-1} = 1$.</p> <p>3. Family $\mathcal{J}_{\max, \tilde{I}}^{(\text{dpma}, \kappa)}$ is constructed by varying $\mathbf{v} = [v_m; m \in \mathcal{Z}_{\Omega(N)-\kappa}]$ with $v_m \in \mathcal{Z}_{A_m^{(\kappa)}-1}^+$ exclusively and has the family size $\Psi^{(\text{dpma}, \kappa)}(N) = \prod_{m \in \mathcal{Z}_{\Omega(N)-\kappa}} (A_m^{(\kappa)} - 1)$.</p>
$\tilde{\mathcal{J}}_{\max, \tilde{I}}^{(\text{dpma}, \kappa)}$	<p>1. Arrange factors in descending order $\tilde{A}_0^{(\kappa)} \leq \tilde{A}_1^{(\kappa)} \leq \dots \leq \tilde{A}_{\Omega(N)-\kappa-1}^{(\kappa)}$.</p> <p>2. An order-$\tilde{I}$ CA sequence $\tilde{\mathcal{J}}_{\tilde{I}}$ is defined as in (1)-(4) with $\phi_m \rightarrow \psi_m$ and $P_m \rightarrow \tilde{A}_m^{(\kappa)}$ for $m \in \mathcal{Z}_{\Omega(N)-\kappa}$, where $\psi_m = N/\phi_{m+1}$ for $m \in \mathcal{Z}_{\Omega(N)-\kappa-1}$ and $\psi_{\Omega(N)-\kappa-1} = 1$.</p> <p>3. Family $\tilde{\mathcal{J}}_{\max, \tilde{I}}^{(\text{dpma}, \kappa)}$ is constructed by varying $\mathbf{v} = [v_m; m \in \mathcal{Z}_{\Omega(N)-\kappa}]$ with $v_m \in \mathcal{Z}_{\tilde{A}_m^{(\kappa)}-1}^+$ exclusively and has the family size $\tilde{\Psi}^{(\text{dpma}, \kappa)}(N) = \prod_{m \in \mathcal{Z}_{\Omega(N)-\kappa}} (\tilde{A}_m^{(\kappa)} - 1)$.</p>

Table IV

Families $\hat{\mathcal{G}}_{\max, \tilde{I}}^{(\text{dpma}, \kappa)}$, $\hat{\mathcal{G}}_{\max, \tilde{I}}^{(\text{adpma}, \kappa)}$, $\hat{\mathcal{J}}_{\max, \tilde{I}}^{(\text{dpma}, \kappa)}$, and $\hat{\mathcal{J}}_{\max, \tilde{I}}^{(\text{adpma}, \kappa)}$ for $\kappa \in \mathcal{Z}_{\tilde{\Omega}(N)-1}^+$ under a proper decomposition $N = \sum_{\rho \in \mathcal{Z}_L} \tilde{N}^{(\rho)}$ and individual proper level- $(\Omega(\tilde{N}^{(\rho)}) - \kappa)$ factorizations $\tilde{N}^{(\rho)} = \prod_{m \in \mathcal{Z}_{\tilde{\Omega}(N)-\kappa}} A_m^{(\rho, \kappa)}$ for all $\rho \in \mathcal{Z}_L$, provided that $\tilde{\Omega}(N) > \Omega(N)$.

For $\hat{\mathcal{G}}_{\max, \tilde{I}}^{(\text{adpma}, \kappa)}$ and $\hat{\mathcal{J}}_{\max, \tilde{I}}^{(\text{adpma}, \kappa)}$, the decomposition $N = \sum_{\rho \in \mathcal{Z}_L} \tilde{N}^{(\rho)}$ has to meet

Restriction A.

Family	Description
$\hat{\mathcal{G}}_{\max, \tilde{I}}^{(\text{dpma}, \kappa)}$	<ol style="list-style-type: none"> 1. Arrange factors in descending order $A_0^{(\rho, \kappa)} \geq A_1^{(\rho, \kappa)} \geq \dots \geq A_{\Omega(N)-\kappa-1}^{(\rho, \kappa)}$ for all $\rho \in \mathcal{Z}_L$. 2. An order-\tilde{I} CA sequence $\hat{\mathcal{G}}_{\tilde{I}}$ is described as $\boldsymbol{\chi} = [\boldsymbol{\chi}_0^t, \boldsymbol{\chi}_1^t, \dots, \boldsymbol{\chi}_{L-1}^t]^t$. 3. Subsequences $\boldsymbol{\chi}_\rho$ for all $\rho \in \mathcal{Z}_L$ are constructed in (1)-(4) with $\phi_m \rightarrow \phi_m^{(\rho)}$ and $P_m \rightarrow A_m^{(\rho, \kappa)}$ for $m \in \mathcal{Z}_{\tilde{\Omega}(N)-\kappa}$, where $\phi_m^{(\rho)} = \prod_{i \in \mathcal{Z}_m} A_i^{(\rho, \kappa)}$ for $m \in \mathcal{Z}_{\Omega(\tilde{N}^{(\rho)})-\kappa-1}^+$ and $\phi_0^{(\rho)} = 1$. 4. Family $\hat{\mathcal{G}}_{\max, \tilde{I}}^{(\text{dpma}, \kappa)}$ is constructed by varying $\mathbf{v}^{(\rho)} = [v_m^{(\rho)}; m \in \mathcal{Z}_{\Omega(\tilde{N}^{(\rho)})-\kappa}]$ with $v_m^{(\rho)} \in \mathcal{Z}_{A_m^{(\rho, \kappa)}-1}^+$ for all $\rho \in \mathcal{Z}_L$ exclusively and has the family size $\hat{\Psi}^{(\text{dpma}, \kappa)}(N) = \min_{\rho \in \mathcal{Z}_L} \prod_{m=0}^{\Omega(\tilde{N}^{(\rho)})-\kappa-1} (A_m^{(\rho, \kappa)} - 1)$.
$\hat{\mathcal{G}}_{\max, \tilde{I}}^{(\text{adpma}, \kappa)}$	<ol style="list-style-type: none"> 1. Family $\hat{\mathcal{G}}_{\max, \tilde{I}}^{(\text{adpma}, \kappa)}$ contains all orthogonal order-\tilde{I} CA sequences in family $\hat{\mathcal{G}}_{\max, \tilde{I}}^{(\text{dpma}, \kappa)}$ and their phase-rotated sequences. 2. From an order-\tilde{I} CA sequence $\hat{\mathcal{G}}_{\tilde{I}}$ in family $\hat{\mathcal{G}}_{\max, \tilde{I}}^{(\text{dpma}, \kappa)}$, one extra order-$\tilde{I}$ CA sequence is augmented by rotating the phases of the subsequences $\boldsymbol{\chi}_\rho$ and described by $\boldsymbol{\chi}^\theta = [e^{j\theta_0} \boldsymbol{\chi}_0^t, e^{j\theta_1} \boldsymbol{\chi}_1^t, \dots, e^{j\theta_{L-1}} \boldsymbol{\chi}_{L-1}^t]^t$.

	<p>3. A proper phase vector $\boldsymbol{\theta} = [\theta_\rho; \rho \in \mathcal{Z}_L]$ is obtained by invoking the procedure in Subsection IV.B.1.</p>
$\hat{\mathcal{J}}_{\max, \tilde{I}}^{(\text{dpma}, \kappa)}$	<ol style="list-style-type: none"> 1. Arrange factors in descending order $A_0^{(\rho, \kappa)} \leq A_1^{(\rho, \kappa)} \leq \dots \leq A_{\Omega(N) - \kappa - 1}^{(\rho, \kappa)}$ for all $\rho \in \mathcal{Z}_L$. 2. An order-\tilde{I} CA sequence $\hat{\mathcal{J}}_{\tilde{I}}$ is described as $\boldsymbol{\chi} = [\boldsymbol{\chi}_0^t, \boldsymbol{\chi}_1^t, \dots, \boldsymbol{\chi}_{L-1}^t]^t$. 3. Subsequences $\boldsymbol{\chi}_\rho$ for all $\rho \in \mathcal{Z}_L$ are constructed in (1)-(4) with $\phi_m \rightarrow \psi_m^{(\rho)}$ and $P_m \rightarrow A_m^{(\rho, \kappa)}$ for $m \in \mathcal{Z}_{\tilde{\Omega}(N) - \kappa}^+$, where $\psi_m^{(\rho)} = N / \phi_{m+1}^{(\rho)}$ for $m \in \mathcal{Z}_{\Omega(\tilde{N}(\rho)) - \kappa - 1}^+$ and $\psi_{\Omega(\tilde{N}(\rho)) - \kappa - 1}^{(\rho)} = 1$. 4. Family $\hat{\mathcal{J}}_{\max, \tilde{I}}^{(\text{dpma}, \kappa)}$ is constructed by varying $\mathbf{v}^{(\rho)} = [v_m^{(\rho)}; m \in \mathcal{Z}_{\Omega(\tilde{N}(\rho)) - \kappa}]$ with $v_m^{(\rho)} \in \mathcal{Z}_{A_m^{(\rho, \kappa)} - 1}^+$ for all $\rho \in \mathcal{Z}_L$ exclusively and has the family size $\hat{\Psi}^{(\text{dpma}, \kappa)}(N) = \min_{\rho \in \mathcal{Z}_L} \prod_{m=0}^{\Omega(\tilde{N}(\rho)) - \kappa - 1} (A_m^{(\rho, \kappa)} - 1)$.
$\hat{\mathcal{J}}_{\max, \tilde{I}}^{(\text{adpma}, \kappa)}$	<ol style="list-style-type: none"> 1. Family $\hat{\mathcal{J}}_{\max, \tilde{I}}^{(\text{adpma}, \kappa)}$ contains all orthogonal order-\tilde{I} CA sequences in family $\hat{\mathcal{J}}_{\max, \tilde{I}}^{(\text{dpma}, \kappa)}$ and their phase-rotated sequences. 2. From an order-\tilde{I} CA sequence $\hat{\mathcal{J}}_{\tilde{I}}$ in family $\hat{\mathcal{J}}_{\max, \tilde{I}}^{(\text{dpma}, \kappa)}$, one extra order-$\tilde{I}$ CA sequence is augmented by rotating the phases of the subsequences $\boldsymbol{\chi}_\rho$ and described by $\boldsymbol{\chi}^\theta = [e^{j\theta_0} \boldsymbol{\chi}_0^t, e^{j\theta_1} \boldsymbol{\chi}_1^t, \dots, e^{j\theta_{L-1}} \boldsymbol{\chi}_{L-1}^t]^t$. 3. A proper phase vector $\boldsymbol{\theta} = [\theta_\rho; \rho \in \mathcal{Z}_L]$ is obtained by invoking the procedure in Subsection IV.B.1.

Table V

The closed-form expressions for proper level- $(\Omega(N) - \kappa)$ factorizations with $\kappa = 1$ and $\kappa = 2$, as well as near-proper level- $(\Omega(N) - \kappa)$ factorizations with $\kappa \in \mathcal{Z}_{\Omega(N)-2}^+ - \mathcal{Z}_2^+$. For $\kappa \in \mathcal{Z}_2^+$, $\{\tilde{A}_m^{(\kappa)}; m \in \mathcal{Z}_{\Omega(N)-\kappa}\}$ is initially assigned by $\tilde{A}_m^{(\kappa)} = A_m^{(\kappa)}$ with the arranged order $1 < A_0^{(\kappa)} \leq A_1^{(\kappa)} \leq \dots \leq A_{\Omega(N)-\kappa-1}^{(\kappa)}$.

Level- $(\Omega(N) - \kappa)$ Factorization	Factor Assignment From $\{P_m; m \in \mathcal{Z}_{\Omega(N)}\}$ With $P_0 \leq P_1 \leq \dots \leq P_{\Omega(N)-1}$
Proper Factorization $(\kappa = 1, \Omega(N) > 2)$ [43]	$A_0^{(1)} = P_0 P_1$ and $A_m^{(1)} = P_{m+1}$ for $m \in \mathcal{Z}_{\Omega(N)-2}^+$
Proper Factorization $(\kappa = 2, \Omega(N) > 3)$ [43]	$A_0^{(2)} = P_0 P_1 P_2$ $A_m^{(2)} = P_{m+2}$ for $m \in \mathcal{Z}_{\Omega(N)-3}^+$, if $P_1 P_2 < P_3$ $A_0^{(2)} = P_0 P_3$, $A_1^{(2)} = P_1 P_2$ and $A_{m+1}^{(2)} = P_{m+3}$ for $m \in \mathcal{Z}_{\Omega(N)-4}^+$, otherwise
Near-Proper Factorization $(\kappa \in \mathcal{Z}_{\Omega(N)-2}^+ - \mathcal{Z}_2^+, \Omega(N) > 4)$	$\tilde{A}_0^{(\kappa)} = \tilde{A}_0^{(\kappa-2)} \tilde{A}_1^{(\kappa-2)} \tilde{A}_2^{(\kappa-2)}$ and $\tilde{A}_m^{(\kappa)} = \tilde{A}_{m+2}^{(\kappa-2)}$ for $m \in \mathcal{Z}_{\Omega(N)-\kappa-1}^+$, if $\tilde{A}_1^{(\kappa-2)} \tilde{A}_2^{(\kappa-2)} < \tilde{A}_3^{(\kappa-2)}$ $\tilde{A}_0^{(\kappa)} = \tilde{A}_0^{(\kappa-2)} \tilde{A}_3^{(\kappa-2)}$, $\tilde{A}_1^{(\kappa)} = \tilde{A}_1^{(\kappa-2)} \tilde{A}_2^{(\kappa-2)}$, and $\tilde{A}_{m+1}^{(\kappa)} = \tilde{A}_{m+3}^{(\kappa-2)}$ for $m \in \mathcal{Z}_{\Omega(N)-\kappa-2}^+$, otherwise

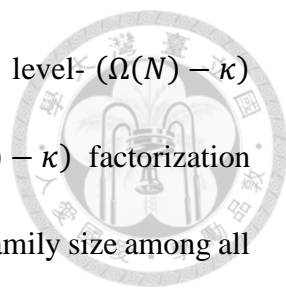
Chapter 3



Families $\mathcal{G}_{\max, \tilde{I}}^{(\text{dpma}, \kappa)}$ and $\tilde{\mathcal{G}}_{\max, \tilde{I}}^{(\text{dpma}, \kappa)}$

Consider a composite length N with the prime factorization $N = \prod_{m=0}^{\Omega(N)-1} P_m$ and $\Omega(N) > 2$. With a given $\kappa \in \mathcal{Z}_{\Omega(N)-1}^+$, many families $\mathcal{G}_{\tilde{I}}^{(\text{dpma}, \kappa)}$ can be degenerated from family $\mathcal{G}_{\tilde{I}}^{(\text{pma})}$ with identical or less sidelobe-decaying order. Based on a particular level- $(\Omega(N) - \kappa)$ factorization $N = \prod_{m=0}^{\Omega(N)-\kappa-1} A_m$ where factors A_m may not be all primes and are arranged in descending order, a family $\mathcal{G}_{\tilde{I}}^{(\text{dpma}, \kappa)}$ can be constructed by the same PMA method constructing family $\mathcal{G}_{\tilde{I}}^{(\text{pma})}$. Specifically, such family $\mathcal{G}_{\tilde{I}}^{(\text{dpma}, \kappa)}$ contains $\prod_{m=0}^{\Omega(N)-\kappa-1} (A_m - 1)$ orthogonal order- \tilde{I} CA sequences $\mathcal{G}_{\tilde{I}}$ by varying the index vector $\mathbf{v} = [v_m; m \in \mathcal{Z}_{\Omega(N)-\kappa}]$ exclusively with $v_m \in \mathcal{Z}_{A_m-1}^+$ for all $m \in \mathcal{Z}_{\Omega(N)-\kappa}$, and exhibits the sidelobe-decaying order $\tilde{I} \geq \Omega(N) - \kappa$ under *Condition A* and $\tilde{I} \geq \lfloor (\Omega(N) - \kappa)/2 \rfloor$ under *Condition B*. As $\Omega(N)$ is odd, any family $\mathcal{G}_{\tilde{I}}^{(\text{dpma}, 1)}$ based on any level- $(\Omega(N) - 1)$ factorization yields the sidelobe-decaying order $\tilde{I} \geq \lfloor \Omega(N)/2 \rfloor$ under *Condition B*, which may exhibit the same sidelobe-decaying as family $\mathcal{G}_{\tilde{I}}^{(\text{pma})}$ based on the prime factorization.

For a fixed $\kappa \in \mathcal{Z}_{\Omega(N)-2}^+$, the family sizes for different families $\mathcal{G}_{\tilde{I}}^{(\text{dpma}, \kappa)}$ are not necessarily identical, depending on corresponding level- $(\Omega(N) - \kappa)$ factorizations. Besides, more orthogonal PMA sequences can be obtained by using a larger κ in $\mathcal{Z}_{\Omega(N)-1}^+$ in that $A_m A_n - 1$ is strictly larger than $(A_m - 1)(A_n - 1)$ for any two integer factors with $A_m, A_n > 1$. The largest family size $\Psi_{\max}(N) = N - 1$ under *Condition A* is exactly achieved by the only family $\mathcal{G}_{\tilde{I}}^{(\text{dpma}, \Omega(N)-1)}$ based on the level-1



factorization $N = A_0$. For a fixed $\kappa \in \mathcal{Z}_{\Omega(N)-2}^+$, a particular level- $(\Omega(N) - \kappa)$ factorization $N = \prod_{m=0}^{\Omega(N)-\kappa-1} A_m^{(\kappa)}$ is said to be a *proper* level- $(\Omega(N) - \kappa)$ factorization if $\Psi^{(\text{dpma},\kappa)}(N) \triangleq \prod_{m=0}^{\Omega(N)-\kappa-1} (A_m^{(\kappa)} - 1)$ is the achievable largest family size among all possible families $\mathcal{G}_I^{(\text{dpma},\kappa)}$. Such proper level- $(\Omega(N) - \kappa)$ factorization may not be unique. Under a proper factorization, the corresponding family $\mathcal{G}_I^{(\text{dpma},\kappa)}$ is dubbed $\mathcal{G}_{\max,I}^{(\text{dpma},\kappa)}$ for notational convenience. Family $\mathcal{G}_{\max,I}^{(\text{dpma},\kappa)}$ consists of $\Psi^{(\text{dpma},\kappa)}(N) / (A_{\max}^{(\kappa)} - 1)$ mutually exclusive CS sequence subfamilies $\mathcal{G}_{\max,I}^{(\text{cs},\kappa)}(\mathbf{q}_{\text{lead}})$ for all permissible subfamily leaders \mathbf{q}_{lead} , where $A_{\max}^{(\kappa)} \triangleq \max_{m \in \mathcal{Z}_{\Omega(N)-\kappa}} A_m^{(\kappa)}$. Each subfamily $\mathcal{G}_{\max,I}^{(\text{cs},\kappa)}(\mathbf{q}_{\text{lead}})$ contains $A_{\max}^{(\kappa)} - 1$ sequences generated by cyclically shifting the inverse DFT of a subfamily leader \mathbf{q}_{lead} in family $\mathcal{G}_{\max,I}^{(\text{dpma},\kappa)}$ with family CSD $\omega_{\mathcal{G}}^{(\kappa)} \triangleq N/A_{\max}^{(\kappa)}$. Below, proper level- $(\Omega(N) - \kappa)$ factorizations with $\kappa = 1$ and $\kappa = 2$ are first developed in closed-form expressions. An exclusive search procedure is then proposed to find proper level- $(\Omega(N) - \kappa)$ factorizations with all $\kappa \in \mathcal{Z}_{\Omega(N)-2}^+$. Last, for sequence lengths N with $\Omega(N) > 4$, near-proper level- $(\Omega(N) - \kappa)$ factorizations $N = \prod_{m=0}^{\Omega(N)-\kappa-1} \tilde{A}_m^{(\kappa)}$ for all $\kappa \in \mathcal{Z}_{\Omega(N)-2}^+ - \mathcal{Z}_2^+$ are presented in closed-form expressions to construct another degenerate PMA sequence family $\tilde{\mathcal{G}}_{\max,I}^{(\text{dpma},\kappa)}$, which also gives a larger family size than $\mathcal{G}_I^{(\text{pma})}$.

For presentation convenience, prime factors in $N = \prod_{m=0}^{\Omega(N)-1} P_m$ are arranged below in ascending order $P_0 \leq P_1 \leq \dots \leq P_{\Omega(N)-1}$ for the development of proper and near-proper level- $(\Omega(N) - \kappa)$ factorizations and the developed factors in $N = \prod_{m=0}^{\Omega(N)-\kappa-1} A_m^{(\kappa)}$ and $N = \prod_{m=0}^{\Omega(N)-\kappa-1} \tilde{A}_m^{(\kappa)}$ are not arranged in any order. Notably, to

construct order- \tilde{I} CA sequences in families $\mathcal{G}_{\max, \tilde{I}}^{(\text{dpma}, \kappa)}$ and $\tilde{\mathcal{G}}_{\max, \tilde{I}}^{(\text{dpma}, \kappa)}$, the developed factors have to be rearranged beforehand in descending order, i.e., $A_0^{(\kappa)} \geq A_1^{(\kappa)} \geq \dots \geq A_{\Omega(N)-\kappa-1}^{(\kappa)}$ and $\tilde{A}_0^{(\kappa)} \geq \tilde{A}_1^{(\kappa)} \geq \dots \geq \tilde{A}_{\Omega(N)-\kappa-1}^{(\kappa)}$. Table V summarizes the developed closed-form expressions for proper level- $(\Omega(N) - \kappa)$ factorizations with $\kappa = 1$ and $\kappa = 2$ as well as near-proper level- $(\Omega(N) - \kappa)$ factorizations for all $\kappa \in \mathcal{Z}_{\Omega(N)-2}^+ - \mathcal{Z}_2^+$.

3.1 Proper Level- $(\Omega(N) - 1)$ Factorization for $\Omega(N) > 2$:

The proper level- $(\Omega(N) - 1)$ factorization was proposed by [43]. With $N = \prod_{m=0}^{\Omega(N)-1} P_m$ and $\Omega(N) > 2$, N can be factorized into $\Omega(N) - 1$ factors only when two specific prime factors P_i and P_n are chosen from $\{P_m; m \in \mathcal{Z}_{\Omega(N)}\}$ and merged into one composite factor $P_i P_n$. Under such factorization, one family $\mathcal{G}_i^{(\text{dpma}, 1)}$ can be formed with the family size $\Psi(N) \times f([P_i, P_n])$, where the function $f(\mathbf{a}^t)$ is defined by

$$f(\mathbf{a}^t) = \frac{\prod_{m \in \mathcal{Z}_M} a_m - 1}{\prod_{m \in \mathcal{Z}_M} (a_m - 1)} \quad (11)$$

with $\mathbf{a} = [a_m; m \in \mathcal{Z}_M]$ being an M -tuple argument with all integer-valued entries $a_m > 1$. This family size can be maximized by choosing P_i and P_n properly based on *Lemma 1*, which is proven in [43].

Lemma 1 : Consider two integer-valued M -tuples $\mathbf{a} = [a_m; m \in \mathcal{Z}_M]$ and $\mathbf{b} = [b_m; m \in \mathcal{Z}_M]$. If $1 < a_m \leq b_m$ for all $m \in \mathcal{Z}_M$, then $f(\mathbf{a}^t) \geq f(\mathbf{b}^t)$. Moreover, $f(\mathbf{a}^t) > f(\mathbf{b}^t)$ if $1 < a_n < b_n$ for some $m \in \mathcal{Z}_M$ and $1 < a_m \leq b_m$ for all the other $m \in \mathcal{Z}_M - \{n\}$.

From *Lemma 1*, the smallest two prime factors should be merged to compose a proper level- $(\Omega(N) - 1)$ factorization $N = \prod_{m=0}^{\Omega(N)-2} A_m^{(1)}$ with $A_0^{(1)} = P_0 P_1$ and

$A_m^{(1)} = P_{m+1}$ for $m \in \mathcal{Z}_{\Omega(N)-2}^+$. This proper factorization results in the largest family size $\Psi^{(\text{dpma},1)}(N) = (P_0 P_1 - 1) \prod_{m=2}^{\Omega(N)-1} (P_m - 1)$. The corresponding family $\mathcal{G}_{\max, \tilde{I}}^{(\text{dpma},1)}$ can provide mutually orthogonal order- \tilde{I} CA sequences with $\tilde{I} \geq \Omega(N) - 1$ under *Condition A* and $\tilde{I} \geq \lfloor (\Omega(N) - 1)/2 \rfloor$ under *Condition B*.

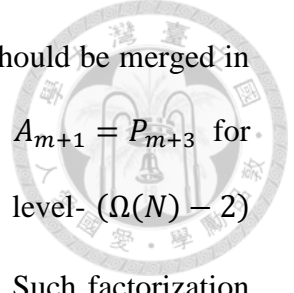
3.2 Proper Level- $(\Omega(N) - 2)$ Factorization for $\Omega(N) > 3$:

The proper level- $(\Omega(N) - 2)$ factorization was proposed by [43]. With $N = \prod_{m=0}^{\Omega(N)-1} P_m$ and $\Omega(N) > 3$, there are two mutually exclusive methods to factorize $N = \prod_{m=0}^{\Omega(N)-3} A_m$ in order to obtain a level- $(\Omega(N) - 2)$ factorization. *Method 1* is to choose any three prime factors from $\{P_m; m \in \mathcal{Z}_{\Omega(N)}\}$ and merge them into one composite factor. *Method 2* is to choose any four prime factors from $\{P_m; m \in \mathcal{Z}_{\Omega(N)}\}$ and merge them into two composite factors in pairs. Both methods are detailed below.

Method 1: From *Lemma 1*, the smallest three prime factors should be merged in order to maximize the family size when a level- $(\Omega(N) - 2)$ factorization is obtained by merging three prime factors. This results in the family size $(P_0 P_1 P_2 - 1) \prod_{m=3}^{\Omega(N)-1} (P_m - 1)$. Thus, one candidate family for $\mathcal{G}_{\max, \tilde{I}}^{(\text{dpma},2)}$ is based on the candidate factorization $A_0 = P_0 P_1 P_2$ and $A_m = P_{m+2}$ for $m \in \mathcal{Z}_{\Omega(N)-3}^+$.

Method 2: When a level- $(\Omega(N) - 2)$ factorization is obtained by merging four prime factors in pairs, the family size can be maximized by choosing and pairing four prime factors properly based on *Lemma 2*, as proven in [43].

Lemma 2: Consider four integers $P_a, P_b, P_c,$ and P_d . If $1 < P_a \leq P_b \leq P_c \leq P_d$, then $f([P_a, P_d]) \times f([P_b, P_c]) \geq f([P_a, P_c]) \times f([P_b, P_d]) \geq f([P_a, P_b]) \times f([P_c, P_d])$.



From *Lemma 1* and *Lemma 2*, the smallest four prime factors should be merged in pairs to form the candidate factorization $A_0 = P_0P_3$, $A_1 = P_1P_2$ and $A_{m+1} = P_{m+3}$ for $m \in \mathcal{Z}_{\Omega(N)-4}^+$, in order to maximize the family size when a level- $(\Omega(N) - 2)$ factorization is obtained by merging four prime factors in pairs. Such factorization results in the other candidate family for $\mathcal{G}_{\max, \tilde{I}}^{(\text{dpma}, 2)}$ having the family size $(P_0P_3 - 1)(P_1P_2 - 1) \prod_{m=4}^{\Omega(N)-1} (P_m - 1)$.

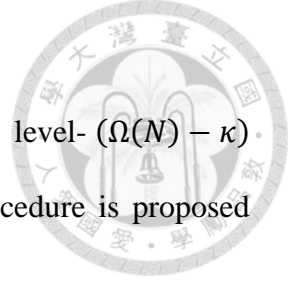
Exclusively, *Method 1* and *Method 2* give two candidate level- $(\Omega(N) - 2)$ factorizations offering the family sizes $\Psi(N) \times f([P_0, P_1, P_2])$ and $\Psi(N) \times f([P_0, P_3]) \times f([P_1, P_2])$, respectively. The factorization that yields the largest family size is thus a proper level- $(\Omega(N) - 2)$ factorization and can be adopted to construct family $\mathcal{G}_{\max, \tilde{I}}^{(\text{dpma}, 2)}$. *Lemma 3* is proven in [43] to support such proper factorization.

Lemma 3: Consider four integers P_a , P_b , P_c , and P_d with $1 < P_a \leq P_b \leq P_c \leq P_d$. If $P_bP_c \leq P_d$, then $f([P_a, P_b, P_c]) \geq f([P_a, P_d]) \times f([P_b, P_c])$.

From *Lemma 3*, a proper level- $(\Omega(N) - 2)$ factorization for $N = \prod_{m=0}^{\Omega(N)-3} A_m^{(2)}$ is obtained by setting $A_0^{(2)} = P_0P_1P_2$ and $A_m^{(2)} = P_{m+2}$ for $m \in \mathcal{Z}_{\Omega(N)-3}^+$ (i.e., *Method 1*) if $P_1P_2 < P_3$, and by setting $A_0^{(2)} = P_0P_3$, $A_1^{(2)} = P_1P_2$ and $A_{m+1}^{(2)} = P_{m+3}$ for $m \in \mathcal{Z}_{\Omega(N)-4}^+$ (i.e., *Method 2*) otherwise. This proper factorization results in the largest family

size $\Psi^{(\text{dpma}, 2)}(N) = \max\left\{(P_0P_1P_2 - 1) \prod_{m=3}^{\Omega(N)-1} (P_m - 1), (P_0P_3 - 1)(P_1P_2 - 1) \prod_{m=4}^{\Omega(N)-1} (P_m - 1)\right\}$. Based on the proper level- $(\Omega(N) - 2)$ factorization, family

$\mathcal{G}_{\max, \tilde{I}}^{(\text{dpma}, 2)}$ is constructed by the PMA method and provides mutually orthogonal order- \tilde{I} CA sequences with $\tilde{I} \geq \Omega(N) - 2$ under *Condition A* and $\tilde{I} \geq \lfloor (\Omega(N) - 2)/2 \rfloor$ under *Condition B*.



3.3 Exclusively Search a Proper Level- $(\Omega(N) - \kappa)$ Factorization

For $\kappa \in \{3, 4, \dots, \Omega(N) - 2\}$, it is difficult to find proper level- $(\Omega(N) - \kappa)$ factorizations in closed-form expressions. An exclusive search procedure is proposed instead to find such proper factorizations.

To obtain a proper level- $(\Omega(N) - \kappa)$ factorization, we need to (i) find all possible factor sets $\{A_m; m \in \mathcal{Z}_{\Omega(N)-\kappa}\}$ satisfying $\prod_{m=0}^{\Omega(N)-\kappa-1} A_m = \prod_{m=0}^{\Omega(N)-1} P_m$ by partitioning the prime factor set $\{P_m; m \in \mathcal{Z}_{\Omega(N)}\}$ into $\Omega(N) - \kappa$ groups first and then taking all group products in the exclusive manner, and (ii) search for a proper factor set $\{A_m^{(\kappa)}; m \in \mathcal{Z}_{\Omega(N)-\kappa}\}$ which yields the largest family size $\Psi^{(\text{dpma}, \kappa)}(N) = \prod_{m=0}^{\Omega(N)-\kappa-1} (A_m^{(\kappa)} - 1)$ among all factor sets. In each partitioning, we denote ω_m as the number of prime factors in the m -th group, i.e., $\omega_m = \Omega(A_m)$ for $m \in \mathcal{Z}_{\Omega(N)-\kappa}$. Thus, each factor set $\{A_m; m \in \mathcal{Z}_{\Omega(N)-\kappa}\}$ is characterized by the corresponding omega pattern $\boldsymbol{\omega} \triangleq [\omega_m; m \in \mathcal{Z}_{\Omega(N)-\kappa}]$ with $\sum_{m=0}^{\Omega(N)-\kappa-1} \omega_m = \Omega(N)$. The exclusive partitioning can be conducted by searching for all possible omega patterns first and then finding all possible groupings for each pattern $\boldsymbol{\omega}$. To avoid repetitive search, $\boldsymbol{\omega}$ is limited to have descending entries $\omega_0 \geq \omega_1 \geq \dots \geq \omega_{\Omega(N)-\kappa-1}$ in the exclusive partitioning. In the following, an exclusive search procedure is proposed accordingly to find a proper level- $(\Omega(N) - \kappa)$ factorization.

Step 1: Obtain and store all admissible patterns for $\boldsymbol{\omega}$ under the constraints $\sum_{m=0}^{\Omega(N)-\kappa-1} \omega_m = \Omega(N)$ and $\omega_0 \geq \omega_1 \geq \dots \geq \omega_{\Omega(N)-\kappa-1} \geq 1$ by the process of integer partitioning in [36, Section 1.1]-[37].

Step 2: Transform the prime factor set $\{P_m; m \in \mathcal{Z}_{\Omega(N)}\}$ into all possible factor sets $\{A_m; m \in \mathcal{Z}_{\Omega(N)-\kappa}\}$ characterized by each admissible pattern $\boldsymbol{\omega}$ exclusively from

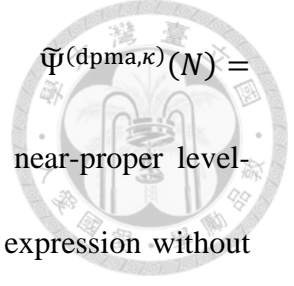
Gosper's Hack algorithm [38, Section 7.1.3]-[39]. Compute family sizes $\prod_{m=0}^{\Omega(N)-\kappa-1} (A_m - 1)$ for all sought factor sets $\{A_m; m \in \mathcal{Z}_{\Omega(N)-\kappa}\}$. Store one candidate factor set which provides the largest family size among all sought factor sets characterized by each admissible pattern ω .

Step 3: Find a proper level- $(\Omega(N) - \kappa)$ factor set $\{A_m^{(\kappa)}; m \in \mathcal{Z}_{\Omega(N)-\kappa}\}$ by choosing one candidate factor set which yields the largest family size $\Psi^{(\text{dpma}, \kappa)}(N) = \prod_{m=0}^{\Omega(N)-\kappa-1} (A_m^{(\kappa)} - 1)$ among all stored factor sets in *Step 2*.

In *Step 1*, the process of integer partitioning in [36, Section 1.1]-[37] finds all possible patterns for ω by dividing the all one $\Omega(N)$ -tuple $[1, 1, \dots, 1]^t$ into the admissible $(\Omega(N) - \kappa)$ -tuple ω in the exclusive manner. For example, the process finds $[3, 1, 1]^t$ and $[2, 2, 1]^t$ by dividing $[1, 1, 1, 1, 1]^t$ into $[\omega_0, \omega_1, \omega_2]^t$ for $\Omega(N) = 5$ and $\kappa = 2$. In *Step 2*, Gosper's Hack algorithm transforms an omega pattern to all possible binary codewords without repetition in the bitwise manner [39, Algorithm 3.1], as detailed in *Appendix A*. In *Step 3*, a proper level- $(\Omega(N) - \kappa)$ factor set $\{A_m^{(\kappa)}; m \in \mathcal{Z}_{\Omega(N)-\kappa}\}$ is found from all stored candidate factor sets stored in *Step 2* by identifying the largest family size. This completes the exclusive search procedure.

3.4 Near-Proper Level- $(\Omega(N) - \kappa)$ Factorization for $\Omega(N) > 4$ and $\kappa \in \{3, 4, \dots, \Omega(N) - 2\}$

A *near-proper* level- $(\Omega(N) - \kappa)$ factorization $\prod_{m=0}^{\Omega(N)-\kappa-1} \tilde{A}_m^{(\kappa)}$ with $\tilde{A}_0^{(\kappa)} \leq \tilde{A}_1^{(\kappa)} \leq \dots \leq \tilde{A}_{\Omega(N)-\kappa-1}^{(\kappa)}$ for all $\kappa \in \mathcal{Z}_{\Omega(N)-2}^+ - \mathcal{Z}_2^+$ is proposed here to construct another degenerate PMA sequence family $\tilde{\mathcal{G}}_{\max, l}^{(\text{dpma}, \kappa)}$ based on the construction method of *Proper Level- $(\Omega(N) - 2)$ Factorization* in Subsection III.B. Under such near-proper



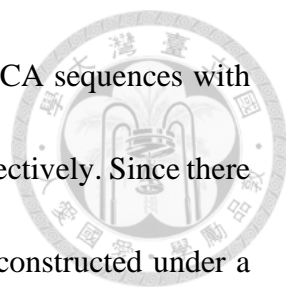
factorization, family $\tilde{\mathcal{G}}_{\max, \tilde{I}}^{(\text{dpma}, \kappa)}$ exhibits the family size $\tilde{\Psi}^{(\text{dpma}, \kappa)}(N) = \prod_{m=0}^{\Omega(N)-\kappa-1} (\tilde{A}_m^{(\kappa)} - 1)$. Despite $\tilde{\Psi}^{(\text{dpma}, \kappa)}(N) \leq \Psi^{(\text{dpma}, \kappa)}(N)$, the near-proper level- $(\Omega(N) - \kappa)$ factorization can be obtained simply in a closed-form expression without resort to exclusive searching.

Following Subsection III.B, a *near-proper* level- $(\Omega(N) - \kappa)$ factorization for $N = \prod_{m=0}^{\Omega(N)-\kappa-1} \tilde{A}_m^{(\kappa)}$ is obtained from a given level- $(\Omega(N) - \kappa + 2)$ factorization $N = \prod_{m=0}^{\Omega(N)-\kappa+1} \tilde{A}_m^{(\kappa-2)}$ with the arranged order $\tilde{A}_0^{(\kappa-2)} \leq \tilde{A}_1^{(\kappa-2)} \leq \dots \leq \tilde{A}_{\Omega(N)-\kappa+1}^{(\kappa-2)}$. Specifically, a near-proper level- $(\Omega(N) - \kappa)$ factorization for $N = \prod_{m=0}^{\Omega(N)-\kappa-1} \tilde{A}_m^{(\kappa)}$ is obtained by setting $\tilde{A}_0^{(\kappa)} = \tilde{A}_0^{(\kappa-2)} \tilde{A}_1^{(\kappa-2)} \tilde{A}_2^{(\kappa-2)}$ and $\tilde{A}_m^{(\kappa)} = \tilde{A}_{m+2}^{(\kappa-2)}$ for $m \in \mathcal{Z}_{\Omega(N)-\kappa-1}^+$ if $\tilde{A}_1^{(\kappa-2)} \tilde{A}_2^{(\kappa-2)} < \tilde{A}_3^{(\kappa-2)}$, and by setting $\tilde{A}_0^{(\kappa)} = \tilde{A}_0^{(\kappa-2)} \tilde{A}_3^{(\kappa-2)}$, $\tilde{A}_1^{(\kappa)} = \tilde{A}_1^{(\kappa-2)} \tilde{A}_2^{(\kappa-2)}$ and $\tilde{A}_{m+1}^{(\kappa)} = \tilde{A}_{m+3}^{(\kappa-2)}$ for $m \in \mathcal{Z}_{\Omega(N)-\kappa-2}^+$ otherwise. For $\kappa \in \mathcal{Z}_2^+$, $\{\tilde{A}_m^{(\kappa)}; m \in \mathcal{Z}_{\Omega(N)-\kappa}\}$ is initially assigned by $\tilde{A}_m^{(\kappa)} = A_m^{(\kappa)}$ where $N = \prod_{m=0}^{\Omega(N)-\kappa-1} A_m^{(\kappa)}$ is a proper level- $(\Omega(N) - \kappa)$ factorization with the arranged order $A_0^{(\kappa)} \leq A_1^{(\kappa)} \leq \dots \leq A_{\Omega(N)-\kappa-1}^{(\kappa)}$.

Notably, families $\tilde{\mathcal{G}}_{\max, \tilde{I}}^{(\text{dpma}, \kappa)}$ contain $\tilde{\Psi}^{(\text{dpma}, \kappa)}(N) / (\tilde{A}_{\max}^{(\kappa)} - 1)$ mutually exclusive CS sequence subfamilies and each subfamily contains $\tilde{A}_{\max}^{(\kappa)} - 1$ sequences generated by cyclically shifting the inverse DFT of a subfamily leader with family CSD $\omega_{\tilde{\mathcal{G}}}^{(\kappa)} \triangleq N / \tilde{A}_{\max}^{(\kappa)}$, where $\tilde{A}_{\max}^{(\kappa)} \triangleq \max_{m \in \mathcal{Z}_{\Omega(N)-\kappa}} \tilde{A}_m^{(\kappa)}$.

3.5 Some Examples of Families $\mathcal{G}_{\max, \tilde{I}}^{(\text{dpma}, \kappa)}$ and $\tilde{\mathcal{G}}_{\max, \tilde{I}}^{(\text{dpma}, \kappa)}$

Based on proper level- $(\Omega(N) - \kappa)$ factorization $N = \prod_{m=0}^{\Omega(N)-\kappa-1} A_m^{(\kappa)}$ and near-proper level- $(\Omega(N) - \kappa)$ factorization $N = \prod_{m=0}^{\Omega(N)-\kappa-1} \tilde{A}_m^{(\kappa)}$, family $\mathcal{G}_{\max, \tilde{I}}^{(\text{dpma}, \kappa)}$ and



family $\tilde{\mathcal{G}}_{\max, \tilde{I}}^{(\text{dpma}, \kappa)}$ can be constructed to contain orthogonal order- \tilde{I} CA sequences with family sizes $\prod_{m=0}^{\Omega(N)-\kappa-1} (A_m^{(\kappa)} - 1)$ and $\prod_{m=0}^{\Omega(N)-\kappa-1} (\tilde{A}_m^{(\kappa)} - 1)$, respectively. Since there is only one level- $\Omega(N)$ factorization, family $\mathcal{G}_I^{(\text{pma})}$ is essentially constructed under a proper level- $(\Omega(N) - \kappa)$ factorization with $\kappa = 0$. The developed degenerate PMA families $\mathcal{G}_{\max, \tilde{I}}^{(\text{dpma}, \kappa)}$ and $\tilde{\mathcal{G}}_{\max, \tilde{I}}^{(\text{dpma}, \kappa)}$ are listed in Table VI for example sequence lengths adopted by the MIMO SCE application in 5G-NR [2, Section 6.4.1.4.3], where the achieved family size, the supporting factor set, and the family CSD are demonstrated for each family. As shown, $\mathcal{G}_{\max, \tilde{I}}^{(\text{dpma}, \kappa)}$ and $\tilde{\mathcal{G}}_{\max, \tilde{I}}^{(\text{dpma}, \kappa)}$ provide much larger family sizes than $\mathcal{G}_I^{(\text{pma})}$ and offer the larger family sizes as κ increases, but they may entail reduced sidelobe-decaying order $\tilde{I} \geq \Omega(N) - \kappa$ under *Condition A* and $\tilde{I} \geq [(\Omega(N) - \kappa)/2]$ under *Condition B*. For a fixed $\kappa \in \{3, 4, \dots, \Omega(N) - 2\}$, the family size of $\tilde{\mathcal{G}}_{\max, \tilde{I}}^{(\text{dpma}, \kappa)}$ is the same as or very close to the family size of $\mathcal{G}_{\max, \tilde{I}}^{(\text{dpma}, \kappa)}$. The latter reveals the advantage of near-proper level- $(\Omega(N) - \kappa)$ factorization for $\kappa \in \{3, 4, \dots, \Omega(N) - 2\}$ in that the closed-form expressions are available for factorization.

For the SCE application in 5G NR, orthogonal Zadoff-Chu sequences are adopted and these sequences are generated by cyclically shifting a root ZC sequence in time domain under the restriction that the minimum CSD ω_{\min} is guaranteed for every shift to avoid sequence ambiguity [2, Section 6.4.1.4.1]. Recall that family $\mathcal{G}_{\max, \tilde{I}}^{(\text{dpma}, \kappa)}$ contains $\Psi^{(\text{dpma}, \kappa)}(N) / (A_{\max}^{(\kappa)} - 1)$ mutually exclusive CS sequence subfamilies and each subfamily contains $A_{\max}^{(\kappa)} - 1$ sequences generated by cyclically shifting the inverse DFT of a subfamily leader with family CSD $\omega_{\mathcal{G}}^{(\kappa)} \triangleq N / A_{\max}^{(\kappa)}$. Thus, not every sequence in family $\mathcal{G}_{\max, \tilde{I}}^{(\text{dpma}, \kappa)}$ can be adopted if $\omega_{\mathcal{G}}^{(\kappa)}$ is smaller than ω_{\min} required by the SCE

application. The same concern exists with family $\tilde{\mathcal{G}}_{\max, \tilde{l}}^{(\text{dpma}, \kappa)}$. For example, family $\mathcal{G}_{\max, \tilde{l}}^{(\text{dpma}, 5)}$ in Table VI(c) contains $\Psi^{(\text{dpma}, 5)}(288)/(A_{\max}^{(5)} - 1) = 15$ CS sequence subfamilies and each subfamily contains $A_{\max}^{(5)} - 1 = 17$ sequences with $\omega_{\mathcal{G}}^{(5)} = 16$. Due to $\omega_{\min} = 24$, at most $\lfloor (A_{\max}^{(5)} - 1) / \lceil \omega_{\min} / \omega_{\mathcal{G}}^{(5)} \rceil \rfloor = 8$ sequences can be adopted in each subfamily to satisfy the CSD restriction and accordingly at most 120 orthogonal sequences from family $\mathcal{G}_{\max, \tilde{l}}^{(\text{dpma}, 5)}$ can be used as the sounding sequences under the restriction $\omega_{\min} = 24$. As such, the number $\Psi(N|\omega_{\min})$ is also given for each family in Table VI to show the maximum number of sounding sequences available for use in the SCE application under the CSD restriction by ω_{\min} .

Remark 1: In 5G NR, there are 12 orthogonal ZC sequences required for all considered sequence lengths [2, Section 6.4.1.4.3] to support simultaneous uplink channel estimation from at most 12 transmit antennas [2, Section 6.4.1.4.1], and the orthogonality among sounding sequences is necessary to identify and separate different channels in order to achieve high estimation accuracy for multipath channels with short-delay channel profiles [14], [22], [24]. In this case, the minimum CSD required to avoid sequence ambiguity is specified by $\omega_{\min} = N/12$ for the adopted ZC sequences of different sequence lengths N . As an example in Table VI(a) with $N = 48$, 12 orthogonal ZC sequences can be generated by cyclically shifting a given ZC sequence (in time domain) with $\omega_{\min} = 4$. As shown in Table VI, all families $\mathcal{G}_{\max, \tilde{l}}^{(\text{dpma}, \kappa)}$ and $\tilde{\mathcal{G}}_{\max, \tilde{l}}^{(\text{dpma}, \kappa)}$ with $\kappa \geq 2$ can offer more than 12 orthogonal sequences than the adopted ZC sequence families for the channel sounding application in 5G NR [2, Section 6.4.1.4.1], while satisfying the same CSD restriction by ω_{\min} and providing the larger sidelobe-decaying order.

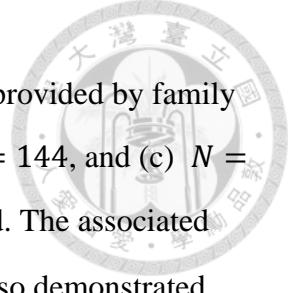


Table VI

The family sizes and the numbers of available sounding sequences provided by family

$\mathcal{G}_{\max, \bar{l}}^{(\text{dpma}, \kappa)}$ and $\tilde{\mathcal{G}}_{\max, \bar{l}}^{(\text{dpma}, \kappa)}$ for sequence lengths (a) $N = 48$, (b) $N = 144$, and (c) $N =$

288 adopted for channel sounding application in 5G NR standard. The associated

factor sets $\{A_m^{(\kappa)}; m \in \mathcal{Z}_{\Omega(N)-\kappa}\}$ and $\{\tilde{A}_m^{(\kappa)}; m \in \mathcal{Z}_{\Omega(N)-\kappa}\}$ are also demonstrated.

(a) $N = 48$ ($\Omega(N) = 5, \omega_{\min} = 4$)

Family (Family CSD)	Family Size ($\Psi(N \omega_{\min})$)	Factor Set
$\mathcal{G}_l^{(\text{pma})}$ (16)	2 (2)	{2,2,2,2,3}
$\mathcal{G}_{\max, \bar{l}}^{(\text{dpma}, 1)}$ (12)	6 (6)	{2,2,3,4}
$\mathcal{G}_{\max, \bar{l}}^{(\text{dpma}, 2)}$ (12)	18 (18)	{3,4,4}
$\mathcal{G}_{\max, \bar{l}}^{(\text{dpma}, 3)}, \tilde{\mathcal{G}}_{\max, \bar{l}}^{(\text{dpma}, 3)}$ (6,6)	35,35 (35,35)	{6,8}, {6,8}

(b) $N = 144$ ($\Omega(N) = 6, \omega_{\min} = 12$)

Family (Family CSD)	Family Size ($\Psi(N \omega_{\min})$)	Factor Set
$\mathcal{G}_l^{(\text{pma})}$ (48)	4 (4)	{2,2,2,2,3,3}
$\mathcal{G}_{\max, \bar{l}}^{(\text{dpma}, 1)}$ (36)	12 (12)	{2,2,3,3,4}
$\mathcal{G}_{\max, \bar{l}}^{(\text{dpma}, 2)}$ (36)	36 (36)	{3,3,4,4}
$\mathcal{G}_{\max, \bar{l}}^{(\text{dpma}, 3)}, \tilde{\mathcal{G}}_{\max, \bar{l}}^{(\text{dpma}, 3)}$ (24,24)	75,75 (75,75)	{4,6,6}, {4,6,6}
$\mathcal{G}_{\max, \bar{l}}^{(\text{dpma}, 4)}, \tilde{\mathcal{G}}_{\max, \bar{l}}^{(\text{dpma}, 4)}$ (12,12)	121,121 (121,121)	{12,12} {12,12}

(c) $N = 288$ ($\Omega(N) = 7, \omega_{\min} = 24$)

Family (Family CSD)	Family Size ($\Psi(N \omega_{\min})$)	Factor Set
$\mathcal{G}_l^{(\text{pma})}$ (96)	4 (4)	{2,2,2,2,2,3,3}
$\mathcal{G}_{\max, \bar{l}}^{(\text{dpma}, 1)}$ (72)	12 (12)	{2,2,2,3,3,4}
$\mathcal{G}_{\max, \bar{l}}^{(\text{dpma}, 2)}$ (72)	36 (36)	{2,3,3,4,4}
$\mathcal{G}_{\max, \bar{l}}^{(\text{dpma}, 3)}, \tilde{\mathcal{G}}_{\max, \bar{l}}^{(\text{dpma}, 3)}$ (48,48)	90,90 (90,90)	{3,4,6,6}, {3,4,6,6}
$\mathcal{G}_{\max, \bar{l}}^{(\text{dpma}, 4)}, \tilde{\mathcal{G}}_{\max, \bar{l}}^{(\text{dpma}, 4)}$ (36,32)	175,168 (175,168)	{6,6,8} {4,8,9}
$\mathcal{G}_{\max, \bar{l}}^{(\text{dpma}, 5)}, \tilde{\mathcal{G}}_{\max, \bar{l}}^{(\text{dpma}, 5)}$ (16,16)	255,255 (120,120)	{16,18} {16,18}

Table VII

The family sizes provided by $\hat{\mathcal{G}}_{\max, \bar{I}}^{(\text{dpma}, \kappa)}$ and $\hat{\mathcal{G}}_{\max, \bar{I}}^{(\text{adpma}, \kappa)}$ with sequence lengths (a) $N = 139$, (b) $N = 571$, (c) $N = 839$, and (d) $N = 1151$ for RA application in 5G NR. In searching θ , the accuracy measure is set to $\epsilon = 10^{-9}$. The proper factor sets for all subsequence lengths $\tilde{N}^{(0)}, \tilde{N}^{(1)}, \dots, \tilde{N}^{(L-1)}$ and the sought $\hat{\theta}$ are also demonstrated.

The largest achievable family size $\Psi_{\max}(N)$ under *Condition B* is given for benchmarking.

(a) $N = 139$ with $(\tilde{N}^{(0)}, \tilde{N}^{(1)}, \tilde{N}^{(2)}) = (50, 45, 44)$,

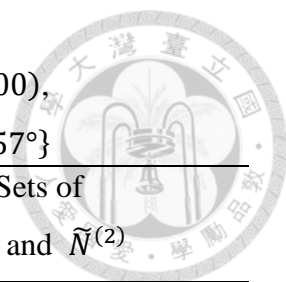
$\tilde{\Omega}(N) = 3$, and $\{\hat{\theta}_0, \hat{\theta}_1, \hat{\theta}_2\} = \{0^\circ, 125.12^\circ, 236.77^\circ\}$

Family	Family Size ($\Psi_{\max}(N)$)	Factor Sets of $\tilde{N}^{(0)}, \tilde{N}^{(1)}$, and $\tilde{N}^{(2)}$
$\hat{\mathcal{G}}_I^{(\text{pma})}, \hat{\mathcal{G}}_I^{(\text{apma})}$	10, 20 (137)	{2,5,5}, {3,3,5}, {2,2,11}
$\hat{\mathcal{G}}_{\max, \bar{I}}^{(\text{dpma}, 1)}, \hat{\mathcal{G}}_{\max, \bar{I}}^{(\text{adpma}, 1)}$	30, 60 (137)	{5,10}, {5,9}, {4,11}

(b) $N = 571$ with $(\tilde{N}^{(0)}, \tilde{N}^{(1)}, \tilde{N}^{(2)}) = (225, 196, 150)$,

$\tilde{\Omega}(N) = 4$, and $\{\hat{\theta}_0, \hat{\theta}_1, \hat{\theta}_2\} = \{0^\circ, 138.98^\circ, 239.06^\circ\}$

Family	Family Size ($\Psi_{\max}(N)$)	Factor Sets of $\tilde{N}^{(0)}, \tilde{N}^{(1)}$, and $\tilde{N}^{(2)}$
$\hat{\mathcal{G}}_I^{(\text{pma})}, \hat{\mathcal{G}}_I^{(\text{apma})}$	32, 64 (567)	{3,3,5,5}, {2,2,7,7}, {2,3,5,5}
$\hat{\mathcal{G}}_{\max, \bar{I}}^{(\text{dpma}, 1)}, \hat{\mathcal{G}}_{\max, \bar{I}}^{(\text{adpma}, 1)}$	80, 160 (569)	{5,5,9}, {4,7,7}, {5,5,6}
$\hat{\mathcal{G}}_{\max, \bar{I}}^{(\text{dpma}, 2)}, \hat{\mathcal{G}}_{\max, \bar{I}}^{(\text{adpma}, 2)}$	125, 252 (569)	{15,15}, {14,14}, {10,15}



(c) $N = 839$ with $(\tilde{N}^{(0)}, \tilde{N}^{(1)}, \tilde{N}^{(2)}) = (396, 243, 200)$,

$\tilde{\Omega}(N) = 5$, and $\{\hat{\theta}_0, \hat{\theta}_1, \hat{\theta}_2\} = \{0^\circ, 156.04^\circ, 509.57^\circ\}$

Family	Family Size ($\Psi_{\max}(N)$)	Factor Sets of $\tilde{N}^{(0)}, \tilde{N}^{(1)}$, and $\tilde{N}^{(2)}$
$\hat{G}_I^{(\text{pma})}, \hat{G}_I^{(\text{apma})}$	16, 32 (835)	$\{2,2,3,3,11\}, \{3,3,3,3,3\},$ $\{2,2,2,5,5\}$
$\hat{G}_{\max, \tilde{I}}^{(\text{dpma},1)}, \hat{G}_{\max, \tilde{I}}^{(\text{adpma},1)}$	48, 96 (835)	$\{3,3,4,11\}, \{3,3,3,9\}, \{2,4,5,5\}$
$\hat{G}_{\max, \tilde{I}}^{(\text{dpma},2)}, \hat{G}_{\max, \tilde{I}}^{(\text{adpma},2)}$	112, 224 (837)	$\{6,6,11\}, \{3,9,9\}, \{5,5,8\}$
$\hat{G}_{\max, \tilde{I}}^{(\text{dpma},3)}, \hat{G}_{\max, \tilde{I}}^{(\text{adpma},3)}$	171, 342 (837)	$\{18,22\}, \{9,27\}, \{10,20\}$

(d) $N = 1151$ with $(\tilde{N}^{(0)}, \tilde{N}^{(1)}, \tilde{N}^{(2)}) = (468, 440, 243)$,

$\tilde{\Omega}(N) = 5$, and $\{\hat{\theta}_0, \hat{\theta}_1, \hat{\theta}_2\} = \{0^\circ, 149.15^\circ, 248.20^\circ\}$

Family	Family Size ($\Psi_{\max}(N)$)	Factor Sets of $\tilde{N}^{(0)}, \tilde{N}^{(1)}$, and $\tilde{N}^{(2)}$
$\hat{G}_I^{(\text{pma})}, \hat{G}_I^{(\text{apma})}$	32, 64 (1147)	$\{2,2,3,3,13\}, \{2,2,2,5,11\},$ $\{3,3,3,3,3\}$
$\hat{G}_{\max, \tilde{I}}^{(\text{dpma},1)}, \hat{G}_{\max, \tilde{I}}^{(\text{adpma},1)}$	64, 128 (1147)	$\{3,3,4,13\}, \{2,4,5,11\}, \{3,3,3,9\}$
$\hat{G}_{\max, \tilde{I}}^{(\text{dpma},2)}, \hat{G}_{\max, \tilde{I}}^{(\text{adpma},2)}$	128, 256 (1149)	$\{6,6,13\}, \{5,8,11\}, \{3,9,9\}$
$\hat{G}_{\max, \tilde{I}}^{(\text{dpma},3)}, \hat{G}_{\max, \tilde{I}}^{(\text{adpma},3)}$	208, 416 (1149)	$\{18,26\}, \{20,22\}, \{9,27\}$

Chapter 4

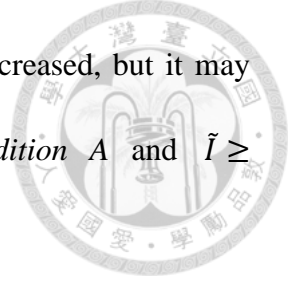


Families $\widehat{\mathcal{G}}_I^{(\text{apma})}$, $\widehat{\mathcal{G}}_{\max, \tilde{I}}^{(\text{dpma}, \kappa)}$, and $\widehat{\mathcal{G}}_{\max, \tilde{I}}^{(\text{adpma}, \kappa)}$

In this section, we consider the sequence length N meeting $\tilde{\Omega}(N) > \Omega(N)$ and construct new families $\widehat{\mathcal{G}}_{\max, \tilde{I}}^{(\text{dpma}, \kappa)}$ and $\widehat{\mathcal{G}}_{\max, \tilde{I}}^{(\text{adpma}, \kappa)}$ for $\kappa \in \mathcal{Z}_{\tilde{\Omega}(N)-1}^+$. Notably, any orthogonal sequence in a new family $\widehat{\mathcal{G}}_{\max, \tilde{I}}^{(\text{dpma}, \kappa)}$ or $\widehat{\mathcal{G}}_{\max, \tilde{I}}^{(\text{adpma}, \kappa)}$ cannot be obtained from cyclically shifting another sequence in the same family, due to the proper decomposition of N .

4.1 Degenerate PMA Sequence Family $\widehat{\mathcal{G}}_{\max, \tilde{I}}^{(\text{dpma}, \kappa)}$ for $\kappa \in \mathcal{Z}_{\tilde{\Omega}(N)-1}^+$

With a given $\kappa \in \mathcal{Z}_{\tilde{\Omega}(N)-1}^+$, the degenerate PMA sequence family $\widehat{\mathcal{G}}_{\max, \tilde{I}}^{(\text{dpma}, \kappa)}$ can be constructed by virtue of the *combined proper* level- $(\tilde{\Omega}(N) - \kappa)$ factorization for sequence $\widehat{\mathcal{G}}_I$, which is composed of *individual proper* level- $(\Omega(\tilde{N}^{(\rho)}) - \kappa)$ factorizations for all component subsequences of lengths $\tilde{N}^{(0)}, \tilde{N}^{(1)}, \dots, \tilde{N}^{(L-1)}$ under the proper decomposition $N = \sum_{\rho \in \mathcal{Z}_L} \tilde{N}^{(\rho)}$ yielding $\tilde{\Omega}(N)$ (see (7)) with $\tilde{N}^{(0)} \geq \tilde{N}^{(1)} \geq \dots \geq \tilde{N}^{(L-1)} \geq 2$. For each $\rho \in \mathcal{Z}_L$, the proper level- $(\Omega(\tilde{N}^{(\rho)}) - \kappa)$ factorization $\tilde{N}^{(\rho)} = \prod_{m=0}^{\Omega(\tilde{N}^{(\rho)}) - \kappa - 1} A_m^{(\rho, \kappa)}$ is used to construct family $\mathcal{G}_{\max, \tilde{I}}^{(\text{dpma}, \kappa)}$ with subsequence length $\tilde{N}^{(\rho)}$, where the factors $A_m^{(\rho, \kappa)}$ are not all primes. Each orthogonal sequence in family $\widehat{\mathcal{G}}_{\max, \tilde{I}}^{(\text{dpma}, \kappa)}$ is thus composed by a concatenation of L PMA subsequences $\mathcal{X}_0, \mathcal{X}_1, \dots, \mathcal{X}_{L-1}$ of lengths $\tilde{N}^{(0)}, \tilde{N}^{(1)}, \dots, \tilde{N}^{(L-1)}$, respectively. Such family $\widehat{\mathcal{G}}_{\max, \tilde{I}}^{(\text{dpma}, \kappa)}$ has the family size $\widehat{\Psi}^{(\text{dpma}, \kappa)}(N) \triangleq \min_{\rho \in \mathcal{Z}_L} \prod_{m=0}^{\Omega(\tilde{N}^{(\rho)}) - \kappa - 1} (A_m^{(\rho, \kappa)} - 1)$.



Notably, $\hat{\mathcal{G}}_{\max, \tilde{I}}^{(\text{dpma}, \kappa)}$ tends to offer the larger family size as κ is increased, but it may reduce the sidelobe-decaying order $\tilde{I} \geq \tilde{\Omega}(N) - \kappa$ under *Condition A* and $\tilde{I} \geq \lfloor (\tilde{\Omega}(N) - \kappa)/2 \rfloor$ under *Condition B*.

4.2 Augmented PMA Sequence Families $\hat{\mathcal{G}}_I^{(\text{apma})}$ and $\hat{\mathcal{G}}_{\max, \tilde{I}}^{(\text{adpma}, \kappa)}$ for $\kappa \in \mathbb{Z}_{\tilde{\Omega}(N)-1}^+$

Augmented PMA sequence family $\hat{\mathcal{G}}_I^{(\text{apma})}$ was proposed from [43], which expands from family $\hat{\mathcal{G}}_I^{(\text{pma})}$ with the same sidelobe-decaying order and a double family size, by virtue of phase-rotating every existing sequence in family $\hat{\mathcal{G}}_I^{(\text{pma})}$ to generate more orthogonal sequence members. Similarly, augmented degenerate PMA sequence family $\hat{\mathcal{G}}_{\max, \tilde{I}}^{(\text{adpma}, \kappa)}$ expands from $\hat{\mathcal{G}}_{\max, \tilde{I}}^{(\text{dpma}, \kappa)}$ and offers a double family size while sustaining the same sidelobe-decaying order. In what follows, the phase-rotating method constructing family $\hat{\mathcal{G}}_I^{(\text{apma})}$ is described in detail, and such method is also applied to construct family $\hat{\mathcal{G}}_{\max, \tilde{I}}^{(\text{adpma}, \kappa)}$. The details of the phase-rotating method were presented in [43] and are reviewed here.

Consider one sequence $\hat{\mathcal{G}}_I$ in family $\hat{\mathcal{G}}_I^{(\text{pma})}$, which is described by $\boldsymbol{\chi} = [\boldsymbol{\chi}_0^t, \boldsymbol{\chi}_1^t, \dots, \boldsymbol{\chi}_{L-1}^t]^t$. From this sequence, one extra order- I CA sequence $\hat{\mathcal{G}}_I$ can be obviously constructed by rotating the phases of the subsequences $\boldsymbol{\chi}_\rho$ and described by $\boldsymbol{\chi}^\theta = [e^{j\theta_0} \boldsymbol{\chi}_0^t, e^{j\theta_1} \boldsymbol{\chi}_1^t, \dots, e^{j\theta_{L-1}} \boldsymbol{\chi}_{L-1}^t]^t$ where $\boldsymbol{\theta} = [\theta_\rho; \rho \in \mathbb{Z}_L]$ is the rotating phase vector. Due to the PMA construction of $\hat{\mathcal{G}}_I^{(\text{pma})}$, such phase-rotated sequence is mutually orthogonal to all the other PMA sequences in family $\hat{\mathcal{G}}_I^{(\text{pma})}$ as well as their phase-rotated sequences. To ensure that two sequences $\hat{\mathcal{G}}_I$ described by $\boldsymbol{\chi}$ and $\boldsymbol{\chi}^\theta$ are mutually orthogonal, $\boldsymbol{\theta}$ should be chosen to meet the orthogonality condition $\boldsymbol{\chi}^h \boldsymbol{\chi}^\theta =$

$\sum_{\rho \in Z_L} \chi_\rho^h \chi_\rho e^{j\theta_\rho} = 0$, or equivalently

$$\sum_{\rho \in Z_L} \tilde{N}^{(\rho)} e^{j\theta_\rho} = 0. \quad (12)$$



Notably, $\sum_{\rho \in Z_L} \tilde{N}^{(\rho)} e^{j\theta_\rho}$ can be regarded as the sum of L vectors $\tilde{N}^{(\rho)} e^{j\theta_\rho}$ in the complex plane. As indicated by (12), these L vectors should be connected to form an L -edge cyclic polygon in the complex plane. According to the cyclic polygon theorem in [40, Theorem 1], a solution to (12) exists iff all edge lengths $\tilde{N}^{(\rho)}$ meet following restriction.

Restriction A: $L \geq 3$ and $\max_{\rho \in Z_L} \tilde{N}^{(\rho)} < \frac{1}{2} \sum_{\rho \in Z_L} \tilde{N}^{(\rho)}$

When *Restriction A* is met, the solution of θ to (12) can be obtained by invoking the following procedure.

4.2.1 Review of the Procedure to Finding a Proper θ

This procedure was proposed in [43] and based on the bisection method to constructing a cyclic polygon given the edge lengths and obtaining the arc angles corresponding to the given edge lengths simultaneously [40, Section 1]. Under *Restriction A*, there must exist a cyclic polygon with prescribed edge lengths $\tilde{N}^{(0)}, \tilde{N}^{(1)}, \dots, \tilde{N}^{(L-1)}$. Denote ξ as the radius of the circumscribed circle and ϑ_ρ as the arc angle corresponding to the edge length $\tilde{N}^{(\rho)}$ of the circumscribed circle. Notably, ξ and $\{\vartheta_\rho\}$ are necessary to calculate $\{\theta_\rho\}$ [40, Section 1]. Moreover, we denote $\hat{\xi}$, $\hat{\vartheta}_\rho$, and $\hat{\theta}_\rho$ as the estimates of ξ , ϑ_ρ , and θ_ρ , respectively, in order to approach (12). The following procedure is then used to find $\{\hat{\theta}_\rho\}$ which can approach (12) within a predetermined accuracy ϵ [40, Section 1], [43].

Step 0: Let $\theta_{\min} = 0$, $\theta_{\max} = 2\pi$, and ϵ be a small positive real number close to



zero.

Step 1: Let $\theta_{\text{mid}} = \frac{1}{2}(\theta_{\text{min}} + \theta_{\text{max}})$ and $\hat{\xi} = \frac{\tilde{N}^{(0)}}{2 \sin(\theta_{\text{mid}}/2)}$.

Step 2: Let $\hat{\vartheta}_0 = \theta_{\text{mid}}$ and $\hat{\vartheta}_\rho = \arccos\left(1 - \frac{(\tilde{N}^{(\rho)})^2}{2\hat{\xi}^2}\right)$ for all $\rho \in \mathcal{Z}_{L+1}^+$.

Step 3: There are three cases in this step.

Case 1: If $|\sum_{\rho \in \mathcal{Z}_L} \hat{\vartheta}_\rho - 2\pi| \leq \epsilon$, go to *Step 4* directly.

Case 2: If $\sum_{\rho \in \mathcal{Z}_L} \hat{\vartheta}_\rho < 2\pi - \epsilon$, let $\theta_{\text{min}} = \theta_{\text{mid}}$ and go back to *Step 1*.

Case 3: If $\sum_{\rho \in \mathcal{Z}_L} \hat{\vartheta}_\rho > 2\pi + \epsilon$, let $\theta_{\text{max}} = \theta_{\text{mid}}$ and go back to *Step 1*.

Step 4: Let $\hat{\vartheta}_0 = 0$ and $\hat{\theta}_\rho = \hat{\theta}_{\rho-1} + \frac{1}{2}(\hat{\vartheta}_{\rho-1} + \hat{\vartheta}_\rho)$ for all $\rho \in \mathcal{Z}_{L-1}^+$.

When $\sum_{\rho \in \mathcal{Z}_L} \hat{\vartheta}_\rho < 2\pi - \epsilon$ occurs, all prescribed edge lengths $\tilde{N}^{(\rho)}$ can not make a cyclic polygon and thus the estimated radius $\hat{\xi}$ is larger than the actual radius ξ . Since \arccos is a monotonically decreasing function and $\hat{\xi} > \xi$, $\hat{\vartheta}_\rho < \vartheta_\rho$ for all $\rho \in \mathcal{Z}_L$ in this case. Conversely, $\hat{\vartheta}_\rho > \vartheta_\rho$ for all $\rho \in \mathcal{Z}_L$ when $\sum_{\rho \in \mathcal{Z}_L} \hat{\vartheta}_\rho > 2\pi + \epsilon$. Through multiple iterations, $\hat{\vartheta}_\rho$ can be obtained for all $\rho \in \mathcal{Z}_L$. At *Step 4*, the absolute error $|\sum_{\rho} \vartheta_\rho - \sum_{\rho} \hat{\vartheta}_\rho|$ is limited to be within ϵ . Thus, $\hat{\theta}_\rho$ for all $\rho \in \mathcal{Z}_L$ can be estimated within an accuracy ϵ .

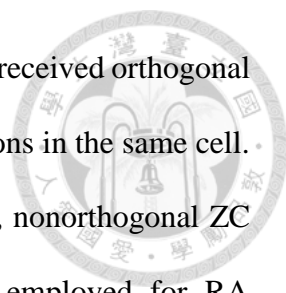
When the proper decomposition $N = \sum_{\rho \in \mathcal{Z}_L} \tilde{N}^{(\rho)}$ for a given family $\hat{\mathcal{G}}_I^{(\text{pma})}$ meets *Restriction A*, family $\hat{\mathcal{G}}_I^{(\text{apma})}$ can be constructed by including all orthogonal order- I CA sequences in family $\hat{\mathcal{G}}_I^{(\text{pma})}$ with size $\hat{\Psi}(N)$ and augmenting another $\hat{\Psi}(N)$ orthogonal order- I CA sequences, where each augmented sequence described by \mathbf{x}^θ can be constructed for each sequence $\hat{\mathcal{G}}_I$ described by \mathbf{x} with θ obtained by invoking the aforementioned procedure. Apparently, all augmented sequences are mutually orthogonal and also orthogonal to all sequences in family $\hat{\mathcal{G}}_I^{(\text{pma})}$. This results in the

family size $2\hat{\Psi}(N)$ and the same sidelobe-decaying order for family $\hat{\mathcal{G}}_I^{(\text{apma})}$. Similarly, family $\hat{\mathcal{G}}_{\max, \tilde{I}}^{(\text{adpma}, \kappa)}$ for $\kappa \in \mathcal{Z}_{\tilde{\Omega}(N)-1}^+$ can be augmented from a given family $\hat{\mathcal{G}}_{\max, \tilde{I}}^{(\text{dpma}, \kappa)}$ and has the family size $2\hat{\Psi}^{(\text{dpma}, \kappa)}(N)$ under the same proper decomposition $N = \sum_{\rho \in \mathcal{Z}_L} \tilde{N}^{(\rho)}$, while sustaining the same sidelobe-decaying order. Notably, $\hat{\mathcal{G}}_I^{(\text{apma})}$ can be regarded as a special case of $\hat{\mathcal{G}}_{\max, \tilde{I}}^{(\text{adpma}, \kappa)}$ with $\kappa = 0$ and $\tilde{I} = I$ since $\hat{\mathcal{G}}_I^{(\text{apma})}$ is essentially constructed under combined proper level- $\tilde{\Omega}(N)$ factorization for $\hat{\mathcal{G}}_{\max, \tilde{I}}^{(\text{adpma}, 0)}$.

4.3 Examples of Families $\hat{\mathcal{G}}_I^{(\text{apma})}$, $\hat{\mathcal{G}}_{\max, \tilde{I}}^{(\text{dpma}, \kappa)}$, and $\hat{\mathcal{G}}_{\max, \tilde{I}}^{(\text{adpma}, \kappa)}$

The developed families $\hat{\mathcal{G}}_I^{(\text{apma})}$, $\hat{\mathcal{G}}_{\max, \tilde{I}}^{(\text{dpma}, \kappa)}$, and $\hat{\mathcal{G}}_{\max, \tilde{I}}^{(\text{adpma}, \kappa)}$ are listed in Table VII for example sequence lengths adopted by the random access application in 5G-NR [2], where the achieved family size and the proper factor sets for all subsequence lengths $\tilde{N}^{(0)}, \tilde{N}^{(1)}, \dots, \tilde{N}^{(L-1)}$ are demonstrated for each family. As shown, family $\hat{\mathcal{G}}_{\max, \tilde{I}}^{(\text{dpma}, \kappa)}$ offers the larger family size as κ increases and much larger family size than $\hat{\mathcal{G}}_I^{(\text{pma})}$. Nevertheless, $\hat{\mathcal{G}}_{\max, \tilde{I}}^{(\text{dpma}, \kappa)}$ may entail reduced sidelobe-decaying order $\tilde{I} \geq \tilde{\Omega}(N) - \kappa$ under *Condition A* and $\tilde{I} \geq \lceil (\tilde{\Omega}(N) - \kappa) / 2 \rceil$ under *Condition B*. For a fixed $\kappa \in \mathcal{Z}_{\tilde{\Omega}(N)-1}^+$, family $\hat{\mathcal{G}}_{\max, \tilde{I}}^{(\text{adpma}, \kappa)}$ exhibits double the size of family $\hat{\mathcal{G}}_{\max, \tilde{I}}^{(\text{dpma}, \kappa)}$ while sustaining the same sidelobe-decaying order. Moreover, the family sizes of $\hat{\mathcal{G}}_{\max, \tilde{I}}^{(\text{dpma}, \kappa)}$ with large κ values approach a good portion of the largest achievable size $\Psi_{\max}(N)$. The latter reveals the advantage of augmented degenerate PMA sequence families.

Remark 2: Orthogonal Zadoff-Chu sequences are desirable for the RA application in 5G NR. Although N orthogonal ZC sequences of length N can be easily generated by cyclically shifting a given ZC sequence with an admissible root index ζ (relatively prime



to N), a large minimum CSD ω_{\min} is generally required to identify received orthogonal ZC sequences transmitted from transmitters located in various locations in the same cell. The larger the cell radius, the larger the required ω_{\min} . As a result, nonorthogonal ZC sequences with different admissible root indices are commonly employed for RA requiring a large number of short-length identification sequences under a limited ω_{\min} . In 5G NR, there are 64 RA identification sequences required in each cell, and many large values for ω_{\min} are specified in [2, Tables 5-7 in Section 6.3.3.1] for the adopted ZC sequences of different lengths $N = 139, 571, 839$, and 1151. In these specifications, the maximum number of orthogonal ZC sequences is limited to $\lfloor N/\omega_{\min} \rfloor < 64$ for many specified pairs (N, ω_{\min}) . For example with $(N, \omega_{\min}) = (839, 26)$, only 32 orthogonal ZC sequences can be generated by cyclically shifting a given ZC sequence with an admissible root index ζ_1 . In this case, additional nonorthogonal ZC sequences are added in [2, Section 6.3.3.1] by cyclically shifting another ZC sequence with an admissible root index ζ_2 so that all 64 sequences are collected. As shown in Table VII(c), families $\hat{\mathcal{G}}_{\max, \tilde{l}}^{(\text{adpma}, \kappa)}$ with $\kappa \in \{2, 3\}$ can provide more than 64 orthogonal order- \tilde{l} CA sequences and thus outperform the adopted ZC sequences [2, Section 6.3.3.1] in RA performance while providing the higher spectral compactness.

Chapter 5

Random-Access Channel Identification



This section demonstrates the performance characteristics of uplink RA channel identification based on the reception of the OFDM preamble waveforms carrying identification sequences from various CA sequence families, including modified PMA, ZC, YL, and PN sequence families, over Rayleigh multipath channels. Here, the interleaving factor $\gamma = 1$ is considered. Spectral compactness of various OFDM preamble waveforms are also shown to justify the spectral compactness achieved by use of order- I CA sequences.

5.1 Scenario for RA Channel Identification

Consider the scenario that a single user terminal transmits a sequence $\mathbf{q}_k \triangleq [q_k[n]; n \in \mathcal{Z}_N]$ from the family of J CA sequences $\{\mathbf{q}_i; i \in \mathcal{Z}_J\}$ for identifying the availability of the k -th access channel [1]-[2]. After applying down-conversion, CP removal, and DFT to the received OFDM preamble signal, the base-station receiver observes the frequency-domain vector $\mathbf{r} \triangleq [r[n]; n \in \mathcal{Z}_N]$ modeled as [17], [19]

$$r[n] = N^{\frac{1}{2}}q_k[n]h[n] + z[n]. \quad (13)$$

Here, $\mathbf{z} \triangleq [z[n]; n \in \mathcal{Z}_N]$ contains independent and identically distributed circularly symmetric complex Gaussian (CSCG) noise samples with mean zero and variance $\mathcal{E}\{|z[n]|^2\} = 1/\varphi$, where φ is the received signal-to-noise power ratio (SNR). $\mathbf{h} \triangleq [h[n]; n \in \mathcal{Z}_N]$ is the channel frequency response (CFR) vector corresponding to the channel impulse response (CIR) $\{\tilde{h}[l], \tau_l; l \in \mathcal{Z}_{L_h}\}$ with L_h resolvable paths, given by

$$h[n] = \sum_{l \in \mathcal{Z}_{L_h}} \tilde{h}[l] e^{-j2\pi\Delta f n \tau_l} \text{ for all } n \in \mathcal{Z}_N \quad (14)$$

where $\Delta f = 1/T_d$ is subcarrier frequency spacing and τ_l denotes the l -th path delay value with $0 \leq \tau_0 < \tau_1 < \dots < \tau_{L_h-1} \leq T_g$. Moreover, all path responses are modeled to be independent CSCGs having means $\mathcal{E}\{\tilde{h}[0]\} = \tilde{\sigma} \exp\{j\theta\}$ and $\mathcal{E}\{\tilde{h}[l]\} = 0$ for $l \in \mathcal{Z}_{L_h}^+$, and correlations $\mathcal{E}\{(\tilde{h}[l] - \mathcal{E}\{\tilde{h}[l]\})^2\} = 0$ and $\mathcal{E}\{|\tilde{h}[l] - \mathcal{E}\{\tilde{h}[l]\}|^2\} = \sigma_l^2$ for $l \in \mathcal{Z}_{L_h}$, where θ is an arbitrary phase, $\tilde{\sigma}^2$ is the direct path power, and σ_l^2 is the l -th diffuse path power for the CIR $\{\tilde{h}[l]; l \in \mathcal{Z}_{L_h}\}$ with $\tilde{\sigma}^2 + \sum_{l \in \mathcal{Z}_{L_h}} \sigma_l^2 = 1$. Additionally, the factor K is the ratio of direct power to diffuse power sum, which is defined as $K = \tilde{\sigma}^2 / \sum_{l \in \mathcal{Z}_{L_h}} \sigma_l^2$. All path responses are also independent of all noise samples $\{z[n]; n \in \mathcal{Z}_N\}$. The RA channel identification is based on the correlations $\{\mathbf{q}_i^h \mathbf{r}; i \in \mathcal{Z}_J\}$, with

$$\mathbf{q}_i^h \mathbf{r} = N^{\frac{1}{2}} \sum_{l \in \mathcal{Z}_{L_h}} \tilde{h}[l] \sum_{n \in \mathcal{Z}_N} q_i^*[n] q_k[n] e^{-j2\pi\Delta f n \tau_l} + \sum_{n \in \mathcal{Z}_N} q_i^*[n] z[n]. \quad (15)$$

To identify \mathbf{q}_k , the squared correlation magnitudes $Y(\mathbf{q}_i) = |\mathbf{q}_i^h \mathbf{r}|^2$ are measured and compared with a positive threshold β for all $i \in \mathcal{Z}_J$. When $Y(\mathbf{q}_i)$ is greater than β , the i -th access channel is considered as a requested one [17]-[18], [20]-[21].

5.2 Performance Analysis

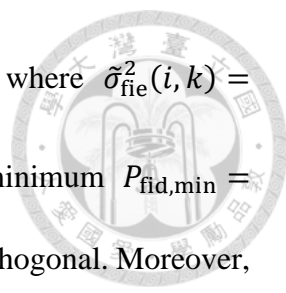
Under Rayleigh channel with $\tilde{\sigma}^2 = 0$, $\mathbf{q}_i^h \mathbf{r}$ for $i \in \mathcal{Z}_J$ is a CSCG having zero mean and variance $\mathcal{E}\{|\mathbf{q}_i^h \mathbf{r}|^2\} = \frac{1}{\phi} + \sigma_{\text{fie}}^2(i, k)$ if $i \neq k$ and $\mathcal{E}\{|\mathbf{q}_i^h \mathbf{r}|^2\} = \frac{1}{\phi} + \sigma_c^2$ otherwise, where $\sigma_{\text{fie}}^2(i, k) \triangleq N \sum_{l \in \mathcal{Z}_{L_h}} \sigma_l^2 |\sum_{n \in \mathcal{Z}_N} q_i^*[n] q_k[n] e^{-j2\pi\Delta f n \tau_l}|^2$ is the variance of the FIE term occurring when \mathbf{q}_i does not match the identification sequence

\mathbf{q}_k and $\sigma_c^2 = \frac{1}{N} \sum_{l \in \mathcal{Z}_{L_h}} \sigma_l^2 \left| \sum_{n \in \mathcal{Z}_N} e^{-j2\pi \Delta f n \tau_l} \right|^2$ is the signaling variance when \mathbf{q}_i matches \mathbf{q}_k correctly. Given the statistic of $\mathbf{q}_i^h \mathbf{r}$, $Y(\mathbf{q}_i)$ is a central chi-square random variable with two degrees of freedom [41].

Three measures P_{fa} , $P_{fid,k}$, and P_c are defined herein to quantify the performance of the threshold-based identification scheme. The false alarm probability P_{fa} denotes the probability of misidentifying \mathbf{q}_i when there is no request (i.e., $r[n] = z[n]$ for all $n \in \mathcal{Z}_N$), defined by $P_{fa} \triangleq \Pr\{Y(\mathbf{q}_i) > \beta | \text{no request}\}$ for some $i \in \mathcal{Z}_J$ and given by $P_{fa} = e^{-\beta\varphi}$, which is invariant with \mathbf{q}_i . The average false identification probability $P_{fid,k}$ is the average probability of identifying the request of an access channel other than the k -th channel that was actually requested [20, Subsection IV.D], and given by

$$\begin{aligned} P_{fid,k} &\triangleq \frac{1}{J-1} \sum_{i \in \mathcal{Z}_J, i \neq k} \Pr\{Y(\mathbf{q}_i) > \beta | \mathbf{q}_k \text{ was requested}\} \\ &= \frac{1}{J-1} \sum_{i \in \mathcal{Z}_J, i \neq k} e^{-\beta\varphi / (1 + \varphi\sigma_{fie}^2(i,k))}. \end{aligned} \quad (16)$$

From the union bound argument, $(J-1)P_{fid,k}$ is also an upper bound to the probability of identifying the request of *any* access channel other than the k -th channel that was actually requested [21, Subsection III.D]. The correct identification probability P_c is the average probability of identifying the request of the k -th access channel correctly, defined by $P_c \triangleq \Pr\{Y(\mathbf{q}_k) > \beta | \mathbf{q}_k \text{ was requested}\}$ and given by $P_c = e^{-\beta\varphi / (1 + \varphi\sigma_c^2)}$, which is irrelevant with \mathbf{q}_k . The identification scheme performs well when P_c is made as large as possible while P_{fa} and all $P_{fid,k}$ are restricted to be small. This can be achieved by properly setting the threshold β since P_{fa} , $P_{fid,k}$, and P_c increase as β is decreased for a given SNR φ . When the channel is flat fading (i.e., $h[n] = \tilde{h}[0]$ for all $n \in \mathcal{Z}_N$, or equivalently $L_h = 1$, $\tau_0 = 0$, and $\sigma_0^2 = 1$), $\mathbf{q}_i^h \mathbf{r}$ for $i \neq k$ simplifies to a



CSCG with mean zero and variance $\mathcal{E}\{|\mathbf{q}_i^h \mathbf{r}|^2\} = \frac{1}{\varphi} + \tilde{\sigma}_{\text{fie}}^2(i, k)$, where $\tilde{\sigma}_{\text{fie}}^2(i, k) = N|\sum_{n \in \mathcal{Z}_N} q_i^*[n]q_k[n]|^2$. In this case, $P_{\text{fid},k}$ in (16) achieves the minimum $P_{\text{fid},\min} = e^{-\beta\varphi}$ when all sequences in the family $\{\mathbf{q}_i; i \in \mathcal{Z}_J\}$ are mutually orthogonal. Moreover, P_c achieves the maximum $P_{c,\max} = e^{-\beta\varphi/(1+\varphi N)}$. When the coherence bandwidth $B_c \approx 1/(5\sigma_{\text{rms}})$ [25, Chapter 4, eq. 39] is much larger than the signaling bandwidth $N\gamma/T_d$ (i.e., $\tau_0 = 0$ and $\sigma_l^2 \ll \sigma_0^2$ for all $l \neq 0$), $\sigma_{\text{fie}}^2(i, k)$ approaches to $\tilde{\sigma}_{\text{fie}}^2(i, k)$ for $i \neq k$ and $P_{\text{fid},k}$ is expected to get close to $P_{\text{fid},\min}$ if all sequences in $\{\mathbf{q}_i; i \in \mathcal{Z}_J\}$ are orthogonal, where σ_{rms} is the root mean square delay spread in CIR. As thus implied, smaller $P_{\text{fid},k}$ values can be achieved when there are more orthogonal sequences in $\{\mathbf{q}_i; i \in \mathcal{Z}_J\}$ available for RA channel identification over multipath channels with large coherence bandwidth, or equivalently short-delay channel profiles.

For Rician channel, $\mathbf{q}_i^h \mathbf{r}$ for $i \in \mathcal{Z}_J$ is a CSCG having mean $\mathcal{E}\{\mathbf{q}_i^h \mathbf{r}\} = \eta_{\text{fie}}(i, k)$ and variance $\mathcal{E}\{|\mathbf{q}_i^h \mathbf{r}|^2\} = \frac{1}{\varphi} + \sigma_{\text{fie}}^2(i, k)$ if $i \neq k$, and $\mathcal{E}\{\mathbf{q}_i^h \mathbf{r}\} = \eta_c$ and variance $\mathcal{E}\{|\mathbf{q}_i^h \mathbf{r}|^2\} = \frac{1}{\varphi} + \sigma_c^2$ otherwise, where $\eta_{\text{fie}} = \sqrt{N}\tilde{\sigma}e^{j\theta} \sum_{n \in \mathcal{Z}_N} q_i^*[n]q_k[n]$ is the mean of the FIE term occurring when \mathbf{q}_i does not match the identification sequence \mathbf{q}_k and $\eta_c = \sqrt{N}\tilde{\sigma}e^{j\theta}$ is the signaling variance when \mathbf{q}_i matches \mathbf{q}_k correctly. Under such derive, the average false identification probability $P_{\text{fid},k}$ is given by $P_{\text{fid},k} = \frac{1}{J-1} \sum_{i \in \mathcal{Z}_J, i \neq k} Q_1\left(\frac{|\eta_{\text{fie}}(i,k)|}{(\frac{1}{2}\sigma_{\text{fie}}^2(i,k) + \frac{1}{2\varphi})^{1/2}}, \frac{\sqrt{\beta}}{(\frac{1}{2}\sigma_{\text{fie}}^2(i,k) + \frac{1}{2\varphi})^{1/2}}\right)$, and the correct identification probability is given by $P_c = Q_1\left(\frac{|\eta_c|}{(\frac{1}{2}\sigma_c^2 + \frac{1}{2\varphi})^{1/2}}, \frac{\sqrt{\beta}}{(\frac{1}{2}\sigma_c^2 + \frac{1}{2\varphi})^{1/2}}\right)$. Here, $Q_m(a, b)$ is called the Marcum Q-function of order m and defined in [49, eq. 2.3-36].

Table VIII

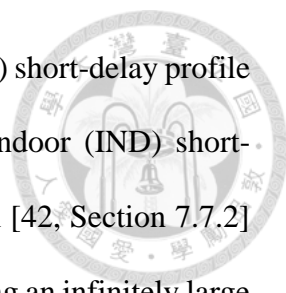
A Typical RA System Parameter Profile in Uplink 5G NR

Sequence Length N	839
Subcarrier Spacing $\Delta f = 1/T_d$	1.25 kHz
Interleaving Factor γ	1
Guard Ratio α	33/256
Total Number of Sequences J	64



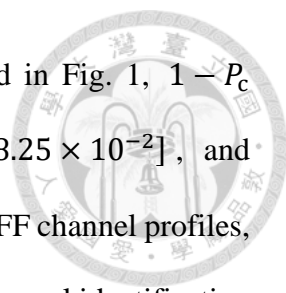
5.3 Performance Results

A total of 64 ZC sequences are required for RA channel identification in uplink 5G-NR [2, Section 6.3.3.1]. To avoid sequence ambiguity, a minimum CSD ω_{\min} is required to extract orthogonal ZC sequences through cyclically shifting a fixed-root-index ZC sequence. As mentioned in *Remark 2*, this causes the shortage of adoptable orthogonal ZC sequences for most specified (N, ω_{\min}) pairs. In [14], orthogonal YL sequences are constructed from phase-rotating the ZC sequences generated from cyclically shifting a fixed-root-index ZC sequence appropriately. When the minimum CSD requirement is imposed, not every cyclically shifted ZC sequence can be used to generate orthogonal YL sequences. The latter limits the number of adoptable orthogonal YL sequences as well in order to avoid sequence ambiguity. For example, we consider a particular RA system parameter profile in Table VIII [2] which adopts the sequence length $N = 839$ and the minimum CSD limit 26. In this case, at most $\lceil 839/26 \rceil = 32$ orthogonal ZC and YL sequences can be respectively adopted and thus nonorthogonal sequences have to be augmented in [2, Section 6.3.3.1] since 64 RA channels are to be identified. The characteristics of the average false identification probability $\frac{1}{J} \sum_{k \in Z_J} P_{\text{fid},k}$ versus SNR φ are demonstrated in Fig. 1 by simulating the threshold-based RA channel identification using such ZC and YL sequence families under three different Rayleigh multipath



channel profiles, namely TDL-B urban micro street-canyon (UMI-SC) short-delay profile (exhibiting $\sigma_{\text{rms}} = 65$ ns and $B_c \approx 2.93 \times N\gamma/T_d$) and TDL-B indoor (IND) short-delay profile (exhibiting $\sigma_{\text{rms}} = 20$ ns and $B_c \approx 9.54 \times N\gamma/T_d$) in [42, Section 7.7.2] as well as the benchmarking flat fading (FF) channel profile (exhibiting an infinitely large B_c). Notably, the UMI-SC short-delay profile exhibits a longer delay spread than the IND short-delay profile, and thus results in a smaller coherence bandwidth. Also compared in Fig. 1 are RA channel identification systems using orthogonal sequence families $\hat{\mathcal{G}}_{\text{max},I}^{(\text{adpma},1)}$ and $\hat{\mathcal{G}}_{\text{max},I}^{(\text{dpma},2)}$, and a nonorthogonal PN sequence family. All 64 PN sequences are constructed from the generator polynomial $X^{15} + X^{14} + 1$ with minimum CSD 26 [3, Section 9.7.1]. When the sequence length N is not any one of the forms in (8)-(10) and has $\tilde{\Omega}(N) > \Omega(N)$, we can construct family $\hat{\mathcal{G}}_{\text{max},I}^{(\text{dpma},\kappa)}$ with larger sidelobe-decaying order than family $\mathcal{G}_{\text{max},I}^{(\text{dpma},\kappa)}$. Different from family $\mathcal{G}_{\text{max},I}^{(\text{dpma},\kappa)}$, all sequences in family $\hat{\mathcal{G}}_{\text{max},I}^{(\text{dpma},\kappa)}$ can not be obtained through mutual cyclic shifting.¹ As described in Table VII(c), families $\hat{\mathcal{G}}_{\text{max},I}^{(\text{adpma},1)}$ and $\hat{\mathcal{G}}_{\text{max},I}^{(\text{dpma},2)}$ can provide 96 and 112 orthogonal sequences, respectively, and 64 sequences are randomly chosen from them in the simulation. To achieve an extremely small $P_{\text{fa}} = 10^{-5}$, the threshold value is set to $\beta = \frac{5}{\varphi} \ln 10$ for a given SNR φ and in this case the correct identification probability is

¹ A large minimum CSD ω_{min} is generally required to identify received orthogonal ZC sequences transmitted from transmitters located in various locations in the same cell for RA channel identification. As a result, multiple root ZC sequences are commonly employed for RA requiring a large number of short-length identification sequences under a limited ω_{min} , which can not be obtained through mutual cyclic shifting [2, Section 6.3.3.1]. Therefore, even though all sequences in family $\hat{\mathcal{G}}_{\text{max},I}^{(\text{dpma},\kappa)}$ can not be obtained from cyclically shifting another sequence (in time domain) in the family, the sequences can be used for RA channel identification.



equivalent to $P_c = 10^{-5/(1+\varphi\sigma_{\tilde{\epsilon}}^2)}$. For the SNR range demonstrated in Fig. 1, $1 - P_c$ falls in the ranges $[8.85 \times 10^{-4}, 8.42 \times 10^{-2}]$, $[8.67 \times 10^{-4}, 8.25 \times 10^{-2}]$, and $[8.65 \times 10^{-4}, 8.23 \times 10^{-2}]$ for TDL-B UMI-SC, TDL-B IND, and FF channel profiles, respectively. Due to the adoption of nonorthogonal sequences, RA channel identification suffers from large FIE (i.e., larger $\sigma_{\text{fie}}^2(i, k)$) and thus entails serious false identification for the systems using ZC, YL, and PN sequence families. On the contrary, false identification is less severe for the systems using orthogonal sequence families $\hat{\mathcal{G}}_{\max, \bar{l}}^{(\text{dpma}, 2)}$ and $\hat{\mathcal{G}}_{\max, \bar{l}}^{(\text{adpma}, 1)}$, particularly in the multipath channels exhibiting larger coherence bandwidths.

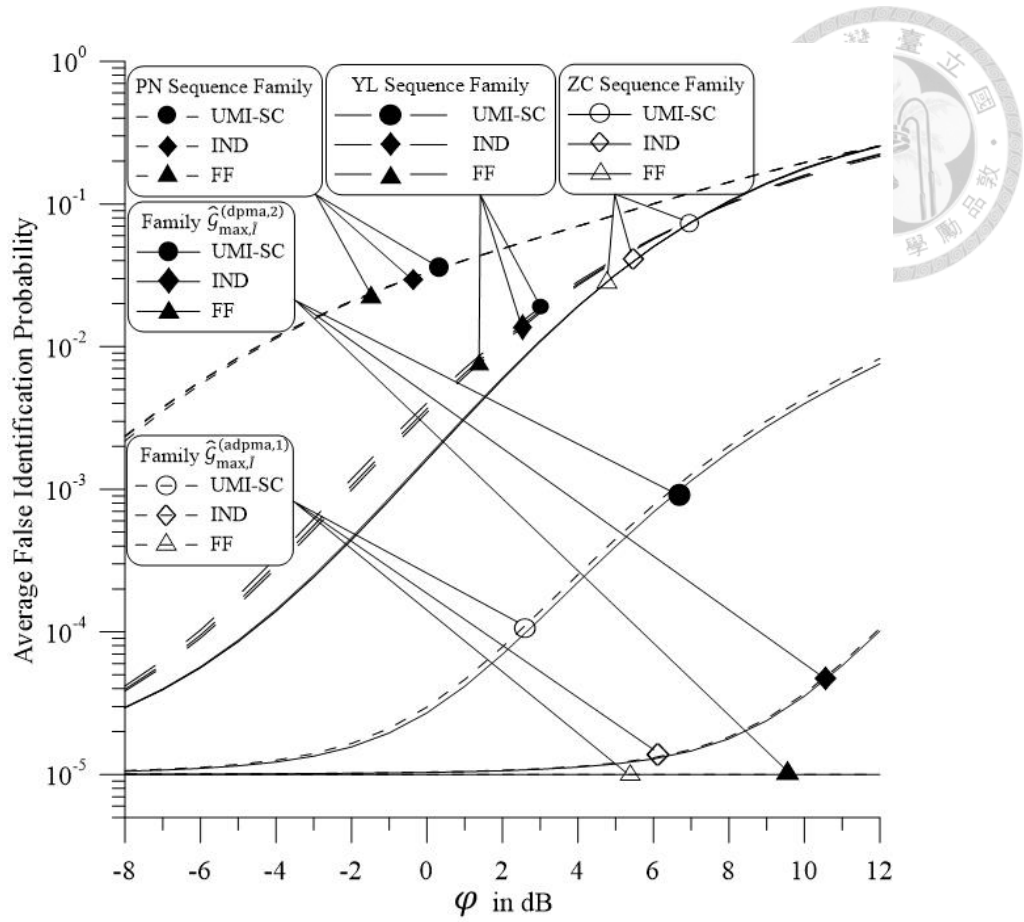


Fig. 1. The characteristics of the average false identification probability versus SNR among the RA channel identification systems using various sequence families under TDL-B UMI-SC short-delay channel profile, TDL-B IND short-delay channel profile, and FF channel profile with K -factor of $K = 0$.

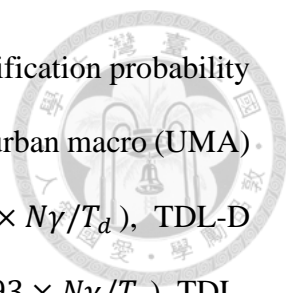


Fig. 2 demonstrates the characteristics of the average false identification probability versus SNR φ under three Rician channel profiles, namely TDL-D urban macro (UMA) normal-delay profile (exhibiting $\sigma_{\text{rms}} = 363$ ns and $B_c \approx 0.52 \times N\gamma/T_d$), TDL-D UMI-SC short-delay profile (exhibiting $\sigma_{\text{rms}} = 65$ ns and $B_c \approx 2.93 \times N\gamma/T_d$), TDL-D IND short-delay profile (exhibiting $\sigma_{\text{rms}} = 20$ ns and $B_c \approx 9.54 \times N\gamma/T_d$) in [42, Section 7.7.2]. TDL-D channel profile is a Rician channel profile with K -factor of $K = 13.3$ dB. Notably, the UMA normal-delay profile exhibits a longer delay spread than the UMI-SC and IND short-delay profile, and thus results in a smaller coherence bandwidth. The demonstration in Fig. 2 uses the same sequence families as Fig. 1. Similar performance trends to those in Fig. 1 can be observed for these systems operating over Rician multipath channels. For the SNR range demonstrated in Fig. 2, $1 - P_c$ falls in the ranges $[1.11 \times 10^{-16}, 7.27 \times 10^{-8}]$, $[2.25 \times 10^{-12}, 3.11 \times 10^{-6}]$, and $[1.14 \times 10^{-11}, 5.9 \times 10^{-6}]$ for TDL-D UMA normal-delay profile, UMI-SC short-delay profile, and TDL-D IND short-delay profiles, respectively.

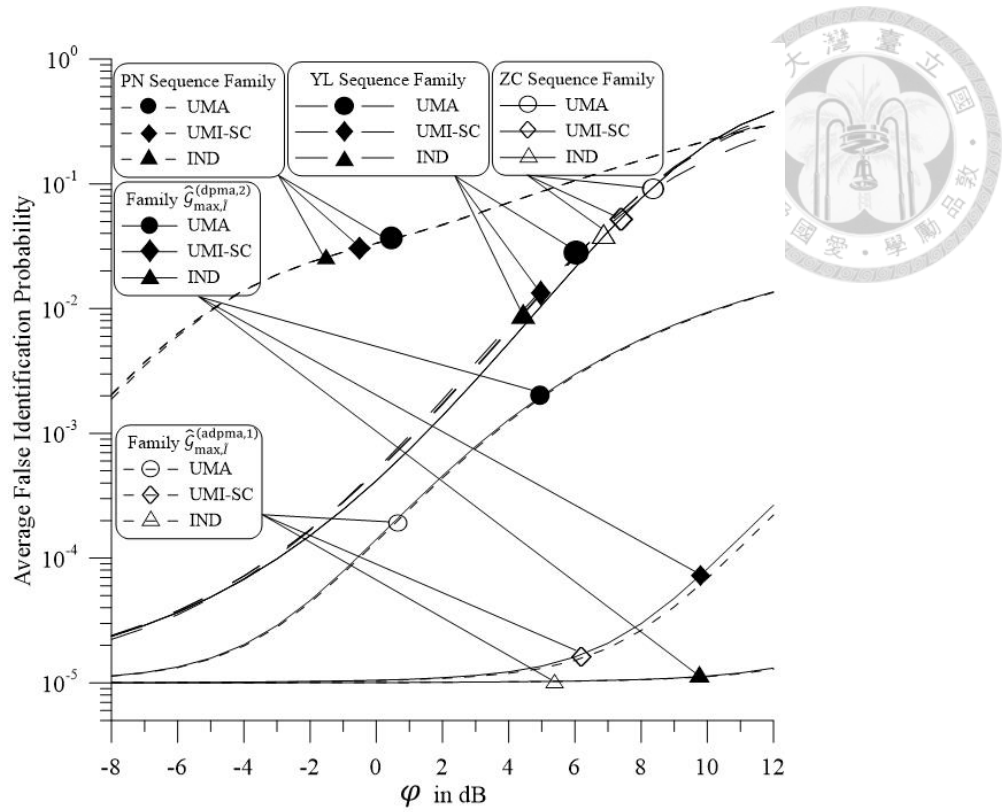


Fig. 2. The characteristics of the average false identification probability versus SNR among the RA channel identification systems using various sequence families under TDL-D UMA normal-delay profile, TDL-D UMI-SC short-delay profile, and TDL-D IND short-delay profile with K -factor of $K = 13.3\text{dB}$.

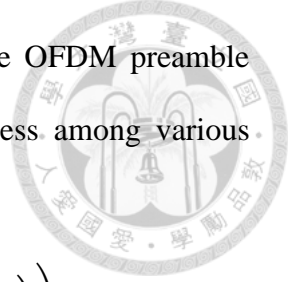


Fig. 3 compares the spectral compactness characteristics of all the OFDM preamble waveforms adopted in Fig. 1. To compare the spectral compactness among various waveforms, the average out-of-band power fraction is defined as

$$\eta \triangleq 10 \log_{10} \left(\frac{1}{J} \sum_{i \in \mathcal{Z}_J} \left(\int_{|f| > \frac{B}{2}} S_B^{(i)}(f) df / \int_{-\infty}^{\infty} S_B^{(i)}(f) df \right) \right) \quad (17)$$

where $S_B^{(i)}(f)$ is the baseband power spectrum of the waveform carrying \mathbf{q}_i [9]. The results on η are presented with respect to the normalized bandwidth $BT_d/(\gamma N)$. For a predetermined η (say -50 dB), the smaller the required bandwidth, the higher the spectral compactness. As shown, preamble waveforms carrying order- \tilde{I} CA sequence families $\hat{\mathcal{G}}_{\max, \tilde{I}}^{(\text{adpma}, 1)}$ (yielding sidelobe-decaying order $\tilde{I} \geq 2$) and $\hat{\mathcal{G}}_{\max, \tilde{I}}^{(\text{dpma}, 2)}$ (yielding sidelobe-decaying order $\tilde{I} \geq 1$) can provide much higher spectral compactness than preamble waveforms carrying ZC, YL, PN sequence families.

The average PAPR is defined as [9, eq. 22]

$$\text{PAPR} = 10 \log_{10} \left(\frac{1}{J} \sum_{i \in \mathcal{Z}_J} \frac{\max_{n \in \mathcal{Z}_{\gamma N}} \left| \tilde{s}^{(i)} \left(-\frac{T_d}{2} + \frac{nT_d}{\gamma N} \right) \right|^2}{\frac{1}{\gamma N} \sum_{n \in \mathcal{Z}_{\gamma N}} \left| \tilde{s}^{(i)} \left(-\frac{T_d}{2} + \frac{nT_d}{\gamma N} \right) \right|^2} \right) \quad (18)$$

where $\tilde{s}^{(i)}(t) = s_k^{(i)}(t) \exp\{-j2\pi f_c t\}$ is the baseband version of $s_k^{(i)}(t)$ by shifting center frequency down by $f_c \triangleq f_0 + \frac{(N-1)\gamma/2 + \kappa^{(k)}}{T_d}$. Here, $s_k^{(i)}(t - T^{(k)})$ is the component waveform carrying \mathbf{q}_i on the k -th training block interval defined in [9, eq. (1)], f_0 is a reference frequency with $f_0 \gg \gamma N/T_d$, and $\kappa^{(k)}$ is the index offset with $\kappa^{(k)} \in \mathcal{Z}_{\gamma}$. Deterministic average PAPR for the sequence families with the parameter adopted in Fig. 1 are demonstrated in Table IX. It is noticed that family $\hat{\mathcal{G}}_{\max, \tilde{I}}^{(\text{dpma}, 2)}$ and $\hat{\mathcal{G}}_{\max, \tilde{I}}^{(\text{adpma}, 1)}$ offer higher waveform PAPR than ZC, YL, and PN sequence families. Thus,

high PAPR turns out to be a major trade-off for the proposed order- I CA sequence families in order to achieve high spectral compactness.

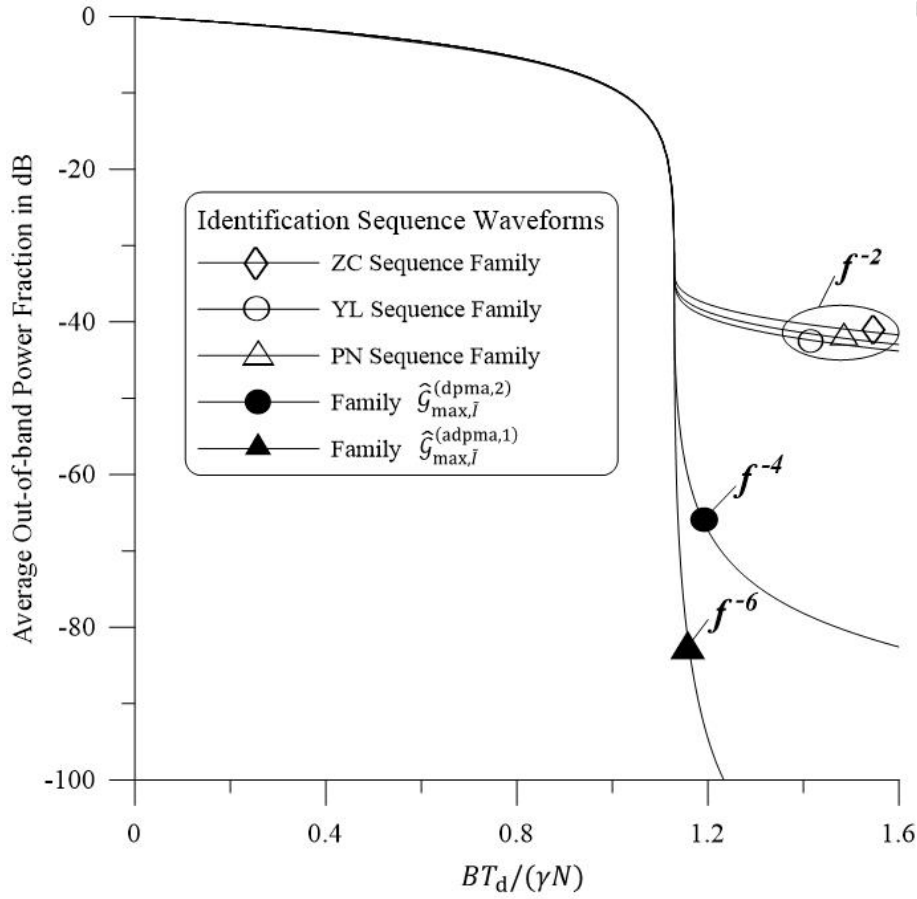
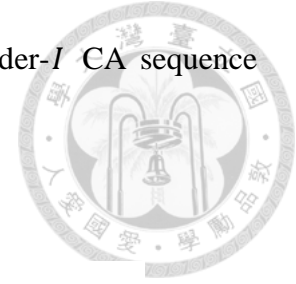


Fig. 3. Average out-of-band power fraction characteristics for OFDM preamble waveforms carrying various CA sequence families.

Table IX

Average PAPR for OFDM preamble waveforms using various sequence families.

Sequence Family	ZC Sequence Family	YL Sequence Family	PN Sequence Family	Family $\hat{\mathcal{G}}_{\max,I}^{(\text{adpma},1)}$	Family $\hat{\mathcal{G}}_{\max,I}^{(\text{dpma},2)}$
Average PAPR	3.93 dB	4.1 dB	7.86 dB	20.16 dB	20.68 dB

Chapter 6

Simultaneous Channel Estimation



6.1 Scenario for Simultaneous Channel Estimation

Consider the uplink MIMO channel sounding scenario that the k -th antenna among a total of K transmit antennas emits the k -th sequence \mathbf{q}_k in a family of J CA sequences $\{\mathbf{q}_l; l \in \mathcal{Z}_J\}$ with $J \geq K$, for the purpose of sounding the uplink channels from the k -th transmit antenna to M receive antennas at the BS receiver [1]-[2], [14], [24], [44]-[48]. In the asynchronously- received sounding intervals of length T , these K transmit antennas send respective rectangularly-pulsed OFDM sounding waveforms, each carrying its respective sounding sequence of N complex symbols. Specifically, N symbols in a sounding sequence are modulated at each transmit antenna site into N uniformly-spaced subcarriers at subcarrier positions $0, \gamma, 2\gamma, \dots, (N-1)\gamma$, which are interleaved among γN subcarriers with the interleaving factor γ . Each sounding time interval can be essentially partitioned into a guard CP subinterval of length T_g followed by a useful sounding subinterval of length $T_d = T - T_g$. To ensure accurate channel estimation in respective SISO channels, \mathbf{q}_k is restricted to have CA symbols with $|q_k[n]|^2 = 1/N$, and thus its inverse DFT $\tilde{\mathbf{q}}_k$ possesses the ZAC property. Within the system setup, the discrete-time sequence transmitted by the k -th transmit antenna contains the n -th entry $\tilde{q}_k \left[\binom{(n)}{N} \right]$ for $n \in \mathcal{Z}_{\gamma N}$ in its useful sounding subinterval.

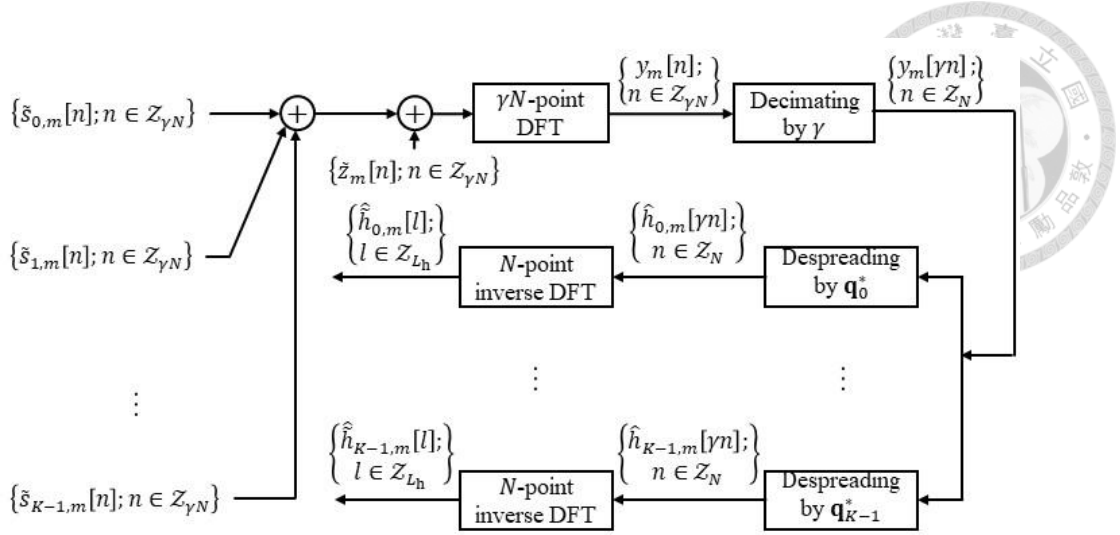
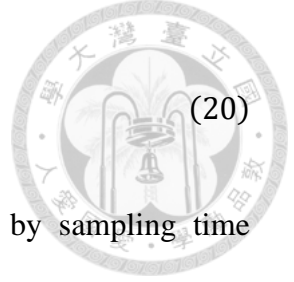


Fig. 4. Simultaneous channel estimation system at the m -th receive antenna.

6.1.1 SCE System

Fig. 4 depicts the considered baseband equivalent SCE system at the m -th receive antenna. After down conversion, sampling at a rate $\gamma N/T_d$, time/frequency synchronization, and guard removal, K (time-domain) baseband signals $\{\tilde{s}_{k,m}[n]; n \in \mathcal{Z}_{\gamma N}\}$ for all $k \in \mathcal{Z}_K$ are extracted simultaneously in a local useful sounding subinterval of length T_d at the m -th receive antenna. Denote $\{\tilde{h}_{k,m}^{(t)}[i]; i \in \mathcal{Z}_N\}$ as the *true* discrete-time channel impulse response (CIR) with at most $L^{(t)}$ paths for all antenna pairs (k, m) , where $\tilde{h}_{k,m}^{(t)}[i] = 0$ for $i \in \mathcal{Z}_N - \mathcal{Z}_{L^{(t)}}$. When all baseband signals are extracted with timing offsets $\tau_{k,m} \in \mathcal{Z}_{\omega_{\min} - L^{(t)}}$ where ω_{\min} is the required minimum CSD and $L^{(t)} < \omega_{\min} \leq \alpha \gamma N$ is assumed throughout, the received baseband signal $\{\tilde{s}_{k,m}[n]; n \in \mathcal{Z}_{\gamma N}\}$ transmitted from the k -th antenna can be modeled as [7, eq. 9]

$$\tilde{s}_{k,m}[n] = \sum_{i \in \mathcal{Z}_{L^{(t)}}} \tilde{q}_k \left[\left((n - \tau_{k,m} - i) \right)_N \right] \tilde{h}_{k,m}^{(t)}[i] \quad (19)$$



$$= \sum_{l=\tau_{k,m}}^{\tau_{k,m}+L^{(t)}-1} \tilde{q}_k \left[\left((n-l) \right)_N \right] \tilde{h}_{k,m}[l]. \quad (20)$$

For each $k \in \mathcal{Z}_K$, $\tau_{k,m}$ is the discrete time offset (normalized by sampling time $T_d/(\gamma N)$) between the local and the received k -th useful sounding subintervals. Under the time synchronization mechanism adopted by the cellular network [1]-[2], [14], [24], [44]-[48], all offsets $\tau_{k,m}$ are not necessarily synchronized to zeros but required to lock into the uncertainty range $\tau_{k,m} \in \mathcal{Z}_{\omega_{\min}-L^{(t)}}$.^{1.5.3} In this case, $\tilde{s}_{k,m}[n]$ is alternatively modeled by (20) where $\{\tilde{h}_{k,m}[l]; l \in \mathcal{Z}_L\}$ represents the *effective* discrete-time CIR which has at most L paths with $L = \omega_{\min}$ and $\tilde{h}_{k,m}[l] \triangleq \tilde{h}_{k,m}^{(t)} \left[\left((l - \tau_{k,m}) \right)_N \right]$. As indicated by (20), the k -th discrete-time sequence $\{\tilde{q}_k \left[\left((n) \right)_N \right], n \in \mathcal{Z}_{\gamma N}\}$ is received after the dispersion by $\{\tilde{h}_{k,m}[l]; l \in \mathcal{Z}_L\}$ in the local useful sounding subinterval. Since all time offsets $\tau_{k,m}$ are uncertain, the effective CIR $\{\tilde{h}_{k,m}[l]; l \in \mathcal{Z}_L\}$ having at most $L^{(t)}$ nonzero path responses are essentially estimated by SCE.

With (20), the received (time-domain) baseband signal at the m -th antenna $\{\tilde{y}_m[n]; n \in \mathcal{Z}_{\gamma N}\}$ is modeled as $\tilde{y}_m[n] = \sum_{k \in \mathcal{Z}_K} \tilde{s}_{k,m}[n] + \tilde{z}_m[n]$ in the local useful sounding subinterval, where $\{\tilde{z}_m[n]; n \in \mathcal{Z}_{\gamma N}\}$ contains independent and identically distributed (i.i.d.) circularly symmetric complex Gaussian (CSCG) noise samples $\tilde{z}_m[n]$ having mean zero and noise power $1/\varphi$. The SCE system first takes the γN -point DFT of $\{\tilde{y}_m[\tilde{n}]; \tilde{n} \in \mathcal{Z}_{\gamma N}\}$ and obtains $\{y_m[n]; n \in \mathcal{Z}_{\gamma N}\}$ with $y_m[n] = \sum_{\tilde{n} \in \mathcal{Z}_{\gamma N}} \tilde{y}_m[\tilde{n}] \omega_{\gamma N}^{n\tilde{n}}$. Then, $\{y_m[n]; n \in \mathcal{Z}_{\gamma N}\}$ is decimated by a factor γ to yield the observable set $\{y_m[\gamma n]; n \in \mathcal{Z}_N\}$, which contains the complete information of all sounding sequences $\mathbf{q}_0, \mathbf{q}_1, \dots, \mathbf{q}_{K-1}$ [16]. Specifically, $y_m[\gamma n]$ is modeled as

$$y_m[\gamma n] = \gamma\sqrt{N} \sum_{k \in \mathcal{Z}_K} q_k[n] h_{k,m}[\gamma n] + z_m[\gamma n]. \quad (21)$$

Here, the noise samples $\{z_m[\gamma n]; n \in \mathcal{Z}_N\}$ for all $m \in \mathcal{Z}_M$ are i.i.d. CSCG with mean zero and noise power $\mathcal{E}\{|z_m[\gamma n]|^2\} = \gamma N / \varphi$. For the channel from the k -th transmit antenna to the m -th receive antenna, $\{h_{k,m}[\gamma n]; n \in \mathcal{Z}_N\}$ is the channel frequency response (CFR) on N uniformly-spaced subcarriers at subcarrier positions $0, \gamma, 2\gamma, \dots, (N-1)\gamma$, which is related to the effective CIR $\{\tilde{h}_{k,m}[l]; l \in \mathcal{Z}_L\}$ by the N -point DFT

$$h_{k,m}[\gamma n] = \sum_{l \in \mathcal{Z}_L} \tilde{h}_{k,m}[l] \omega_{\gamma N}^{\gamma n l} \quad (22)$$

$$= \omega_N^{n\tau_{k,m}} \sum_{i \in \mathcal{Z}_L^{(t)}} \tilde{h}_{k,m}^{(t)}[i] \omega_N^{ni}. \quad (23)$$

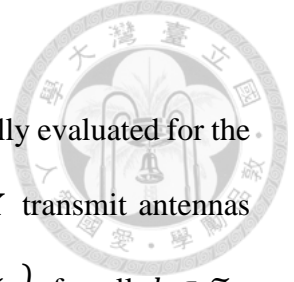
Operating on $\{y_m[\gamma n]; n \in \mathcal{Z}_N\}$, the simultaneous estimation of K effective CIRs $\{\tilde{h}_{k,m}[l]; l \in \mathcal{Z}_L\}$ is conducted in two steps. At the first step, the approximate least-square estimates of K CFRs $\{h_{k,m}[\gamma n]; n \in \mathcal{Z}_N\}$ are formed by despreading $\{y_m[\gamma n]; n \in \mathcal{Z}_N\}$ respectively with K identification sequences \mathbf{q}_k [24], [44]-[46] as

$$\hat{h}_{k,m}[\gamma n] = \gamma^{-1} \sqrt{N} q_k^*[n] y_m[\gamma n] \quad (24)$$

for $n \in \mathcal{Z}_N$ and $k \in \mathcal{Z}_K$. Second, K effective CIR estimates $\{\hat{\tilde{h}}_{k,m}[l]; l \in \mathcal{Z}_L\}$ are made by taking the (N -point) inverse DFT of $\{\hat{h}_{k,m}[\gamma n]; n \in \mathcal{Z}_N\}$ respectively for all $k \in \mathcal{Z}_K$, as

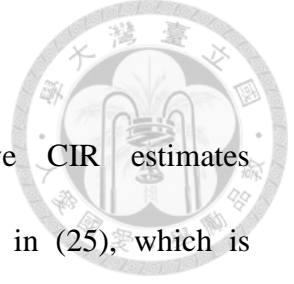
$$\hat{\tilde{h}}_{k,m}[l] = \frac{1}{N} \sum_{n \in \mathcal{Z}_N} \hat{h}_{k,m}[\gamma n] \omega_N^{-nl}, \quad l \in \mathcal{Z}_L. \quad (25)$$

This enables SCE for MK MIMO channels.



6.2 Performance Analysis

Here, the estimation performance of the SCE system is analytically evaluated for the following MIMO multipath channel. For the uplink MIMO with K transmit antennas and M receive antennas, there are MK true CIRs $\{\tilde{h}_{k,m}^{(t)}[i]; i \in \mathcal{Z}_N\}$ for all $k \in \mathcal{Z}_M$ and $m \in \mathcal{Z}_M$, each following the Rician multipath model. For a given antenna pair (k, m) , each CIR consists of one direct path response $\tilde{h}_{k,m}^{(t)}[0]$ and $L^{(t)} - 1$ diffuse path responses $\tilde{h}_{k,m}^{(t)}[i]$ for all $i \in \mathcal{Z}_{L^{(t)}-1}^+$, followed by zero path responses $\tilde{h}_{k,m}^{(t)}[i] = 0$ for all $i \in \mathcal{Z}_N - \mathcal{Z}_{L^{(t)}}$. All path responses are modeled to be independent CSCGs having means $\mathcal{E}\{\tilde{h}_{k,m}^{(t)}[0]\} = \tilde{\sigma}_{k,m} \exp\{j\theta_{k,m}\}$ and $\mathcal{E}\{\tilde{h}_{k,m}^{(t)}[i]\} = 0$ for $i \in \mathcal{Z}_{L^{(t)}-1}^+$, and correlations $\mathcal{E}\left\{\left(\tilde{h}_{k,m}^{(t)}[i] - \mathcal{E}\{\tilde{h}_{k,m}^{(t)}[i]\}\right)^2\right\} = 0$ and $\mathcal{E}\left\{\left|\tilde{h}_{k,m}^{(t)}[i] - \mathcal{E}\{\tilde{h}_{k,m}^{(t)}[i]\}\right|^2\right\} = \sigma_{k,m}^2[i]$ for $i \in \mathcal{Z}_{L^{(t)}}$, where $\theta_{k,m}$ is an arbitrary phase, $\tilde{\sigma}_{k,m}^2$ is the direct path power, and $\sigma_{k,m}^2[i]$ is the i -th diffuse path power for the CIR $\{\tilde{h}_{k,m}^{(t)}[i]; i \in \mathcal{Z}_{L^{(t)}}\}$. All path responses for all antenna pairs are mutually independent and also independent of all noise samples $\{z_m[\gamma n]; m \in \mathcal{Z}_M, n \in \mathcal{Z}_N\}$. Under such MIMO channel modeling, the received channel power for antenna pair (k, m) is given by $\zeta_{k,m} = \tilde{\sigma}_{k,m}^2 + \sum_{i \in \mathcal{Z}_{L^{(t)}}} \sigma_{k,m}^2[i]$. Further, provided with the minimum CSD ω_{\min} and time offsets $\tau_{k,m} \in \mathcal{Z}_{\omega_{\min} - L^{(t)}}$, effective CIRs $\{\tilde{h}_{k,m}[l]; l \in \mathcal{Z}_L\}$ and CFRs $\{h_{k,m}[\gamma n]; n \in \mathcal{Z}_N\}$ for all antenna pairs can be modeled accordingly with $L = \omega_{\min}$ and $\tilde{h}_{k,m}[l] = \tilde{h}_{k,m}^{(t)}\left[\left((l - \tau_{k,m})\right)_N\right]$. Such effective CIRs $\{\tilde{h}_{k,m}[l]; l \in \mathcal{Z}_L\}$ and CFRs $\{h_{k,m}[\gamma n]; n \in \mathcal{Z}_N\}$ can be also characterized by the root-mean-square (rms) delay spread $\sigma_{\text{rms},k,m} = \left[\mu_{k,m}^{(2)} - \left(\mu_{k,m}^{(1)}\right)^2\right]^{1/2}$ [25, Chapter 4, eq. 36], where $\mu_{k,m}^{(2)} = \sum_{i=1}^{L^{(t)}-1} \left(\frac{iT_d}{\gamma N}\right)^2 \sigma_{k,m}^2[i] / \zeta_{k,m}$ and



$$\mu_{k,m}^{(1)} \sum_{i=1}^{L^{(t)}-1} \left(\frac{iT_d}{\gamma N} \right) \sigma_{k,m}^2 [i] / \varsigma_{k,m}.$$

Operating on $\{y_m[\gamma n]; m \in \mathcal{Z}_M, n \in \mathcal{Z}_N\}$, MK effective CIR estimates $\{\hat{h}_{k,m}[l]; l \in \mathcal{Z}_L\}$ for all $k \in \mathcal{Z}_K$ and $m \in \mathcal{Z}_M$ can be made as in (25), which is rewritten by using (21)-(24) as

$$\begin{aligned} \hat{h}_{k,m}[l] &= \frac{1}{\gamma \sqrt{N}} \sum_{n \in \mathcal{Z}_N} q_k^*[n] y_m[\gamma n] \omega_N^{-nl} \\ &= \tilde{h}_{k,m}[l] + \varrho_{k,m}[l] + \lambda_{k,m}[l]. \end{aligned} \quad (26)$$

In (26), the noise term $\lambda_{k,m}[l] \triangleq \frac{1}{\gamma \sqrt{N}} \sum_{n \in \mathcal{Z}_N} q_k^*[n] z_m[\gamma n] \omega_N^{nl}$ is CSCG with mean zero and noise power $\mathcal{E}\{|\lambda_{k,m}[l]|^2\} = \frac{1}{\gamma \varphi}$. $\rho_{k,m}[l]$ is the ISI term caused by the mismatching between the local identification sequence $q_k[n]$ and the sounding sequences transmitted from other than the k -th transmit antenna, with

$$\varrho_{k,m}[l] \triangleq \sum_{u \in \mathcal{Z}_K, u \neq k} \sum_{s \in \mathcal{Z}_L^{(t)}} \tilde{h}_{u,m}^{(t)}[s] \sum_{n \in \mathcal{Z}_N} q_k^*[n] q_u[n] \omega_N^{n(s-l+\tau_{u,m})}. \quad (27)$$

Given $\tau_{u,m}$, the ISI term $\varrho_{k,m}[l]$ is CSCG with mean

$$\mathcal{E}\{\varrho_{k,m}[l]\} = \sum_{u \in \mathcal{Z}_K, u \neq k} \tilde{\sigma}_{k,m} e^{j\theta_{k,m}} \sum_{n \in \mathcal{Z}_N} q_k^*[n] q_u[n] \omega_N^{n(\tau_{u,m}-l)} \quad (28)$$

$$= \sum_{u \in \mathcal{Z}_K, u \neq k} \tilde{\sigma}_{k,m} e^{j\theta_{k,m}} \sum_{n \in \mathcal{Z}_N} \tilde{q}_k^*[n] \tilde{q}_u \left[\left((n+l-\tau_{u,m}) \right)_N \right] \quad (29)$$

and mean square

$$\begin{aligned} \mathcal{E}\{|\varrho_{k,m}[l]|^2\} &= |\mathcal{E}\{\varrho_{k,m}[l]\}|^2 + \\ &\sum_{u \in \mathcal{Z}_K, u \neq k} \sum_{s \in \mathcal{Z}_L^{(t)}} \sigma_{u,m}^2 [s] \left| \sum_{n \in \mathcal{Z}_N} q_k^*[n] q_u[n] \omega_N^{n(s-l+\tau_{u,m})} \right|^2 \end{aligned} \quad (30)$$

$$= |\mathcal{E}\{q_{k,m}[l]\}|^2 + \sum_{u \in \mathcal{Z}_K, u \neq k} \sum_{s \in \mathcal{Z}_{L(t)}} \sigma_{u,m}^2[s] \left| \sum_{n \in \mathcal{Z}_N} \tilde{q}_k^*[n] \tilde{q}_u \left[\left((n + l - s - \tau_{u,m}) \right)_N \right] \right|^2 \quad (31)$$



Where the equalities (29) and (31) come from Parseval's relation. With $L = \omega_{\min}$, the cyclic shifts $l - \tau_{u,m}$ in (29) and $l - s - \tau_{u,m}$ in (31) meet the restriction $|l - \tau_{u,m}| < \omega_{\min}$ and $|l - s - \tau_{u,m}| < \omega_{\min}$. As indicated by (29) and (31) together with the latter restriction, the effect of ISI vanishes when all time-domain sequences in $\{\tilde{\mathbf{q}}_k; k \in \mathcal{Z}_K\}$ can be cyclically shifted to each other by a CSD not smaller than ω_{\min} , e.g., the sequences obtained from cyclically-shiftable ZC sequence family, YL sequence family, and CS sequence subfamily $\mathcal{G}_{\max, \bar{l}}^{(\text{cs}, 4)}(\mathbf{q}_{\text{lead}})$, all meeting the minimum CSD constraint. When all sequences in $\{\mathbf{q}_k; k \in \mathcal{Z}_K\}$ are mutually orthogonal but not necessarily cyclically shiftable (e.g., the sequences obtained from an orthogonal sequence family $\mathcal{G}_{\max, \bar{l}}^{(\text{dpma}, \kappa)}$), all ISI terms in $\{q_{k,m}[l + \tau_{u,m}]; l \in \mathcal{Z}_{L(t)}\}$, which disturb the estimation of all nonzero path responses $\{\tilde{h}_{k,m}[l + \tau_{u,m}]; l \in \mathcal{Z}_{L(t)}\}$ for each antenna pair (k, m) , yield $|\mathcal{E}\{q_{k,m}[\tau_{u,m}]\}|^2 = 0$ and $\mathcal{E}\{|q_{k,m}[s + \tau_{u,m}]|^2\} = 0$ for $s \in \mathcal{Z}_{L(t)}$ and are thus suppressed remarkably. However, when the sequences in $\{\mathbf{q}_k; k \in \mathcal{Z}_K\}$ are not all orthogonal mutually, the ISI terms disturb the effective CIR estimation significantly.

The estimation performance provided by all CIR estimates $\hat{h}_{k,m}[l]$ is characterized by the average MSE [45] as

$$\begin{aligned} \sigma_{\text{ave}}^2 &\triangleq \frac{1}{MK} \sum_{m \in \mathcal{Z}_M} \sum_{k \in \mathcal{Z}_K} \sum_{l \in \mathcal{Z}_L} \mathcal{E} \left\{ \left| \hat{h}_{k,m}[l] - \tilde{h}_{k,m}[l] \right|^2 \right\} \\ &= \frac{1}{MK} \sum_{m \in \mathcal{Z}_M} \sum_{k \in \mathcal{Z}_K} \sum_{l \in \mathcal{Z}_L} \mathcal{E} \left\{ |q_{k,m}[l] + \lambda_{k,m}[l]|^2 \right\}. \end{aligned}$$

since $q_{k,m}[l]$ is independent of $\lambda_{k,m}[l]$. σ_{ave}^2 is derived as

$$\sigma_{\text{ave}}^2 = \frac{1}{MK} \sum_{m \in \mathcal{Z}_M} \sum_{k \in \mathcal{Z}_K} \sum_{l \in \mathcal{Z}_L} \varepsilon \left\{ |e_{k,m}[l]|^2 \right\} + \frac{L}{\gamma\varphi}. \quad (32)$$



Using (30)-(31) in (32), the average MSE performance can be numerically evaluated for SCE over independent Rician multipath channels.

6.3 Performance Results

The performance characteristics of the average MSE versus the total number of transmit antennas are demonstrated in Figs. 4-5 for the SCE systems using ZC, YL, PN, and modified PMA sequence family in Table VI(b) which operate over uplink MIMO multipath channels exhibiting exponentially decaying path power profiles. Specifically, the path power profiles are characterized by factors $K_{k,m}^{(h)}$ and $D_{k,m}$. Here, $K_{k,m}^{(h)}$ is the ratio of direct power to diffuse power sum (i.e., $K_{k,m}^{(h)} = \tilde{\sigma}_{k,m}^2 / \sum_{l \in \mathcal{Z}_{L(t)}} \sigma_{k,m}^2[l]$), making $\tilde{\sigma}_{k,m}^2 = \varsigma_{k,m} K_{k,m}^{(h)} / (K_{k,m}^{(h)} + 1)$ and $\sum_{l \in \mathcal{Z}_{L(t)}} \sigma_{k,m}^2[l] = \varsigma_{k,m} / (K_{k,m}^{(h)} + 1)$. $D_{k,m}$ is an exponential decaying factor used to specify $\sigma_{k,m}^2[l] = C_{k,m} \exp\{-l/D_{k,m}\}$ for $l \in \mathcal{Z}_{L(t)}$ with the normalization $C_{k,m} = \varsigma_{k,m} / \left[(K_{k,m}^{(h)} + 1) \sum_{l \in \mathcal{Z}_{L(t)}} \exp\{-l/D_{k,m}\} \right]$. In the demonstration, we fix $\varsigma_{k,m} = 1$, $K_{k,m}^{(h)} = K^{(h)}$, $D_{k,m} = D$, and $\sigma_{\text{rms},k,m} = \sigma_{\text{rms}}$ for all $k \in \mathcal{Z}_K$ and all $m \in \mathcal{Z}_M$. Under this setup, φ is the received signal to noise power ratio (SNR).

Table X lists the considered system and channel parameters, where a particular system setup in 5G-NR [2, Section 6.4.1.4.1] is followed. To calculate (32), all discrete time offsets $\tau_{k,m}$ for all $k \in \mathcal{Z}_K$ and all $m \in \mathcal{Z}_M$ are randomly selected in the uncertainty range $\tau_{k,m} \in \mathcal{Z}_{L-L(t)}$, and the average MSE results are obtained by simulating all offsets $\tau_{k,m}$ for 1000 trials and averaging the calculated σ_{ave}^2 values from all trials.

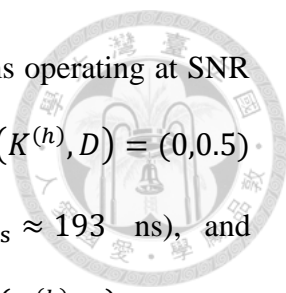


Fig. 5 shows the performance characteristics of all SCE systems operating at SNR $\varphi = 35$ dB over three Rayleigh multipath channels with $(K^{(h)}, D) = (0, 0.5)$ (exhibiting $\sigma_{\text{rms}} \approx 48$ ns), $(K^{(h)}, D) = (0, 2)$ (exhibiting $\sigma_{\text{rms}} \approx 193$ ns), and $(K^{(h)}, D) = (0, 10)$ (exhibiting $\sigma_{\text{rms}} \approx 260$ ns). These sets for $(K^{(h)}, D)$ result in similar σ_{rms} values to the three TDL-B channel profiles in 5G-NR with maximum delay time spreads $T_{\text{max}} \approx 2 \times T_d/(\gamma N)$, $T_{\text{max}} \approx 8 \times T_d/(\gamma N)$, and $T_{\text{max}} \approx 11 \times T_d/(\gamma N)$, respectively [42, Section 7.7.2]. As shown, the performance characteristics are less sensitive to channel delay spread for a fixed true CIR length $L^{(t)}$ as long as all time offsets $\tau_{k,m}$ are well restricted to $\tau_{k,m} \in \mathcal{Z}_{L-L^{(t)}}$. Due to serious ISI caused by K nonorthogonal sequences, the system using the PN sequence family provides the worst average MSE. When $K < 12$, the systems using ZC, YL, and $\mathcal{G}_{\text{max},l}^{(\text{dpma},4)}$ sequence families operate without ISI and provide the best average MSE due to the adoption of K cyclically-shiftable CA sequences (see (29) and (31)). When $K = 12$, such advantage remains with the systems using ZC and YL sequences, but vanishes for the system using $\mathcal{G}_{\text{max},l}^{(\text{dpma},4)}$ since ISI occurs from the adoption of one more orthogonal sequence from a second CS subfamilies $\mathcal{G}_{\text{max},l}^{(\text{cs},4)}(\mathbf{q}_{\text{lead}})$. When $K > 12$, all systems using ZC, YL, and $\mathcal{G}_{\text{max},l}^{(\text{dpma},4)}$ sequence families suffer from ISI due to the use of some pairs of CA sequences which are not cyclically shiftable to each other. The ISI effect gets worse as K is larger since there are more of such CA sequence pairs. Nevertheless, the system using family $\mathcal{G}_{\text{max},l}^{(\text{dpma},4)}$ outperforms all the other systems significantly for $K > 12$, due to the use of orthogonal sequences.

TABLE X
A SCE System and Channel Parameters.

Sequence Length N	144
Subcarrier Spacing $\Delta f = 1/T_d$	15 kHz
Interleaved Length γ	4
Guard Ratio α	9/128
Number of Receive Antennas M	64
Minimum CSD ω_{\min} ($L = \omega_{\min}$)	12
True CIR Length $L^{(t)}$	8
Effective CIR Length L	12

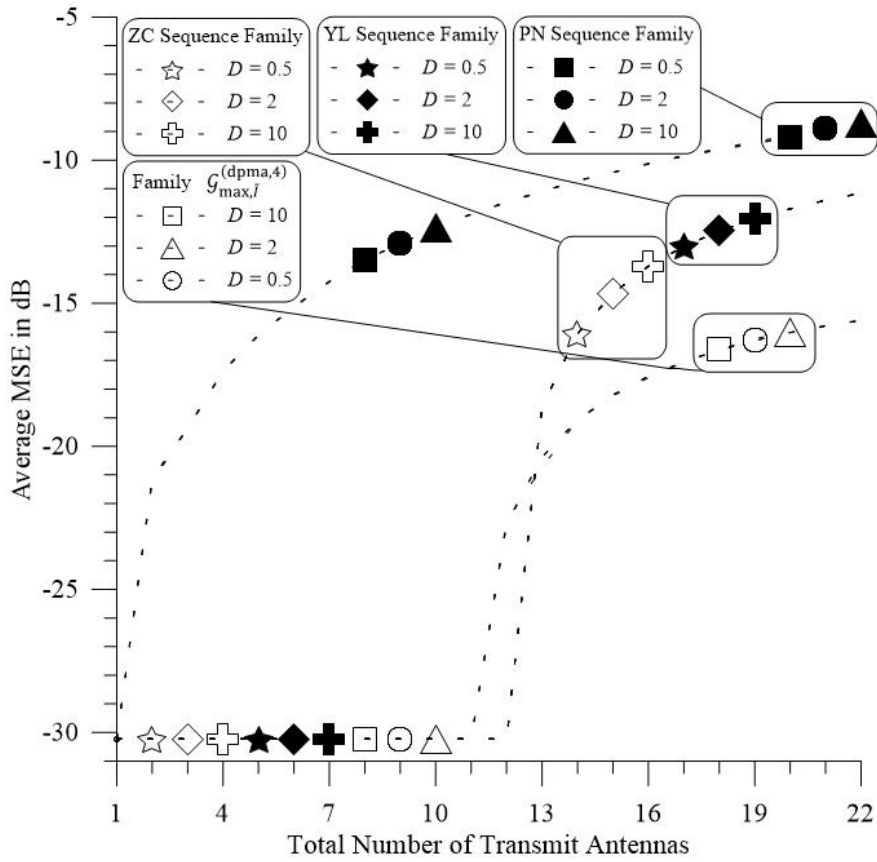


Fig. 5. The characteristics of the average MSE versus the total number of transmit antennas among the simultaneous MIMO channel estimation using various sequence families under Rayleigh multipath channels with $L^{(t)} = 8$, $\varphi = 35$ dB, $K^{(h)} = 0$, and various D .

Fig. 6 shows the performance characteristics of all SCE systems operating at SNR $\varphi = 35$ dB and over three Rician multipath channels with $(K^{(h)}, D) = (10, 0.5)$ (exhibiting $\sigma_{\text{rms}} \approx 15$ ns), $(K^{(h)}, D) = (10, 2)$ (exhibiting $\sigma_{\text{rms}} \approx 73$ ns), and $(K^{(h)}, D) = (10, 10)$ (exhibiting $\sigma_{\text{rms}} \approx 126$ ns). Similar performance trends to those in Fig. 5 can be observed for these systems operating over Rician multipath channels. Due to the strong leading path response (having a large $K^{(h)}$), the SCE system using family $\mathcal{G}_{\text{max}, \bar{l}}^{(\text{dpma}, 4)}$ provides the better performance in the Rician multipath channel than in the Rayleigh multipath channel.

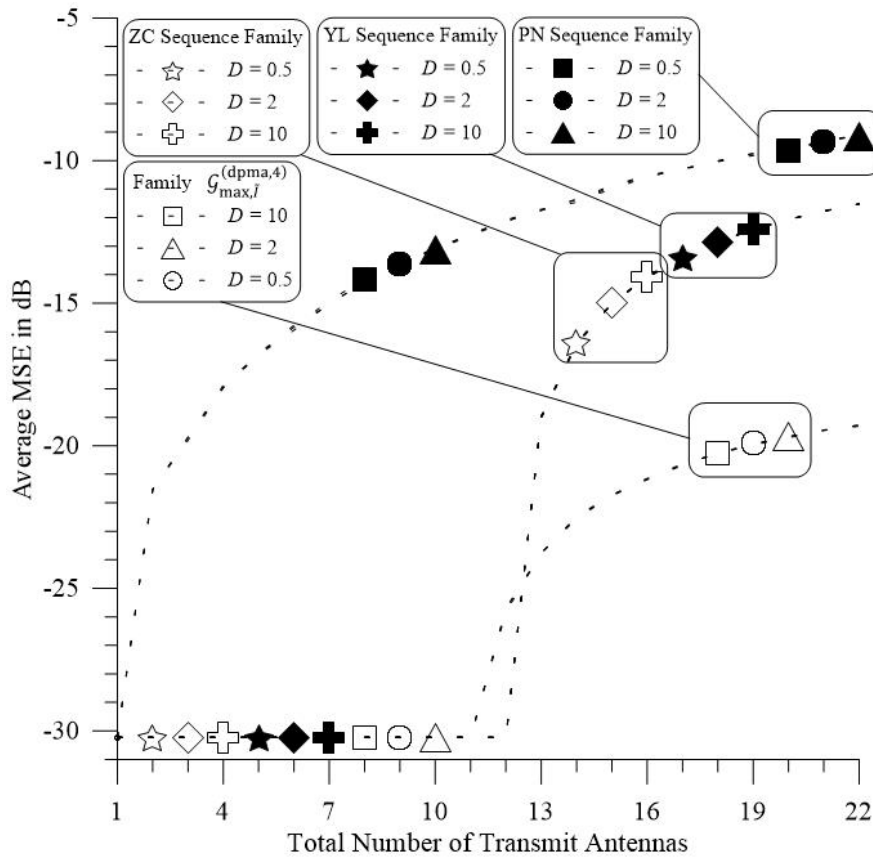


Fig. 6. The characteristics of the average MSE versus the total number of transmit antennas among the simultaneous MIMO channel estimation using various sequence families under Rician multipath channels with $L^{(t)} = 8$, $\varphi = 35$ dB, $K^{(h)} = 10$, and various D .

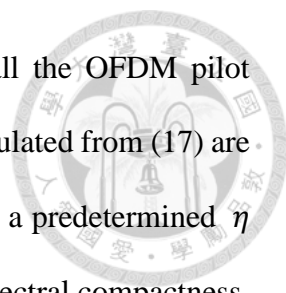


Fig. 7 compares the spectral compactness characteristics of all the OFDM pilot waveforms (with $K = J$) adopted in Figs. 4-5. The results on η calculated from (17) are presented with respect to the normalized bandwidth $BT_d/(\gamma N)$. For a predetermined η (say -40 dB), the smaller the required bandwidth, the higher the spectral compactness. As shown, pilot waveforms carrying order- \tilde{I} CA sequence family $\mathcal{G}_{\max, \tilde{I}}^{(\text{dpma}, 4)}$ (yielding sidelobe-decaying order $\tilde{I} \geq 1$) can provide much higher spectral compactness than pilot waveforms carrying ZC, YL, PN sequence families.

Deterministic average PAPR for the sequence families with the parameter adopted in Fig. 5 are calculated from (18) and demonstrated in Table XI. It is noticed that family $\mathcal{G}_{\max, I}^{(\text{dpma}, 4)}$ offer higher waveform PAPR than ZC, YL, and PN sequence families. Thus, high PAPR turns out to be a major trade-off for the proposed order- I CA sequence families in order to achieve high spectral compactness.

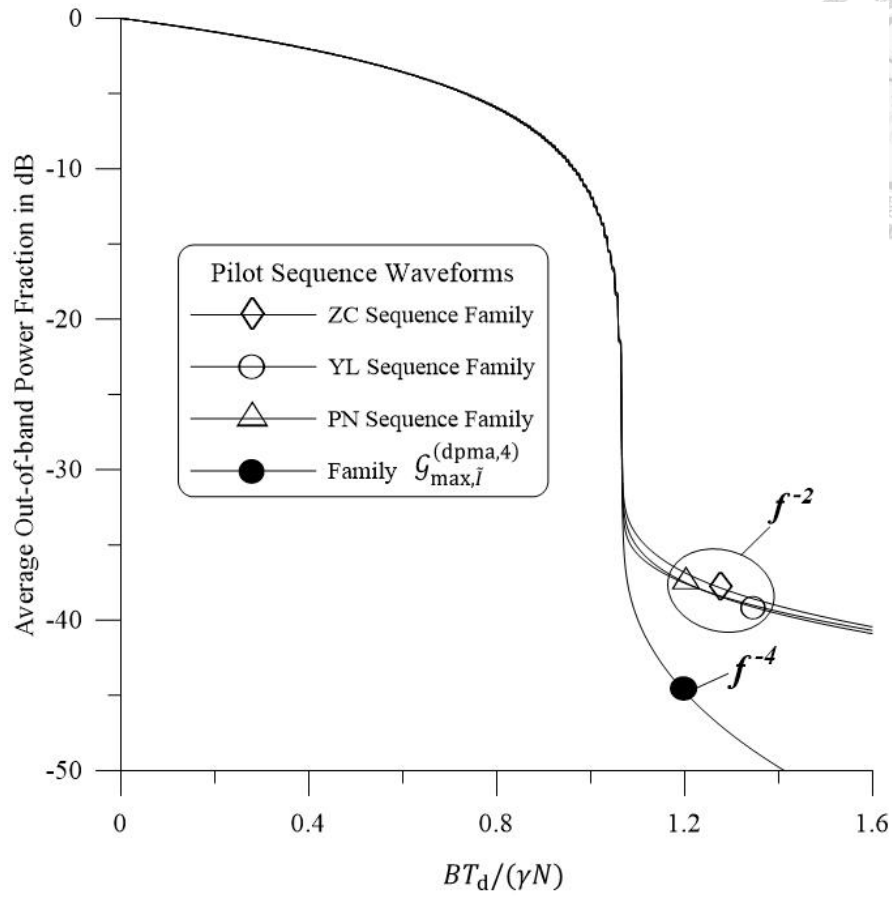


Fig. 7. Average out-of-band power fraction characteristics for OFDM preamble waveforms carrying various CA sequence families.

Table XI

Average PAPR of OFDM pilot waveforms using various sequence families.

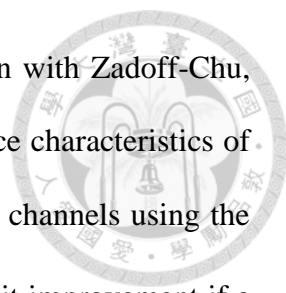
Sequence Family	ZC Sequence Family	YL Sequence Family	PN Sequence Family	Family $\mathcal{G}_{\max, \bar{l}}^{(\text{dpma}, 4)}$
Average PAPR	3.2 dB	3.08 dB	5.95 dB	20.25 dB

Chapter 7

Conclusion



Several modified PMA sequence families are constructed in the paper to provide more orthogonal order- I CA sequences for RA applications and SCE estimation (i.e. SPI applications), while facilitating the composition of spectrally compact OFDM preamble/pilot waveforms. The higher the sidelobe-decaying order, the higher spectral compactness the preamble/pilot waveform exhibits. By use of the developed orthogonal order- I CA sequences, the SPI system requiring a large number of identification/sounding sequences can achieve the better performance in multipath channels while exhibiting high spectral compactness. Specifically, degenerate PMA sequence families $\mathcal{G}_{\max, \tilde{I}}^{(\text{dpma}, \kappa)}$ and $\tilde{\mathcal{G}}_{\max, \tilde{I}}^{(\text{dpma}, \kappa)}$ for $\kappa \in \mathcal{Z}_{\Omega(N)-1}^+ - \mathcal{Z}_2^+$ can provide more orthogonal order- \tilde{I} CA sequences than the family $\mathcal{G}_I^{(\text{pma})}$ and families $\mathcal{G}_{\max, \tilde{I}}^{(\text{dpma}, \kappa)}$ for $\kappa \in \mathcal{Z}_2^+$ proposed from [43], with or without trading off sidelobe-decaying order. Augmented PMA sequence families $\hat{\mathcal{G}}_I^{(\text{apma})}$ proposed from [43] and $\hat{\mathcal{G}}_{\max, \tilde{I}}^{(\text{adpma}, \kappa)}$ for $\kappa \in \mathcal{Z}_{\Omega(N)-1}^+$ are further constructed to double the family size by augmenting the phase-rotated replicas of all PMA sequences in families $\hat{\mathcal{G}}_I^{(\text{pma})}$ and $\hat{\mathcal{G}}_{\max, \tilde{I}}^{(\text{dpma}, \kappa)}$, respectively, without trading off the sidelobe-decaying order. When compared with conventional Zadoff-Chu, Yu-Lee, and pseudorandom-noise CA sequence families, these modified PMA sequence families are shown to provide noticeable performance improvement in random-access channel identification over indoor and urban multipath environments exhibiting short-delay channel profiles. Additionally, it is desirable for simultaneous channel estimation to adopt the orthogonal sequence family containing as many



orthogonal cyclically-shiftable sequences as possible. In comparison with Zadoff-Chu, Yu-Lee, and pseudorandom-noise sequence families, the performance characteristics of simultaneous channel estimation over independent Rician multipath channels using the degenerate phase-model assigning sequence family $\mathcal{G}_{\max, I}^{(\text{dpma}, \kappa)}$ exhibit improvement if a large number of uplink channels were required to be estimated simultaneously under asynchronous signal reception. Meanwhile, the preamble/pilot waveforms carrying order- I CA sequences in these modified PMA sequence families are attributed with much higher spectral compactness than those carrying conventional CA sequences.

Appendix



A) Gosper's Hack Algorithm

Gosper's Hack algorithm in [38]-[39] can assist in finding all possible factor sets $\{A_m; m \in \mathcal{Z}_{\Omega(N)-\kappa}\}$ which satisfy $\prod_{m=0}^{\Omega(N)-\kappa-1} A_m = \prod_{m=0}^{\Omega(N)-1} P_m$ and are all characterized by an admissible pattern $\boldsymbol{w} = [w_m; m \in \mathcal{Z}_{\Omega(N)-\kappa}]$ with $w_m = \Omega(A_m)$. To find all possible factor sets $\{A_m; m \in \mathcal{Z}_{\Omega(N)-\kappa}\}$, we aim to (i) first find all possible partitions of $\{P_m; m \in \mathcal{Z}_{\Omega(N)}\}$ into $\Omega(N) - \kappa$ prime factor subsets $\{P_m^{(n)}; m \in \mathcal{Z}_{w_n}\}$ for $n \in \mathcal{Z}_{\Omega(N)-\kappa}$, where $P_0^{(n)} \leq P_1^{(n)} \leq \dots \leq P_{w_n-1}^{(n)}$, with the aid of Gosper's Hack algorithm and (ii) then compose all possible factor sets by computing $A_n = \prod_{m=0}^{w_n-1} P_m^{(n)}$ accordingly. To describe step (i), we define $\tilde{\boldsymbol{w}} = [\tilde{w}_n; n \in \mathcal{Z}_{\Omega(N)-\kappa}]$ with $\tilde{w}_n \triangleq \sum_{m=n}^{\Omega(N)-\kappa-1} w_m$ and $\mathbf{b}^{(n)} \triangleq [b_m^{(n)}; m \in \mathcal{Z}_{\tilde{w}_n}]$ as a binary codeword with length \tilde{w}_n and Hamming weight w_n .^{1.5.4} For a given \boldsymbol{w} , there are a total of $\prod_{n \in \mathcal{Z}_{\Omega(N)-\kappa}} \binom{\tilde{w}_n}{w_n}$ possible binary codeword sets for $\{\mathbf{b}^{(n)}; n \in \mathcal{Z}_{\Omega(N)-\kappa}\}$ and they can be exclusively obtained by Gosper's Hack algorithm in Fig. 8 [39, Algorithm 3.1]. To obtain a partition of $\{P_m; m \in \mathcal{Z}_{\Omega(N)}\}$ for each given $\{\mathbf{b}^{(n)}; n \in \mathcal{Z}_{\Omega(N)-\kappa}\}$, a binary codeword set $\{\tilde{\mathbf{b}}^{(n)}; n \in \mathcal{Z}_{\Omega(N)-\kappa}\}$ is converted from $\{\mathbf{b}^{(n)}; n \in \mathcal{Z}_{\Omega(N)-\kappa}\}$ by the proposed codeword conversion algorithm in Fig. 9, in a way that each codeword $\tilde{\mathbf{b}}^{(n)} \triangleq [\tilde{b}_m^{(n)}; m \in \mathcal{Z}_{\Omega(N)}]$ contains $\Omega(N)$ entries and the same Hamming weight as $\mathbf{b}^{(n)}$. Notably, there are a total of $\Omega(N)$ ones in $\{\tilde{\mathbf{b}}^{(n)}; n \in \mathcal{Z}_{\Omega(N)-\kappa}\}$. From $\{\tilde{\mathbf{b}}^{(n)}; n \in \mathcal{Z}_{\Omega(N)-\kappa}\}$, a partition of $\{P_m; m \in \mathcal{Z}_{\Omega(N)}\}$ into $\Omega(N) - \kappa$ prime factor subsets $\{P_{\tilde{m}}^{(n)}; \tilde{m} \in \mathcal{Z}_{w_n}\}$ can be thus specified by

$$P_{\mathcal{E}_m^{(n)}}^{(n)} = P_m \text{ if } \tilde{b}_m^{(n)} = 1 \quad (32)$$

For $n \in \mathcal{Z}_{\Omega(N)-\kappa}$ and $m \in \mathcal{Z}_{\Omega(N)}$, where $\mathcal{E}_m^{(n)} = \sum_{m'=0}^m \tilde{b}_{m'}^{(n)} - 1$. Accordingly, all possible partitions of $\{P_m; m \in \mathcal{Z}_{\Omega(N)}\}$ and thereby all possible factor sets for $\{A_m; m \in \mathcal{Z}_{\Omega(N)-\kappa}\}$ can be found in steps (i) and (ii) from $\prod_{n \in \mathcal{Z}_{\Omega(N)-\kappa}} \binom{\tilde{w}_n}{w_n}$ possible codeword sets for $\{\mathbf{b}^{(n)}; n \in \mathcal{Z}_{\Omega(N)-\kappa}\}$.

Consider the example with $\Omega(N) = 6$, $\kappa = 3$, and a given pattern $\mathbf{w} = [3,2,1]^t$. Such \mathbf{w} determines $\tilde{\mathbf{w}} = [6,3,1]^t$ uniquely and thus fixes the lengths 6, 3, 1 and Hamming weights 3, 2, 1 of the binary codeword set $\{\mathbf{b}^{(0)}, \mathbf{b}^{(1)}, \mathbf{b}^{(2)}\}$ accordingly. From Gosper's Hack algorithm, there are $\binom{6}{3} \binom{3}{2} \binom{1}{1} = 60$ possible codeword sets meeting such length and weight distributions. For example, $\mathbf{b}^{(0)} = [0,1,0,1,1,0]^t$, $\mathbf{b}^{(1)} = [0,1,1]^t$, and $\mathbf{b}^{(2)} = [1]$ form one possible codeword set. From the codeword conversion algorithm, the corresponding codeword set $\{\tilde{\mathbf{b}}^{(n)}; n \in \mathcal{Z}_{\Omega(N)-\kappa}\}$ is obtained as $\tilde{\mathbf{b}}^{(0)} = [0,1,0,1,1,0]^t$, $\tilde{\mathbf{b}}^{(1)} = [0,0,1,0,0,1]^t$, and $\tilde{\mathbf{b}}^{(2)} = [1,0,0,0,0,0]^t$. In turns, such $\{\tilde{\mathbf{b}}^{(n)}; n \in \mathcal{Z}_{\Omega(N)-\kappa}\}$ determines a partition of $\{P_m; m \in \mathcal{Z}_{\Omega(N)}\}$ into $\{P_m^{(0)}; m \in \mathcal{Z}_{w_0}\} = \{P_1, P_3, P_4\}$, $\{P_m^{(1)}; m \in \mathcal{Z}_{w_1}\} = \{P_2, P_5\}$, and $\{P_m^{(2)}; m \in \mathcal{Z}_{w_2}\} = \{P_0\}$. The corresponding $\{A_m; m \in \mathcal{Z}_{\Omega(N)-\kappa}\}$ becomes $\{P_1 P_3 P_4, P_2 P_5, P_0\}$. All 60 possible partitions can be thus obtained from 60 codeword sets $\{\mathbf{b}^{(0)}, \mathbf{b}^{(1)}, \mathbf{b}^{(2)}\}$ exclusively obtained by Gosper's Hack algorithm.



Algorithm Gosper's Hack

Input: ω , $\Omega(N)$, and κ

Initialization: Set $i = \Omega(N) - \kappa - 2$ and the initial binary codewords $\mathbf{b}^{(n)}$'s for $n \in Z_{\Omega(N)-\kappa}$ as $b_m^{(n)} = 1$ for $m \in Z_{\omega_n}$ and $b_m^{(n)} = 0$ otherwise. Let \mathcal{S} denote the set containing all binary codeword sets that we have found currently. Initially, we have $\mathcal{S} = \{\{\mathbf{b}^{(n)}; n \in Z_{\Omega(N)-\kappa}\}\}$.

repeat

if $b_{\omega_i-1-m}^{(i)} = 0$ for some $m \in Z_{\omega_i}$, **then**

1. Find the smallest integer v such that $b_v^{(i)} = 1$ and $b_{v+1}^{(i)} = 0$ and then compute the Hamming weight w of $[b_m^{(i)}; m \in Z_v]$.
2. After setting $b_m^{(i)} = 1$ for $m \in Z_w$, $b_m^{(i)} = 0$ for $m \in Z_{v+1} - Z_w$, and $b_{v+1}^{(i)} = 1$, a new binary codeword set $\{\mathbf{b}^{(n)}; n \in Z_{\Omega(N)-\kappa}\}$ is obtained and added into \mathcal{S} .
3. Set $i = \Omega(N) - \kappa - 2$.

Else

1. Set $b_m^{(i)} = 1$ for $m \in Z_{\omega_i}$ and $b_m^{(i)} = 0$ otherwise.
2. Decrease i by 1.

until $b_{\omega_n-1-m}^{(n)} = 1$ for $m \in Z_{\omega_n}$ and $n \in Z_{\Omega(N)-\kappa}$

Output: The set \mathcal{S} which contains all possible binary codeword sets.

Fig. 8.
Gosper's Hack Algorithm

Algorithm Codeword Conversion

Input: $\{\mathbf{b}^{(n)}; n \in Z_{\Omega(N)-\kappa}\}$

Initialization: Set $\tilde{b}_i^{(0)} = b_i^{(0)}$ for $i \in Z_{\Omega(N)}$, $m = \varepsilon = 0$, and $n = 1$.

repeat

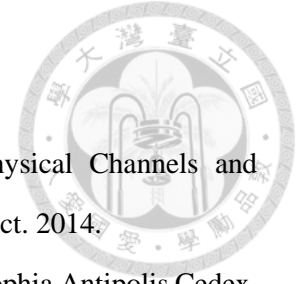
1. If $\sum_{v=0}^{n-1} \tilde{b}_m^{(v)} \neq 0$, set $\tilde{b}_m^{(n)} = 0$. Otherwise, set $\tilde{b}_m^{(n)} = b_\varepsilon^{(n)}$ and increase ε by 1.
2. If $m < \Omega(N) - 1$, increase m by 1. Otherwise, set $m = \varepsilon = 0$ and increase n by 1.

until $n = \Omega(N) - \kappa$

Output: The binary codeword set $\{\tilde{\mathbf{b}}^{(n)}; n \in Z_{\Omega(N)-\kappa}\}$ with $\tilde{\mathbf{b}}^{(n)} = [\tilde{b}_m^{(n)}; m \in Z_{\Omega(N)}]$.

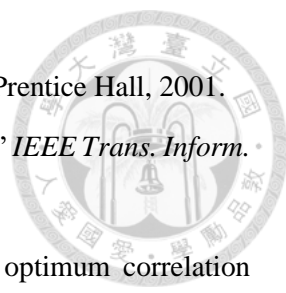
Fig. 9.
Codeword Conversion Algorithm

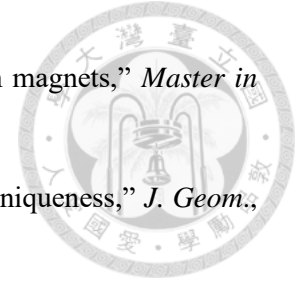
References



- [1] LTE: Evolved Universal Terrestrial Radio Access (E-UTRA): Physical Channels and Modulation, 3GPP TS 36.211 V12.3.0, Sophia Antipolis Cedex, France, Oct. 2014.
- [2] 5G NR: Physical Channels and Modulation, 3GPP TS 38.211 V15.4, Sophia Antipolis Cedex, France, Dec. 2018.
- [3] Part 22: Cognitive Wireless RAN Medium Access Control (MAC) and Physical Layer (PHY) Specifications: Policies and Procedures for Operation in the TV Bands, IEEE Standard 802.22-2011, Jul. 2011
- [4] H. Minn, V. K. Bhargava, and K. K. B. Letaief, "A robust timing and frequency synchronization for OFDM systems," *IEEE Trans. Wireless Commun.*, vol. 2, no. 4, pp. 822-839, Jul. 2003.
- [5] K. S. Kim, S. W. Kim, Y. S. Cho, and J. Y. Ahn, "Synchronization and cell-search technique using preamble for OFDM cellular systems," *IEEE Trans. Veh. Technol.*, vol. 56, no. 6, pp. 3469-3485, Nov. 2007.
- [6] M. M. Gul, X. Ma, and S. Lee, "Timing and frequency synchronization for OFDM downlink transmissions using Zadoff-Chu sequences," *IEEE Trans. Wireless Commun.*, vol. 14, no. 3, pp. 1716-1729, Mar. 2015.
- [7] S. Johnson and O. A. Dobre, "Time and carrier frequency synchronization for coherent optical communication: Implementation considerations, measurements, and analysis," *IEEE Trans. Instrum. Meas.*, vol. 69, no. 8, pp. 5810-5820, Aug. 2020.
- [8] C.-D. Chung and W.-C. Chen, "Preamble sequence design for spectral compactness and initial synchronization in OFDM," *IEEE Trans. Veh. Technol.*, vol. 67, no. 2, pp. 1428-1443, Feb. 2018.
- [9] C.-D. Chung, W.-C. Chen, and C.-K. Yang, "Constant-amplitude sequences for spectrally compact OFDM training waveforms," *IEEE Trans. Veh. Technol.*, vol. 69, no. 11, pp. 12974-12991, Nov. 2020.
- [10] W.-C. Chen and C.-D. Chung, "Spectrally efficient OFDM pilot waveform for channel estimation," *IEEE Trans. Commun.*, vol. 65, no. 1, pp. 387-402, Jan. 2017.
- [11] W.-C. Chen, C.-K. Yang, P.-T. Chi, and C.-D. Chung, "Pilot sequence design for spectral compactness and channel estimation in OFDM," in *Proc. IEEE Veh. Technol. Conf.*, Honolulu, track 7A, pp. 1-5, Sep. 2019.

- 
- [12] R. Negi and J. Cioffi, "Pilot tone selection for channel estimation in a mobile OFDM system," *IEEE Trans. Consumer Electron.*, vol. 44, no. 3, pp. 1122-1128, Aug. 1998.
- [13] P. Stoica and O. Besson, "Training sequence design for frequency offset and frequency-selective channel estimation," *IEEE Trans. Commun.*, vol. 51, no. 11, pp. 1910-1917, Nov. 2003.
- [14] S. Yu and J.-W. Lee, "Channel sounding for multi-user massive MIMO in distributed antenna system environment," *Electronics*, vol. 8, no. 1, pp. 1-14, Jan. 2019.
- [15] L. Kundu, G. Xiong, and J. Cho, "Physical uplink control channel design for 5G new radio," in *Proc. IEEE 5G World Forum (5GWF)*, Silicon Valley, pp. 233-238, Nov. 2018.
- [16] J. Y. Han, O. Jo, and J. Kim, "Exploitation of channel-learning for enhancing 5G blind beam index detection," *IEEE Trans. Veh. Technol.*, vol. 71, no. 3, pp. 2925-2938, Mar. 2022.
- [17] T. Kim, I. Bang, and D.-K. Sung, "An enhanced PRACH preamble detector for cellular IOT communications," *IEEE Commun. Lett.*, vol. 21, no. 12, pp. 2678-2681, Dec. 2017.
- [18] L. Zhen et al., "Random access preamble design and detection for mobile satellite communication systems," *IEEE J. Sel. Areas Commun.*, vol. 36, no. 2, pp. 280-291, Feb. 2018.
- [19] B. Liang, Z. He, K. Niu, B. Tian, and S. Sun, "The research on random access signal detection algorithm in LTE systems," in *Proc. IEEE Int. Symp. Microwave, Antenna, Propag. and EMC Technol. for Wireless Commun.*, Chengdu, China, pp. 115-118, Dec. 2013.
- [20] A.-E. Mostafa, et al., "Aggregate preamble sequence design and detection for massive IOT with deep learning," *IEEE Trans. Veh. Technol.*, vol. 70, no. 4, pp. 3800-3816, Apr. 2021.
- [21] L. Zhen, H. Kong, Y. Zhang, W. Wang, and K. Yu, "Efficient collision detection based on Zadoff-Chu sequences for satellite-enabled M2M random access," in *Proc. IEEE Int. Conf. Commun.*, Montreal, QC, Canada, pp. 1-6, Aug. 2021.
- [22] S. Ali, Z. Chen, and F. Yin, "Design of orthogonal uplink pilot sequences for TDD massive MIMO under pilot contamination," *J. Commun.*, vol. 12, no. 1, pp. 40-48, Jan. 2017.
- [23] L. G. Giordano et al., "Uplink sounding reference signal coordination to combat pilot contamination in 5G massive MIMO," in *Proc. IEEE Wireless Commun. Netw. Conf.*, Barcelona, Spain, pp. 1-6, Apr. 2018.
- [24] F. Yang, P. Cai, H. Qian, and X. Luo, "Pilot contamination in massive MIMO induced by timing and frequency errors," *IEEE Trans. Wireless Commun.*, vol. 17, no. 7, pp. 4477-4492, Jul. 2018.

- 
- [25] T. S. Rappaport, *Wireless Communications*, Upper Saddle River, NJ: Prentice Hall, 2001.
- [26] D. C. Chu, "Polyphase codes with good periodic correlation properties," *IEEE Trans. Inform. Theory*, vol. 18, pp. 531-532, Jul. 1972.
- [27] B. M. Popovic, "Generalized chirp-like polyphase sequences with optimum correlation properties," *IEEE Trans. Inform. Theory*, vol. 38, pp. 1406-1409, Jul. 1992.
- [28] J. J. Benedetto and J. J. Donatelli, "Ambiguity function and frame theoretic properties of periodic zero-autocorrelation waveforms," *IEEE J. Select. Topics Signal Process.*, vol. 1, no. 1, pp. 6-20, Jun. 2007.
- [29] R.-A. Pitaval, B. M. Popovic, P. Wang, and F. Berggren, "Overcoming ' 5G PRACH capacity shortfall: Supersets of Zadoff-Chu sequences with low-correlation zone," *IEEE Trans. Commun.*, vol. 68, no. 9, pp. 5673- 5688, Sep. 2020.
- [30] M. Faulkner, "The effect of filtering on the performance of OFDM systems," *IEEE Trans. Veh. Technol.*, vol. 49, no. 5, pp. 1877-1884, Sep. 2000.
- [31] C.-D. Chung, "Spectrally precoded OFDM," *IEEE Trans. Commun.*, vol. 54, no. 12, pp. 2173-2185, Dec. 2006.
- [32] H.-M. Chen, W.-C. Chen, and C.-D. Chung, "Spectrally precoded OFDM and OFDMA with cyclic prefix and unconstrained guard ratios," *IEEE Trans. Wireless Commun.*, vol. 10, no. 5, pp. 1416-1427, May 2011.
- [33] M. Ma, X. Huang, B. Jiao, and Y. J. Guo, "Optimal orthogonal precoding for power leakage suppression in DFT-based systems," *IEEE Trans. Commun.*, vol. 59, no. 3, pp. 844-853, Mar. 2011.
- [34] C.-D. Chung and K.-W. Chen, "Spectrally precoded OFDM without guard insertion," *IEEE Trans. Veh. Technol.*, vol. 66, no. 1, pp. 107-121, Jan. 2017.
- [35] K. Hussain and R. Lopez-Valcarce, "Joint precoder and window design for OFDM sidelobe suppression," *IEEE Commun. Lett.*, vol. 26, no. 12, pp. 3044-3048, Dec. 2022.
- [36] G. E. Andrews, *The Theory of Partitions*. Cambridge: Cambridge University Press, 1998.
- [37] N. M. Chase, "Global structure of integer partitions sequences," *Electron. J. Comb.*, vol. 1, pp. 1-25, Apr. 2004.
- [38] D. E. Knuth, *The Art of Computer Programming*, vol. 4. Upper Saddle River, NJ, USA: Addison-Wesley, 2005.



- [39] A. M. Foggia, "Massively parallel approaches to frustrated quantum magnets," *Master in High Performance Computing*, vol. 4, pp. 1-46, Jan. 2019.
- [40] I. Pinelis, "Cyclic polygons with given edge lengths: Existence and uniqueness," *J. Geom.*, vol. 82, no. 1-2, pp. 156-171, Aug. 2005.
- [41] J. G. Proakis and M. Salehi, *Digital Communications, 5th ed.* New York: McGraw-Hill, 2008.
- [42] "NR; Study on channel model for frequencies from 0.5 to 100 GHz," 3GPP, Sophia Antipolis Cedex, France, TS 38.901 V16.1, Nov. 2020.
- [43] P.-F. Tsou (2021), *Orthogonal Constant-Amplitude Sequence Families for Spectrally Compact OFDM Training Waveforms* (Unpublished master's dissertation). National Taiwan University, Taipei, Taiwan.
- [44] Y. Wang, A. Zheng, J. Zhang, and D. Yang, "A novel channel estimation algorithm for sounding reference signal in LTE uplink transmission," *IEEE International Conf. on Commun. Tech. and Applications*, Beijing, China, pp. 412-415, Dec. 2009.
- [45] P. Xu, J. Wang, J. Wang, and F. Qi, "Analysis and design of channel estimation in multicell multiuser MIMO OFDM systems," *IEEE Trans. Veh. Tech.*, vol. 64, no. 2, pp. 610-620, Feb. 2015.
- [46] B. M. Popović, P. Wang, and F. Berggren, "Signals with sparse mutual interference for sounding massive MIMO channels," *IEEE Trans. Commun.*, vol. 69, no. 8, pp. 5608-5619, Aug. 2021.
- [47] H.-S. Kim, S.-H. Lee, and Y.-H. Lee, "Channel sounding for multi-sector cooperation in OFDM-based wireless cellular systems," *International Conf. on Advanced Commun. Tech.*, Gangwon, Korea (South), pp. 313-317, Apr. 2010.
- [48] A. Kalachikov and A. Stenin, "Performance evaluation of the SRS based MIMO channel estimation on 5G NR open source channel model," in *Proc. IEEE International Conf. of Young Professionals in Electron Devices and Materials*, Souzga, the Altai Republic, Russia, pp. 124-127, Aug. 2021.
- [49] J. G. Proakis and M. Salehi, *Digital Communications, 5th ed.* New York: McGraw-Hill, 2008.